UNIVERSITY OF CALIFORNIA
RIVERSIDE

Chemistry at the Dirac Point of Graphene

A Dissertation submitted in partial satisfaction
of the requirements for the degree of

Doctor of Philosophy

in

Chemistry

by

Santanu Sarkar

December 2013

Dissertation Committee:
Dr. Robert C. Haddon, Chairperson
Dr. Thomas Morton
Dr. Michael Marsella

The Dissertation of Santanu Sarkar is approved:

Committee Chairperson

University of California, Riverside

ACKNOWLEDGEMENTS

With gratitude and pleasure, I sincerely thank my advisor Professor Robert C. Haddon for his enthusiastic guidance, unflinching support, profound understanding and interest in my personal and professional welfare during my four-year-long graduate research and training in his pioneering group. I deeply acknowledge and appreciate the mentoring from Dr. Elena Bekyarova throughout my graduate studies – she has always been a great teacher, very motivating guide, ready to discuss, encourage and help at any point of time, and a wonderful person. I express my sincere gratitude towards my committee members: Dr. Thomas Morton and Dr. Michael Marsella for their sincere attention to my research progress and suggestions for improvement.

I express my sincere thanks to Dr. Sandip Niyogi for his guidance and help during my initial stages of research. I immensely appreciate his great help, guidance and important suggestions during first and second year of my research. I greatly thank my lab members: Dr. Mikhail E. Itkis, Dr. Aron Pekker, Dr. Irina Kalinina, Xiaojuan Tian, and Matthew L. Moser for their experimental help and insightful discussions, and for making the lab a very cheerful and enjoyable place to work. I would like to convey my deepest thanks to the CNSE Staff, Mr. Dexter Humphrey for his continuous help, sincere guidance, training and helpful discussions in the UCR Cleanroom (nanofabrication) facility.

With great pleasure, I convey my deepest gratitude to my beloved parents, Mr. Pradip Sarkar and Mrs. Mukta Sarkar, my sister, Bulbul, and my beloved wife, Sharmistha for their unconditional love, constant encouragement, support and discipline to achieve my long-cherished goal.

I would like to thank the publishers for allowing me to reprint materials in my dissertation. The text and figures in this dissertation, in part, is a reprint of the materials as appeared in the following publications and are duly cited in my dissertation: Sarkar, S.; Bekyarova, E.; Niyogi, S.; Haddon, R. C. *J. Am. Chem. Soc.* **2011***,* 133, 3324-3327. Sarkar, S.; Niyogi, S.; Bekyarova, E.; Haddon, R. C. *Chem. Sci.* **2011**, 2, 1326-1333. Sarkar, S.; Bekyarova, E.; Haddon, R. C. *Angew. Chem. Int. Ed.* **2012**, 51, 4901-4904. Sarkar, S.; Bekyarova, E.; Haddon, R. C. *Acc. Chem. Res.* **2012**, 45, 673-682. Sarkar, S.; Bekyarova, E.; Haddon, R. C. *Mater. Today* **2012**, 15, 276-285. Sarkar, S.; Zhang, H.; Huang, J-W.; Wang, F,; Bekyarova, E.; Lau, C. N.; Haddon, R. C. *Adv. Mater.* **2013**, 25, 1131-1136. Sarkar, S.; Moser, M. L.; Tian, X.; Zhang, X.; Al-Hadeethi, Y. F.; Haddon, R.C. *Chem. Mater.* **2013**, in press. Sarkar, S.; Bekyarova, E.; Haddon, R. C. Carbon Nanotubes and Graphene (Edited by S. Iijima and K. Tanaka), 2nd Edition, Elsevier.

- Santanu Sarkar
University of California – Riverside

ABSTRACT OF THE DISSERTATION

Chemistry at the Dirac Point of Graphene

by

Santanu Sarkar

Doctor of Philosophy, Graduate Program in Chemistry
University of California, Riverside, December 2013
Dr. Robert C. Haddon, Chairperson

Graphene holds great potential as an electronic material because of its excellent transport properties, which derive from its unique Fermi surface and ballistic conductance. It exhibits extremely high mobility (~250,000 $cm^2V^{-1}s^{-1}$), which exceeds by orders of magnitude that of silicon. Despite its extraordinary properties, the absence of a band-gap in graphene makes it unsuitable for its use as an active element in conventional field effect transistors (FETs). Another problem with pristine graphene is its lack of solution processability, which inhibits it applications in numerous fields such as printed electronics, transparent conductors, nano-biodevices, and thin film technologies involving fuel cells, capacitors and solar cells.

My thesis is focused on addressing theses issue by application of covalent chemistry to graphene. Chemical functionalization of graphene has emerged as a promising approach in modifying the electronic structure and magnetic properties of graphene. Generally, chemical modification of graphene leads to the creation of new sp^3 carbon centers in the graphene lattice, thereby influencing the electron-scattering and creating dielectric regions in graphene wafers by partial breakdown of the electronic conjugation pathway. This approach provides a non-invasive route to the creation of energy band-gaps in graphene and offers the possibility of patterning graphene to form specific conducting, ballistically

conducting, insulating, semiconducting and magnetic patterns – paving the way for wave function engineering of graphene devices using covalent chemistry.

We have applied the **Kolbe electro-oxidation** strategy to achieve an efficient quasi-reversible electrochemical grafting of α-naphthylmethyl radicals to graphene. The method facilitates reversible bandgap engineering in graphene and preparation of electrochemically erasable organic dielectric films. We have discovered that the zero-band-gap electronic structure of graphene enables it to function as either the diene or the dienophile in the **Diels−Alder (DA) reaction** and we show that the application of the Diels-Alder (DA) chemistry to graphene, which is capable of simultaneous formation of a pair of sp^3-carbon centers (balanced sub-lattice functionalization) in graphene, can selectively produce DA-modified graphene FET devices with mobility between 1,000-6,000 $cm^2V^{-1}s^{-1}$ (with a variable range hopping transport mechanism).

Most of the covalent chemistry applied to graphene leads to a change in hybridization of graphene sp^2 carbon to sp^3 (destructive hybridization) and the FET devices based on such covalently modified graphene shows a drastic reduction of device mobility. To this end, we find that the **organometallic hexahapto (η^6) metal complexation** chemistry of graphene, in which the graphene π-band constructively hybridizes with the vacant d-orbitals of transition metals, allows the fabrication of field effect devices which retain a high degree of the mobility with enhanced on-off ratio.

In summary, we conclude that the singular electronic structure of graphene at the Dirac point govern the chemical reactivity of graphene and this chemistry will play a vital role in propelling graphene to assume its role as the next generation electronic material beyond silicon.

TABLE OF CONTENTS

Chemistry at the Dirac Point of Graphene

List of Acronyms

AFM	Atomic Force Microscopy
ARPES	Angle-Resolved Photoemission Spectroscopy
BLG	Bilayer Graphene, n = 2
CNT	Carbon Nanotubes
DMBD	2,3-Dimethoxy-1,3-butadiene
DOS	Density of States
EG	Epitaxial Graphene on SiC substrates
FLG	Few Layer Graphene $n \geq 4$
HOPG	Highly Oriented Pyrolytic Graphite
MA	Maleic Anhydride
MeA	9-Methylanthracene
μG	Microcrystalline Graphite
NP	Nitrophenyl
NM	Naphthylmethyl
SLG	Single Layer (monolayer) Graphene, n = 1
SWNTs	Single-Walled Carbon Nanotubes
SEM	Scanning Electron Microscopy
STM	Scanning Tunneling Microscopy
TCNE	Tetracyanoethylene
TEM	Transmission Electron Microscopy
TGA	Thermogravimetric Analysis
TLG	Tri-layer Graphene, n = 3
FET	Field Effect Transistor
XG	Exfoliated Graphene
XG_{flake}	Exfoliated Graphene Flake
XG_{sol}	Liquid Phase (Solvent) Exfoliated Graphene

CHAPTER 1. Introduction to Graphene Chemistry

1.1. INTRODUCTION

The allotropes of carbon have fascinated mankind for centuries and have been at the epicenter of intensive research interest for their scientific value and potential for technological applications. The element carbon is capable of forming a wide variety of structures due to its valency and existence in different hybridization states leading to catenation of carbon with covalently linking carbon–carbon chains. The new carbon age,[1] which is the third wave in the carbon revolution, has witnessed overwhelming interest in low-dimensional carbon materials, with particular attention to graphene, the newest member of the series of carbon allotropes.[2-6] Graphene is the basic building block for graphitic materials of all other dimensionalities: it can be wrapped up into 0D fullerenes, rolled into 1D carbon nanotubes or stacked into 3D graphite (**Figure 1.1**).[7,8]

This two-dimensional form of pure sp^2 hybridized carbon allotrope of atomic thickness has garnered tremendous attention among both physicists and chemists and has provided a test-bed for fundamental and device physics[3,9,10] and a unique chemical substrate.[11-15] In line with theoretical predictions, charge carriers in graphene behave like massless Dirac fermions, which is a direct consequence of the linear energy dispersion relation.[16] Such features serve to

recommend graphene for mechanical, thermal, electronic, magnetic and optical applications. But the absence of a band-gap in graphene makes it unsuitable for conventional field effect transistors (FETs),[17,18] and its lack of solution processability remains to be resolved.[19] These issues are potentially amenable to solution by chemical techniques, but the effect of chemistry on the mobility of functionalized graphene devices is an imposing challenge.[20]

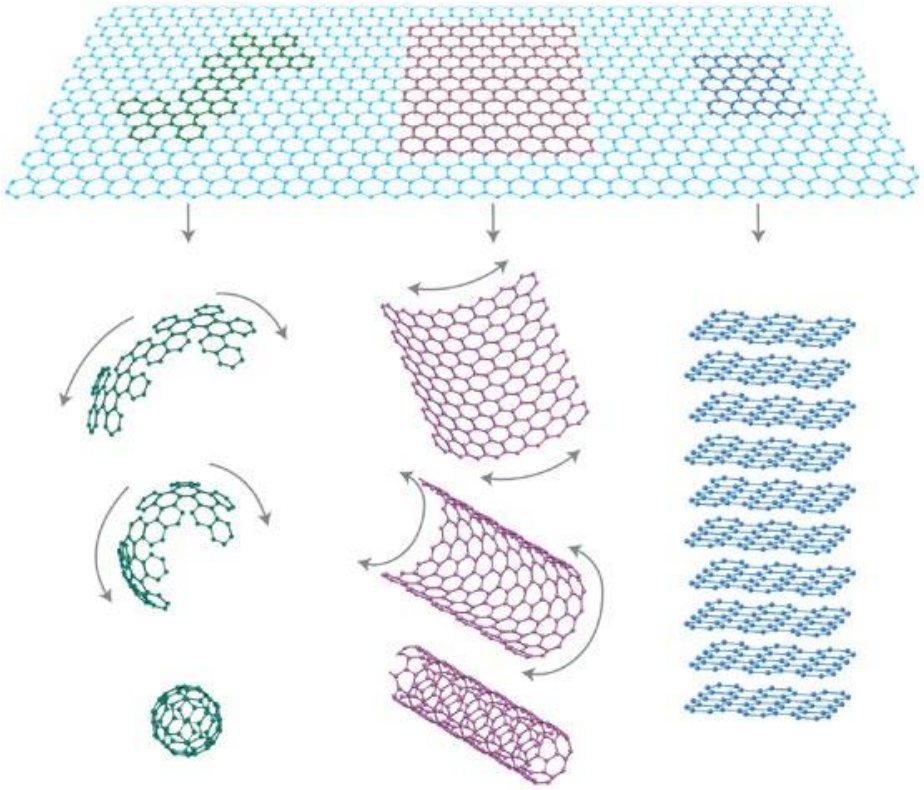

Figure 1.1. Graphene is the mother of other graphitic materials of different dimensionalities. It can be wrapped up into 0D buckyballs, rolled into 1D nanotubes or stacked into 3D graphite. Reprinted with permission from ref.[7] (Copyright © 2007 Nature Publishing Group).

While the fundamental physics of graphene has been extensively studied and experimentally demonstrated,[2,3,9,16] the exciting chemical implications of the massless two-dimensional gas of Dirac fermions in graphene is just now coming into focus.[21,22] The recent exploration of the chemistry of graphene at the Dirac point has provided a rational understanding of the chemical reactivity of graphene in Diels-Alder pericyclic reactions, based on the graphene frontier molecular orbitals at the Dirac point as they relate to the original frontier molecular (FMO) theory and orbital symmetry conservation concepts.[18,21,23-25] This understanding provides the basis of a unified theory of graphene reactivity, including radical addition chemistry, Diels-Alder pericyclic chemistry, and organometallic mono- and bis-hexahapto complexation chemistry.[26-28]

1.2. THE PURPOSE OF GRAPHENE FUNCTIONALIZATION

The pursuit of the chemical functionalization of graphene is based on a number of motivations: (i) modification of the electronic structure of graphene with focus on band-gap engineering for transistors [26] and fabrication of dielectrics, (ii) creation of magnetism in graphene for applications in spintronics,[29-32] and (iii) bulk preparation of solution-processable derivatives of graphene for a broad range of applications including printable electronics, energy storage, thermal interface materials (TIMs), nano-bio hybrid composites.[33]

From a fundamental stand point graphene chemistry is the solid state counterpart of classical small molecule electrocyclic organic reactions, including Diels-Alder chemistry,[18,21] and the Claisen rearrangement.[34]

However, the basal plane chemical modification of graphene is not straightforward because normal aromatic substitution reactions cannot be applied, and in this respect graphene chemistry resembles that of fullerenes and carbon nanotubes, but without the role of strain in promoting addition chemistry.[35,36] Nevertheless, it has already been demonstrated that the atomically flat surface of graphene provides an opportunity to apply carbon-carbon bond formation chemistry with subsequent creation of sp^3 carbon centers in place of sp^2 carbons.[15,30] This chemistry has a pronounced effects on the electronic and phonon properties of graphene as evidenced by Raman spectroscopy, transport and magnetic measurements and scanning tunneling microscopy. The covalent modification of the two-dimensional π-electron system of graphene provides a novel protocol to impart patterning that can modulate the energy band gap, influence electron scattering, affect the flow of current by creating dielectric regions over the graphene wafer,[30] and potentially address some of the issues in the fabrication of molecular level electronic circuitry.[37] The fundamental concept is the generation of new carbon-carbon bonds to redirect the electronic conjugation pathway and to form specific conducting, ballistically conducting, insulating, semiconducting, and magnetic patterns.[22]

1.3. A BRIEF HISTORY OF GRAPHENE

Graphite oxide (GO), graphene oxide (i.e. exfoliated GO), and graphite intercalation compounds (GICs) have been studied extensively for more than 170 years.[38-42] The evolution of graphene as a two-dimensional material[43] is presented below from a historical perspective with the most important timeline presented in **Figure 1.2**.[5,44] It should be noted that the history of graphene is rich and there are a number of reviews, which focus on different aspects of the development of scientific knowledge, which led to the current explosion of interest in graphene.[4,7,10,11,13,45-47]

The “lead pencil” (historically also called: blacklead and plumbago)[48] based on graphite was invented as early as 1564, marking the first informal synthesis of graphene, which went unnoticed. The term “graphite” is derived from the Greek word “graphein” (to write). This three dimensional material with its lamellar structure bestows unique electronic and mechanical properties, particularly when the individual layers of graphite (held together by van der Waals forces) are considered as independent entities.[44]

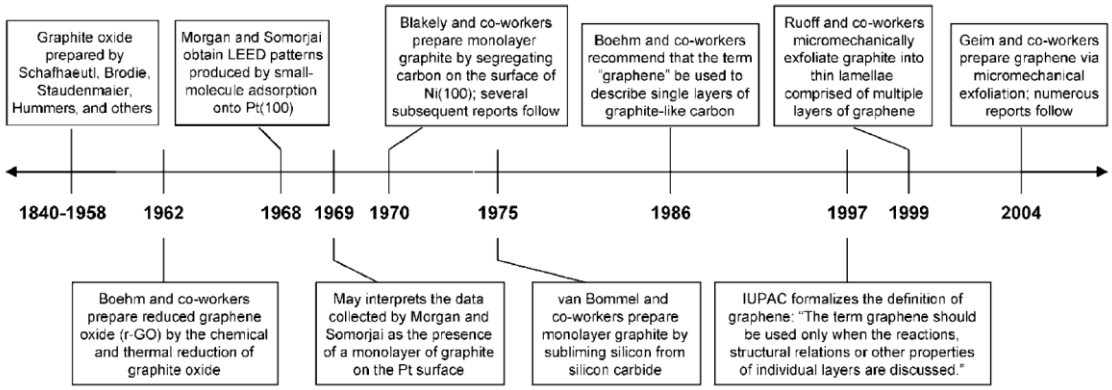

Figure 1.2. Timeline of selected events in the history of the preparation, isolation, and characterization of graphene. Reprinted with permission from ref.[44] (Copyright © 2010 Wiley-VCH Verlag GmbH & Co. KGaA, Weinheim).

The earliest reports of GO and graphite intercalation compounds (GICs) can be tracked back to the 1840s, when the German scientist Schafhaeutl reported the intercalation and exfoliation of graphite with sulphuric and nitric acids.[38-40] In GICs the stacked structure of graphite is retained, but the interlayer spacing is widened, resulting in electronic decoupling of the individual layers. Such electronic decoupling, in some cases, may lead to interesting phenomena including superconductivity.[49]

In 1859, the British chemist Brodie used what may be recognized as modification of the methods described by Schafhaeutl in an effort to characterize the molecular weight of graphite by using strong acids (sulphuric and nitric acids) as well as strong oxidants (e.g. $KClO_3$).[50] Interestingly these

drastic chemical environments not only led to the intercalation of graphite layers, but also to chemical oxidation of the graphite surfaces and formation of graphite oxide (GO).

In 1898, Staudenmaier reported a slightly different version of the Brodie's oxidation method for making GO by addition of chlorine salts in multiple aliquots over the course of the reaction instead of in a single portion.[51] Moreover, these modification methods are still used today for the preparation of graphene oxide, rGO and other chemically modified graphene (CMGs) derivatives of GOs.[52,53]

As early as the 1940s, a series of theoretical analyses suggested that the graphene layers—if isolated—might exhibit extraordinary electronic characteristics (such as 100 times greater conductivity within a plane than between planes).[54] In 1946, P. R. Wallace published the band structure of graphene,[54] which provided the key to its electronic structure and showed that the conduction and valence bands touch at the K-point in momentum space.

Nearly a century after the studies reported by Brodie, in 1962 Boehm found that the chemical reductions of dispersions of GO in dilute alkaline media with hydrazine, hydrogen sulfide, or iron(II) salts produced thin, lamellar carbon that contained only small amounts of hydrogen and oxygen.[55,56] The crucial task of determining the number of layers present in the lamellae was accompanied

by densitometry against a set of standardized films of known thickness by using transmission electron microscopy (TEM). The carbon material was found to exhibit a minimum thickness of 4.6 Å, which deviates slightly from the thickness observed in recent studies (4.0 Å).[7] Thus, Boehm concluded, "this observation confirms the assumption that the thinnest of the lamellae really consisted of single carbon layers".[56]

In a separate study in 1968, Morgan and Somorjai used low-energy electron diffraction (LEED) to investigate the adsorption of various gaseous organic molecules (CO, C_2H_4, C_2H_2) onto a platinum(100) surface at high temperature.[57] In 1969, May postulated that single as well as multiple layers of a material that features a graphitic structure were present.[58] He also deduced that "the first monolayer of graphite minimizes its energy of placement on each of the studied faces of platinum". Between 1970 and 1974, a number of reports by Blakely and co-workers indicated surface segregation of mono- and multilayers of carbon from various crystalline faces of transition metal substrates, including Ni (100) and (111), Pt (111), Pd (100), and Co (0001).[59-65] In 1974, Shelton reported the surface phase transition and equilibrium segregation of carbon on the Ni(111) surface.[65] They pointed out three distinct equilibrium states of carbon with Ni, namely (a) dilute carbon phase at high temperature, (b) a condensed graphitic monolayer (single-layer "graphene", as it is called now), separated from "a" by a sharp transition with temperature, and

(c) precipitation of multilayer epitaxial graphite.[65] This work marks the discovery of monolayer graphene from CVD synthesis on Ni substrates as early as in 1970s. In addition to that, Land reported the growth of monolayer graphene in 1992 from ethylene as precursor and over Pt (111) metal surface at 1230 K (**Figure 1.3**).[66]

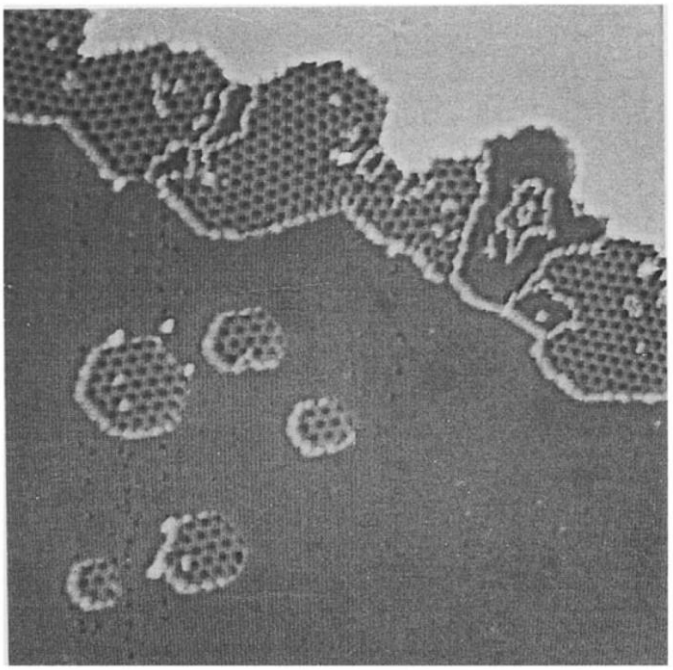

Figure 1.3. STM image (1000 Å × 1000 Å) showing the formation of a graphitic structure on a metal surface; the image was obtained at room temperature after annealing of ethylene over Pt (111) at 1230 K. Most of the graphite is now seen at the lower step edges with a few large regularly shaped islands remaining on the terraces. The sides of the hexagonal graphite islands follow the Pt substrate <110> directions. Reprinted with permission from ref.[66] (Copyright © 1992 Elsevier Inc.).

In 1975, van Bommel et al. described the epitaxial sublimation of silicon from single crystals of silicon carbide (0001). At elevated temperatures under ultrahigh vacuum (UHV; $<10^{-10}$ Torr), monolayered flakes of carbon with the structure of graphene were seen, as was evidenced by LEED and Auger electron spectroscopy.[67] Moreover, the disappearance of the carbide peak in the Auger spectrum was reported to be coupled to the appearance of the graphitic peak.[68]

To the best of our knowledge the term graphene was first coined by Boehm in 1986.[69,70] Boehm recommended standardizing the term: "the ending -ene is used for fused polycyclic aromatic hydrocarbons, even when the root of the name is of trivial origin, for example, naphthalene, anthracene, tetracene, coronene, ovalene. A single carbon layer of the graphitic structure would be the final member of infinite size of this series. The term graphene layer should be used for such a single carbon layer."[5,69,71,72]

In 1997, IUPAC formalized these recommendations by incorporating them into their Compendium of Chemical Technology, which states: "previously, descriptions such as graphite layers, carbon layers or carbon sheets have been used for the term graphene. Because graphite designates that modification of the chemical element carbon, in which planar sheets of carbon atoms, each atom bound to three neighbours in a honeycomb- like structure, are stacked in

a three-dimensional regular order, it is not correct to use for a single layer a term which includes the term graphite, which would imply a three- dimensional structure. The term graphene should be used only when the reactions, structural relations or other properties of individual layers are discussed."[73]

These predictions were not only proven correct, but the isolated layers of graphite were also found to display favorable properties, such as high carrier mobilities (> 200000 $cm^2 V^{-1}s^{-1}$ at electron densities of 2×10^{11} cm^{-2}),[3,74,75] exceptional Young modulus values (> 0.5–1 TPa), and large spring constants (1–5 N m^{-1}).[76] Geim and Novoselov. at the University of Manchester realized and identified graphene experimentally by micro-mechanical exfoliation in 2004.[3] At about the same time Walt de Heer at the Georgia Institute of Technology reported the realization of electronic devices based on "ultrathin graphitic films" (graphene).[2,77]

In 2005, Phillip Kim at Columbia University observed the quantum Hall effect and Berry's phase in graphene.[9] At about the same time Geim, Novoselov and co-workers at the University of Manchaster reported similar observation on graphene.[78]

The stability and isolation of this two dimensional atomic crystal, graphene was first demonstrated using the micro-mechanically exfoliation of

graphite by Scotch tape with subsequent placement on an oxidized silicon wafer.[3] Today chemical vapor deposition (CVD) growth of graphene is the most popular synthetic technique and graphene is generally grown on copper foil or nickel metal substrates from methane, methanol or other carbon sources.[79] Large-area CVD graphene seems to offer a scalable approach for high quality graphene. Recently rapid thermal annealing (RTA) of sputtering deposited amorphous carbon and nickel was also shown to be effective in single-step growth of wafer scale graphene directly on any dielectric substrate.[80]

Graphene nanoribbons (GNRs), thin strips of graphene,[81] have been suggested as a promising material in which there exits a band gap (mobility gap) due to quantum confinement.[82] These GNRs were originally introduced as a model for theoretical studies by Mitsutaka and Fujita to examine the edge and nanoscale size effects in graphene,[83-85] and currently these GNRs are very popular as a superior candidate in graphene-based nanoelectronics.

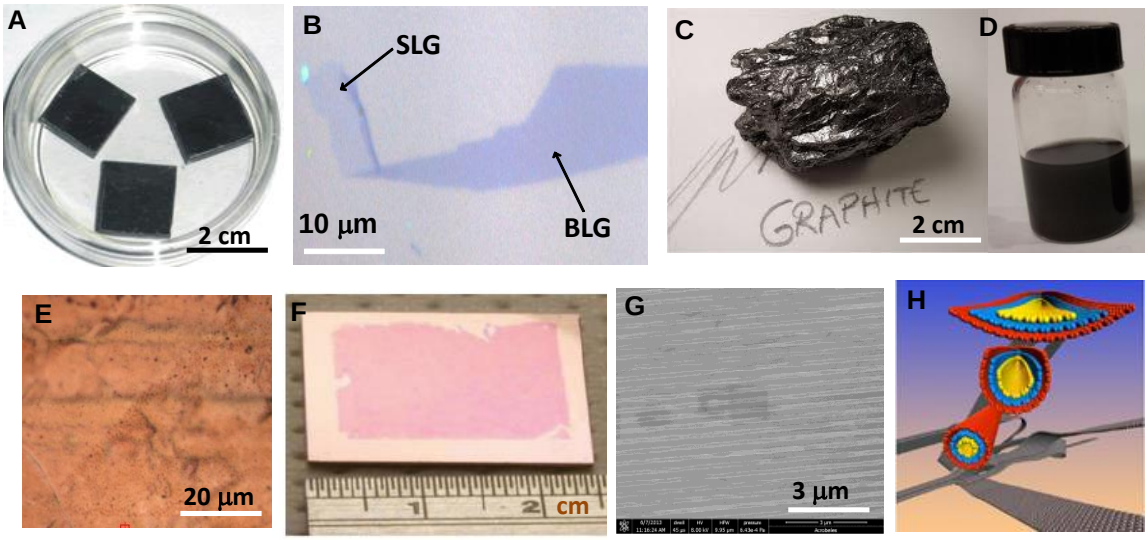

Figure 1.4. Graphene synthesis. (A) Image of highly oriented pyrolytic graphite (HOPG) which is often chosen due to its high atomic purity and smooth surface for the micromechanical (Scotch tape) exfoliation to produce (B) single layer, bi-layer of multilayer graphene flakes. (C) Image of nature graphite, which can be subjected to liquid phase exfoliation (LPE) in aromatic solvent (e.g. ortho-dicholorobenzene) to produce (D) stable dispersions of exfoliated graphene.[14] (E) Optical image of chemical vapor deposition (CVD) grown graphene on copper surface (carbon source: methane, temperature: 1000 ^{o}C), which can be transferred onto (F) oxidized silicon wafer, in which the optical (phase) contrast of graphene makes it visible under white light. (G) Scanning electron microscopy (SEM) of an array of epitaxial graphene nanoribbons (EGNRs) grown on the lithographically patterned step edges of SiC(0001) crystals.[82] (H) Schematic representation of the gradual longitudinal unzipping of multiwall carbon nanotube (MWNTs) to form a graphene nanoribbons (GNRs) by chemical oxidation methods. Reproduced from ref.[81] Copyright 2009 Nature Publishing Group.

1.4. MICROSCOPIC VISUALIZATION OF GRAPHENE LAYERS

Despite the atomic thickness of graphene, optical microscopy can be conveniently employed to identify a monolayer of graphite (single-layer graphene, SLG, with number of layers n = 1), bi-layer graphene (BLG, n =2), tri-layer graphene (TLG, n = 3), few-layer graphene (FLG, $n \geq 4$) along with thicker graphite flakes [$n = \propto$, such as highly oriented pyrolytic graphite (HOPG)] from the color contrast (phase contrast) when the graphene flakes rest on the top of an oxidized Si wafer (**Figure 1.5**).[43] SLG on an SiO_2 substrate, although atomically thin, has the capability to interfere with the optical path of reflected light, and consequently results in a change in the interference color with respect to bare Si/SiO_2 substrate (typically about 300 nm SiO_2, and is purple-to-violet in color).[43]

As can be seen in **Figure 1.5**, SLG is very light violet in color (**Fig. 1.5a**), BLG appears as violet (**Fig. 1.5b**), TLG is dark violet (**Fig. 1.5c**), while FLG flakes are blue in color (**Fig. 1.5b**). Microscopic quality and macroscopic continuity are two essential ingredients in judging the quality of a graphene sample. In contrast to exfoliated graphene, epitaxial graphene (EG) samples grown by vacuum graphitization of SiC(0001) are almost transparent (**Fig. 1.5d**). In the case of supported graphene, the substrate has a strong influence on the subsequent chemistry and device performance. On the other hand, the

chemistry of epitaxial graphene (EG) on SiC substrates shows the effects of the interface layer between the graphene monolayers and the underlying SiC substrate.[26,86,87]

1.5. RAMAN SPECTROSCOPIC CHARACTERIZATION OF GRAPHENE LAYERS

Beyond microscopic visualization, Raman spectroscopy provides the most convenient and powerful tool for characterization of graphene. In the Raman spectra of graphene, the G peak (frequency, ω_G ~ 1580 cm^{-1}), arises from a first order Raman effect where the energy of the scattered incident monochromatic light is proportional to the energy of quantized lattice vibrations (E_{2g} phonon) created by the scattering process.[30,88-91] On the other hand, the 2D band (ω_{2D} ~2670 cm^{-1}, also referred to as the G' peak) results from a second order Raman effect, which arises from lattice vibrations when first order processes activate another phonon. In the case of a single-layer graphene (SLG), the 2D peak appears as a single peak and the intensity of 2D peak is generally higher than the intensity of G-peak [$I_{2D}/I_G \geq 1$, **Fig. 1.5e(i)**].

The covalent chemical modification of graphene, which is usually accompanied by conversion of sp^2 hybridized carbons to sp^3, leads to the activation of the A_{1g} breathing vibration mode and this results in the appearance

of a sharp D-peak (ω_D ~1345 cm^{-1}); broad D-peaks can also be seen in physically defective graphitic materials, such as graphene nanoribbons (GNRs), the edges of graphene, disordered graphene samples, and in graphene oxide.[92]

Raman spectroscopy provides a wealth of information about the number of graphene layers (based on the position and shape of the 2D band, and the ratio of the intensities of the 2D to G band, **Fig. 1.5e**),[88] quality of the samples,[93] types and degree of doping (based on observed shift of G and 2D band),[94] and can even provide insight into the mobility of the graphene devices.[95]

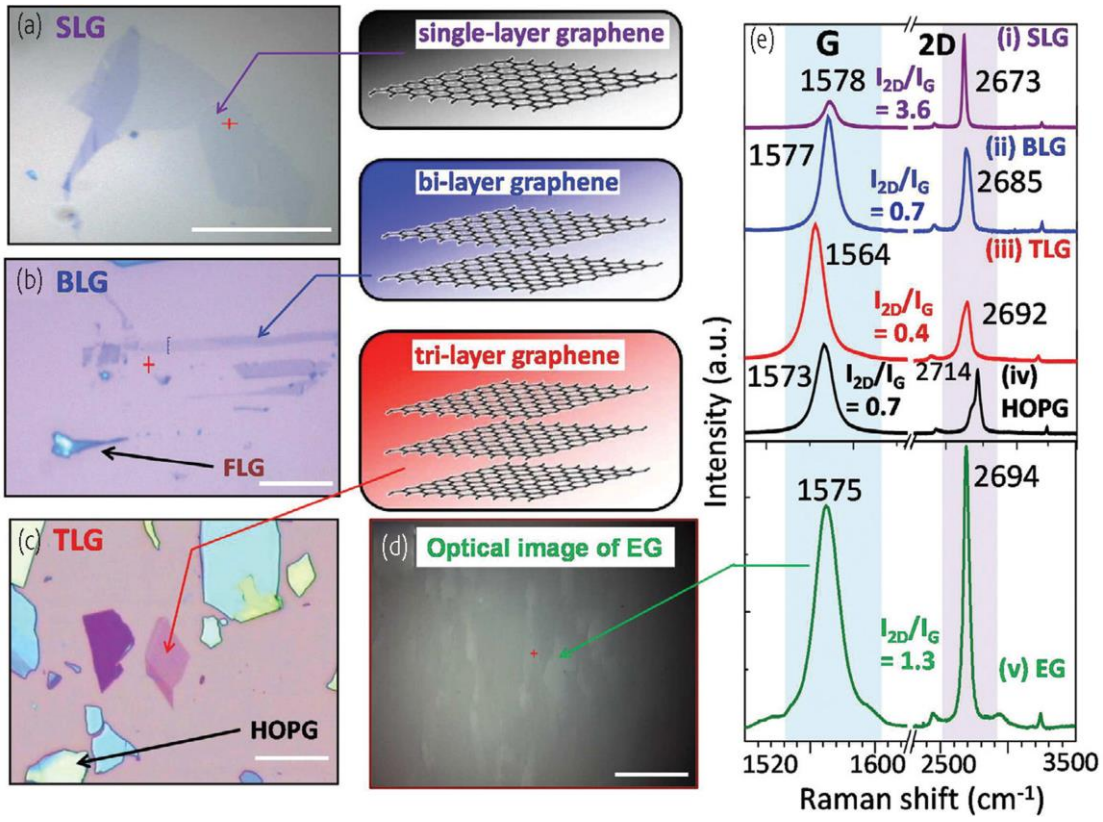

Figure 1.5. Characterization of graphene layers. Optical microscopic image of (a) single-layer graphene (SLG), (b) bilayer grahene (BLG), (c) trilayer graphene (TLG), along with few-layer graphene (FLG in b), and graphite (HOPG in c), obtained by micromechanical cleavage of graphite and imaged on an oxidized Si wafer. The corresponding chemical structures are shown in the right frame. (d) Optical image of epitaxial graphene (EG) grown by vacuum graphitization on SiC(0001). Scale bar is 20 μm. (e) Raman spectral signatures (λ_{ex} = 532 nm) of the corresponding (i) SLG, (ii) BLG, (iii) TLG, (iv) HOPG, and EG (after subtraction of Raman signals due to SiC).[22] Reprinted with permission from ref.[22] (Sarkar, S. et al. *Mater. Today* **2012**, 15, 276-285; Copyright © 2012 Elsevier Inc.).

1.6. ELECTRONIC STRUCTURE OF GRAPHENE

The electronic structure of graphene is very well known in the literature of physics and chemistry. A knowledge of the electronic structure of graphene is helpful to understand its unique physical and chemical properties.[17,21] While all of the carbon atoms in graphene are equivalent in a chemical sense, there are two atoms in the unit cell, and thus in a crystallographic sense the honeycomb structure of graphene is viewed as two interpenetrating triangular Bravais lattices, as depicted in **Figure 1.6** because it is not possible to generate all of the lattice sites by simple translations of a single carbon atom.

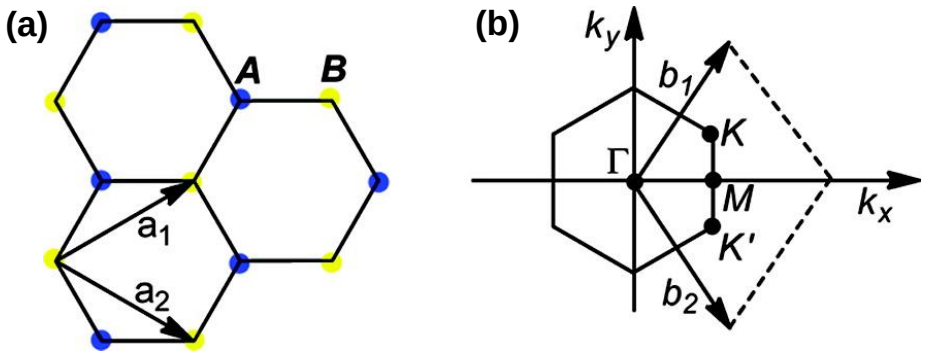

Figure 1.6. (a) Real space graphene lattice, showing the unit cell vectors, (b) Brillouin zone of graphene in momentum space.[17]

The Bravais lattices are traditionally labeled A and B, and the two different sets of carbon atoms are apparent in Figure 1.6; the primitive lattice vectors are given by $\mathbf{a}_1 = (3a/2)\,\mathbf{i} + (\sqrt{3}a/2)\,\mathbf{j}$ and $\mathbf{a}_2 = (3a/2)\,\mathbf{i} - (\sqrt{3}a/2)\,\mathbf{j}$ where a is the carbon–carbon bond length (1.421 Å) and **i** and **j** are the usual unit

vectors along the x, y Cartesian axes; the reciprocal lattice vectors are given by $\mathbf{b}_1 = (2\pi/3a)\,\mathbf{i} + (2\pi/\sqrt{3}a)\,\mathbf{j}$ and $\mathbf{b}_2 = (2\pi/3a)\,\mathbf{i} - (2\pi/\sqrt{3}a)\,\mathbf{j}$. The first Brillouin zone may thus be obtained by taking perpendicular planes, which bisect the vectors to the 6 nearest reciprocal lattice points. Thus the shape of the Brillouin zone is of the same form as the original six-membered rings of the honeycomb lattice in direct space, but rotated by 90^{o}.

The band structure of graphene at the level of tight-binding theory with transfer integral t (resonance integral β, equivalent to the Huckel Molecular Orbital Theory), was solved in 1947 by Wallace[54] (**Figure 1.7**). Two of the points at the corners of the Brillouin zone are distinct and are labeled by K and K', whereas the other points are related to them by symmetry. As may be seen in **Figure 1.7**, the K points are particularly important because this is where the valence and conduction bands meet and cross, but it is important to note that the bands touch at a single point in k space – the Dirac point, as a result of the crossing of the valence and conduction bands. For this reason graphene is referred to as a zero band gap semiconductor, and the density of states (DOS) at the Fermi level is zero (at the absolute zero of temperature).

Nevertheless the conductivity of graphene is always finite even when the chemical potential is at the Dirac point, and there are effectively no free carriers.

The transport properties of graphene are still the subject of intense research, and the high current densities that can be sustained in graphene together with the outstanding mobilities have motivated very strong interest in the use of graphene in the electronics industry. Graphene is now on the International Roadmap for Semiconductors and in this regard the absence of a band gap in graphene is a serious problem as field-effect transistor devices fabricated from pristine graphene cannot be turned off – the main objective of this thesis work is to use chemistry as an enabling tool in the band gap engineering of graphene.

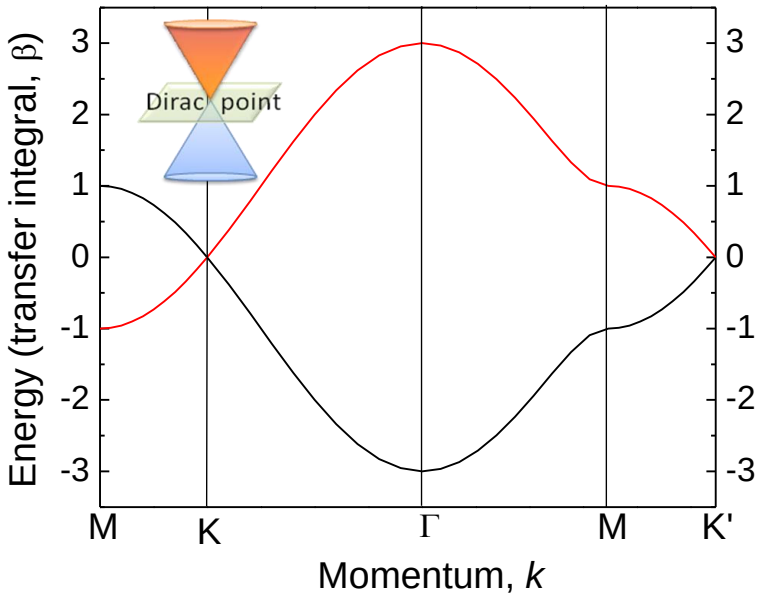

Figure 1.7. Graphene energy band dispersion in momentum space within simple tight-binding (HMO) theory; the resonance or transfer integral (β, t) has a value of about 3 eV.[21]

1.7. CHEMICAL REACTIVITY OF GRAPHENE

Graphene is a unique chemical substrate. As discussed above, the two adjacent carbon atoms in graphene are crystallographically non-equivalent (referred as A and B sub-lattices), but are chemically equivalent.[21] Modification of graphene is not easy because high energy barriers need to be overcome due to intra-layer conjugation and interlayer van der Waals forces between the individual layers in multilayer graphene. Selective functionalization and patterning of graphene with nanometer accuracy is of extreme importance for the electronics industry. The effect of the underlying substrate[96] on the chemical reactivity of graphene must be better understood because graphene is usually used on a substrate, whether it is silica, silicon, SiC, or graphite (multilayer graphene). The understanding of the effects of heterogeneity and defects on chemical interactions and properties of graphene requires further study. Ideal graphene is an infinite two-dimensional sheet of sp^2-carbon atoms without basal plane fluctuations and edge states.[97] In contrast to such ideal graphene, real graphene unavoidably contains edges, suffers from basal plane fluctuations, atom vacancies (defects) and other chemical impurities, which lead to an inevitable alteration of its electronic structure and increased chemical reactivity.[97]

Based on the observed chemical behavior of graphene, a number of structural and electronic features have been found important in understanding the reactivity of graphene as a chemical substrate. (i) **Role of dangling bonds**: Edges containing dangling bonds which are thought to be the most reactive,[98] and within basal plane chemistry, the thermodynamically (energetically) favorable processes involve the pairwise chemisorption of functional groups in different sublattices, rather than on the same sublattice.[13,99] Theoretical calculations suggest that the pairwise chemisorption of a species in different sublattices is favored by 0.5 eV per addition.[99,100] (ii) **Minimization of geometric strain**: In analogy with the fullerenes and carbon nanotubes, which contain curved graphitic surfaces,[35,36] geometrically strained areas and ripples in graphene undergo preferential reactivity in order for these regions to relax by rehybridization.[13,92,101] Strain engineering on the surface lattice of graphene in a periodic manner can control the reactivity and degree of functionalization of graphene.[13] (iii) **Reactivity due to basal plane fluctuations of graphene:** Basal plane fluctuations cause curvature of graphene sheets. This curvature reduces the overlap of the p_z atomic orbital of one carbon with p_z orbitals of surrounding three carbons. Thus, the curvature can lead to localized states with higher energies, which enhances the reactivity of that particular sites.[92,97] (iv) **Role of defects:** Vacancies (defects) present within the basal plane of graphene are as reactive as graphene edges. There are several cases in which such defect sites are believed to be the reaction site in which the first covalent

addition of functional groups occurs, and then propagates around this center leading to a cluster distribution of functional groups.[102,103] Since in general covalent addition leads to the formation of non-planar sp^3 carbon centers in graphene, such addition of functional groups (which is equivalent to addition of defect sites) can lead to increased reactivity of graphene with these reaction centers acting as catalytic centers for the reaction progress (autocatalytic).[104]

(v) **Effect of multiple graphene layers**: Single layer graphene is reported to be 10-14 times more reactive than double layer graphene in radical addition chemistry.[98,104] Brus, Nuckolls, Steigerwald and co-workers has attributed this high reactivity of single layer graphene to the surface induced corrugation (presence of curvature), proximity of the graphene with the substrate, and the lack of interlayer π stacking,[104-106] while Strano has suggested the contribution from the effect of electron and hole puddles (and consequently by deviation of the position of the Dirac point spatially).[98] In the case of multilayer graphene supported on a substrate, covalent functionalization typically changes the surface layer only. The non-stoichiometric nature of the graphene functionalization makes it difficult to control its end-composition and the resulting properties. (vi) **Role of aromatic sextets in graphene rings at basal plane and edges**: The Clar sextet is the most stable resonance structure and those graphene structures that maximize the number of Clar sextets will be preferred. At the graphene edges, which can be either zig-zag or arm-chair structures, the attainment of aromatic sextets is frustrated in most of the rings

where zig-zag edges are concerned, and are therefore thermodynamically unstable and more reactive than arm-chair edges.[13,107,108] (vii) **Chemical Reactivity Influenced by Graphene Electronic Structure (Chemistry at the Dirac Point – frontier molecular orbitals and conservation of orbital symmetry)**: The graphene valence band (HOMO) and conduction band (LUMO) cross at the Dirac point, which defines the work function (W = 4.6 eV). Consequently, the HOMO and LUMO of graphene form a degenerate pair of orbitals at this point in momentum space with the same ionization potential (IP) and electron affinity (EA), and these states determine the reactivity. Pericyclic reactions are subject to the Woodward-Hoffmann rules, and inspection of the orbital symmetries of the degenerate pair of half-occupied HOMO and LUMO band orbitals at the Dirac point confirms that with the appropriate orbital occupancies, both diene and dienophile reaction partners should undergo Woodward-Hoffmann allowed, concerted Diels-Alder reactions with graphene.[18,21] Because of the orbital crossing at the Dirac point, the π-bonds in graphene can access diene or olefinic (quinonoid) resonance structures.[18,21] This behavior is manifested by the reactivity of graphene with electron-rich dienes in Diels-Alder chemistry (as diene and dienophile),[18,21] in nitrene addition chemistry,[109] in Bingel [2+1] cyclopropanation reaction,[110] and 1,3-dipolar cycloaddition reactions.[111] (viii) **Substrate effect**: Substrate-supported graphene (unlike a suspended/ free-standing graphene membrane) usually rests on a substrate, such as silicon dioxide (SiO_2), organic monolayer [e.g.

OTS (oxytriethoxy silane)]-terminated silicon oxide wafer, silicon (Si), SiC, boron nitride (BN), metal substrates (in case of CVD graphene, including Cu, Ni, Pt, Ir) or graphite (multilayer graphene).[96] The effect of the underlying substrate on chemical interaction of graphene must be further studied to understand the substrate dependent reactivity of graphene.[96]

1.8. COVALENT BOND FORMING REACTIONS OF GRAPHENE

Graphene chemistry is a rapidly emerging field and a number of useful functionalization reactions have been reported. We note the following graphene functionalization reactions:[13] radical addition,[12,15,104,112], nitrene addition,[109,113], 1,3-dipolar cycloaddition,[111] Diels-Alder chemistry[18,21,114-116] and benzyne cycloaddition,[117] graphene oxide transformations,[72,118] hydrogenation[106,119] and fluorination.[120-124] The application of organic reactions to graphene will substantially influence the development of graphene-based devices.[47]

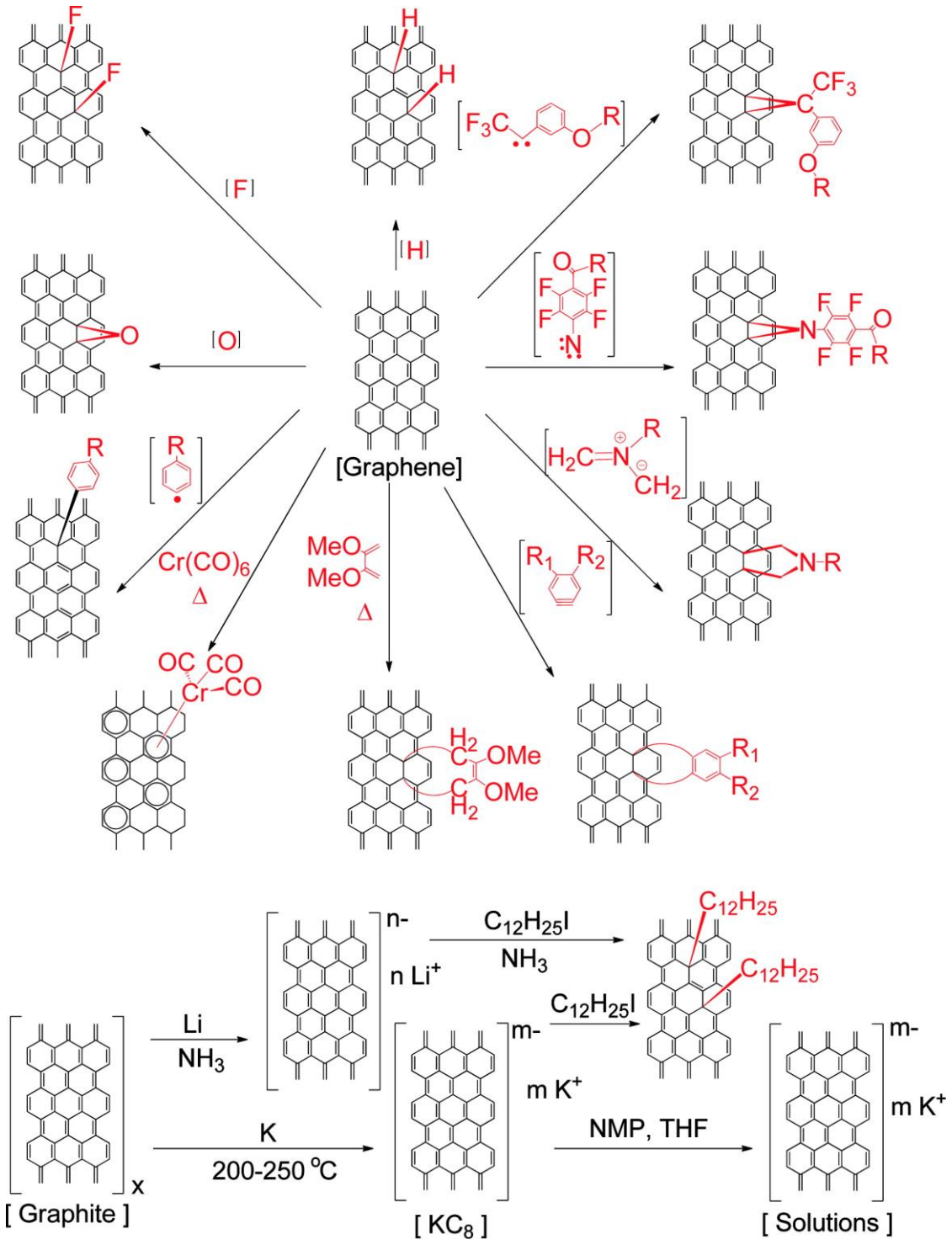

Figure 1.8. Reactions of graphene. Adapted with permission from ref.[125] (Copyright © 2013 American Chemical Society).

1.9. APPLICATIONS OF THE CHEMICALLY MODIFIED GRAPHENE (CMG)

Covalent chemistry of graphene has been employed in engineering the electronic, magnetic and solubility (surface and bulk) properties of graphene.[26,27] For example, addition of nitrophenyl (NP) radicals to epitaxial graphene (EG) has produced chemically modified graphene materials with room-temperature ferromagnetism[29,31] and a band-gap of 0.36 eV (measured by ARPES).[91] The same NP radical addition to suspended single layer graphene (SG) films, which offers double-sided covalent functionalization, has rendered graphene to be a granular metal at low NP coverage, and a gapped semiconductor at high NP coverage;[20] thus allowing band gap engineering in graphene field effect transistor (FET) devices.

Surface and bulk functionalization of graphene with appropriate functional groups has provides opportunities for high throughput bulk synthesis of solution-processable graphene needed for a wide variety of energy conversion and storage applications.[126-128] Chemically modified graphene has been employed as ultrasensitive single molecule sensing devices.[129] Reduced graphene oxide (rGO)-derived graphene[118] (a widely used route to graphene by thermal, laser or chemical reduction of graphene oxide)[52,53] has been employed as transparent conductive electrodes[130] (due to extraordinary high transparency yet superior conductivity of graphene),[131] as composite filler[132] (in thermal

interface materials)[133-135] and as supercapacitors (alone or in conjugation with carbon nanotubes).[128,136] Research in the magnetism of chemically modified graphene and its applications in spintronics is being actively pursued.[32]

1.10. CONCLUSION

Several important challenges emerge regarding the design and implementation of the CMGs into functional/ working devices.

(1) **Growing high quality wafer scale graphene single crystals**: The key to most applications of graphene lies in controlling the quality of the produced graphene (preferably the scalable growth of single crystal materials) by optimizing the growth techniques to ensure that its unusual superlative properties are retained.[53,79]

(2) **Towards nanoscale electronics manufacturing technology**: The post-CMOS manufacturing technology requires the development of selective high precision chemical functionalization strategies for device fabrication, in conjunction with associated techniques for patterning graphene wafers with atomic accuracy.[22] The need is the identification of the chemistry to be applied, its precise control, and implementation of the device chemistry of graphene by a thorough understanding of the principles governing the reactivity and patterning

of graphene at the sub-nanometer length scale.[22] The question of regiochemistry (regioselectivity), whether the chemistry occurs preferentially at edges or basal plane or at specific sites on the basal plane (not everywhere) should be firmly addressed and experimentally established with the aim of regiospecificity.[97,126]

(3) **Knowledge and engineering the graphene edges and defects**: Understanding the electronic and chemical structure of graphene edges and the nature of the defects (structural imperfections) needs specific attention.[137-139]

(4) **Developing high aspect ratio solution processable materials**: The availability of solution processable graphene can make an important contribution to emerging fields such as printable electronics, and is expected to enable chemical modification, purification, and transfer of graphene from solution phase to substrates by means of spin-, spray-, drop-, or dip- casting methods.[22,140]

(5) **Graphene nanoribbon (GNR) electronics via quantum confinement of dimensionality**: The 2D structure, high electrical and thermal conductivity, and low noise of GNRs make this material a possible alternative to copper for integrated circuit interconnects.[82,141] Research is also being done to create quantum dots by changing the width of GNRs at select points along the

ribbon, creating quantum confinement. [83-85]

(6) **Creating architectures of extended dimensionality**: The integration of 2D graphene into 3D architectures will extend its properties from the low-dimensional to the 3D world for applications yet to be conceived.

(7) **High quality electrical contacts to graphene**: Future applications of graphene in nanoscale electronics require defining high quality metal contacts to graphene, which in turn call for an in-depth understanding of the conditions necessary for the growth of uniform metal films (by e-beam evaporation or sputtering deposition) and the nature of metal-graphene interfaces at a fundamental level.[28,142] Additionally, the fundamental understanding of the interaction between mobile metal atoms or metal nano-clusters and graphitic surfaces is crucial from the standpoint of CVD growth of graphitic materials on metal surfaces (surface catalysis),[79] spintronics (spin filters),[143] electronic devices (ultrafast graphene transistors, memory devices),[143] atomic interconnects,[144-147] and superconducting phenomena.[28]

Experiments on the basal plane chemical functionalization of graphene have produced graphene-based materials with semiconducting and magnetic properties, thereby demonstrated the basic thesis behind our work: the possibility of using chemistry to modify the electronic and magnetic structure of

graphene so as to produce a wafer patterned with dielectric, semiconducting metallic, and magnetic regions that would function as a very large scale integration (VLSI) electronic device.[21,26,27] In the pursuit of this chemistry we have also learned that the singular electronic structure of graphene at the Dirac point can profoundly affect the course of classical pericyclic chemical processes such as the Diels-Alder reaction.[21] There is every reason to believe that the chemistry beyond the Dirac point will prove equally fascinating and that chemistry will play a vital role in propelling graphene to assume its role as the next generation electronic material beyond silicon.

CHAPTER 2. Radical Addition Chemistry of Graphene

2.1. INTRODUCTION

Graphene is a particularly intriguing material from the chemical standpoint.[148-151] Although graphene is the thermodynamic ground state of carbon and is solely comprised of sp^2 hybridized carbon atoms, the unique electronic structure of graphene allows it to participate in surprisingly mild reaction processes.[14,15,18]

The nitrophenyl radical addition to various forms of graphene (such as epitaxial graphene, exfoliated graphene, and CVD graphene) has received immense attention from researchers worldwide[12,112 152 150 98,153] and this covalent chemistry of graphene has found application in engineering an electronic band gap into graphene[20,91,154] and modifying the magnetic properties.[29-32]

However, nitrophenyl (NP) radicals are highly reactive in nature and generally lead to kinetically controlled products, which makes the control of functionalization difficult.[155] In contrast to NP radicals,[30] the α-naphthylmethyl (α-NM) radicals are resonance stabilized and can lead to thermodynamically controlled products.[15] Moreover, previous research reports have indicated that

α-NM groups are capable of forming well-ordered structures on graphitic (HOPG) surfaces.[156]

It is known that graphene readily undergoes the Kolbe reaction (eq. 2.1),[157-159] which involves the electrochemical oxidation of carboxylates with subsequent grafting of the derived carbon radicals to graphitic surfaces (**Scheme 2.1**).[15]

$$RCOO^- \xrightarrow{\text{electro-oxidation}} R\bullet + CO_2 + e^- \quad \ldots\ldots\ldots\ldots\ldots\ldots\ldots\ldots\ldots\ldots\ldots \text{(2.1)}$$

We demonstrated that the reversible grafting of α-naphthylmethyl groups to epitaxial graphene (EG) constitutes a versatile approach for engineering the electronic band structure of graphene.[15] The advantages of the Kolbe electro-oxidation in the chemical modification of graphene are: (i) reversibility of the reaction - the grafted functionality can be electrochemically erased, (ii) α-naphthylmethyl (α-NM) groups are found to offer well-ordered structural patterning on graphite surfaces,[156] and thus the resulting graphene derivative is anticipated to exhibit interesting magnetic and electronic behavior, and (iii) the simplicity, versatility and efficiency of the reaction that makes possible the covalent binding of a wide variety of arylmethyl groups with appropriate substituents on the phenyl rings.[15,156]

2.2. RADICAL ADDITION TO GRAPHENE

As discussed in **Chapter 1**, consideration of the band structure allows the development of a unified treatment of the chemical reactivity of graphene.[27] In **Figure 2.1** we show the simple tight binding band structure of graphene at the level of HMO theory, which gives the dispersions of the π-bands along the high symmetry directions in *k*-space,[17,21,160] together with the HMO energy levels for benzene, the allyl radical, and trimethylenemethane diradical (**Figure 2.1**).[27]

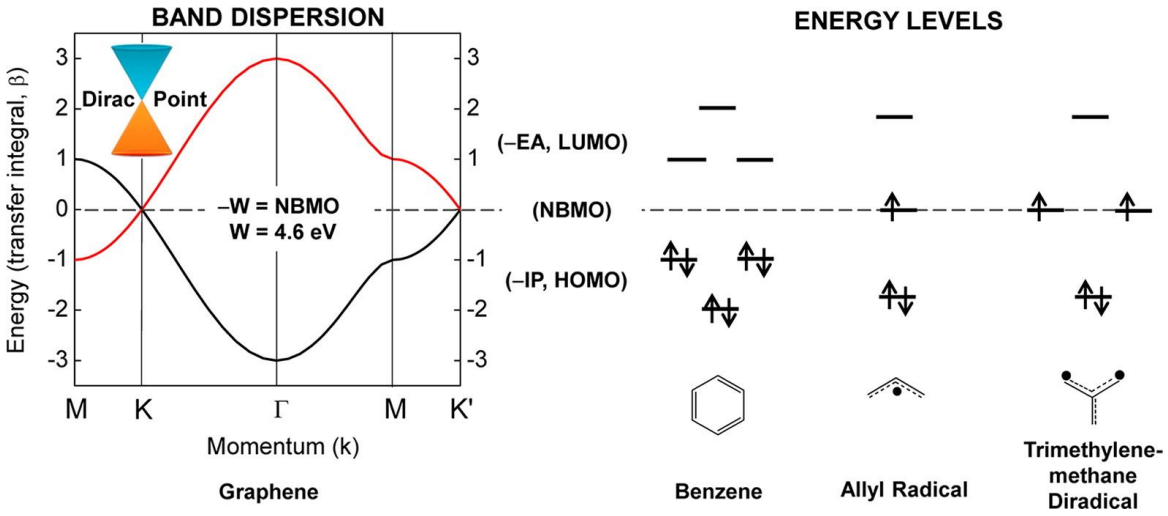

Figure 2.1. Electronic band structure of graphene, at the level of simple tight-binding (HMO) theory,[21] together with HMO energy levels for benzene, allyl radical, and trimethylenemethane diradical.[27] Reprinted with permission from ref. [27] (Copyright © 2013 Amercan Chemical Society).

2.2.1. ROOM TEMPERATURE FERROMAGNETISM IN NP-EG: QUASI-LOCALIZED π-RADICALS

The addition of a single hydrogen (or fluorine) atom to graphene leads to the formation of a delocalized spin in the graphene π-system, in which the spin is delocalized over more than 10,000 carbon atoms.[30] This situation is analogous to the addition of a nitrophenyl radical to graphene (**structure 2** in **Figure 2.2**, where addition has occurred in the A sublattice).[30 26]

Such an intermediate π-radical (**2**) is an odd-alternant hydrocarbon (OAH) and paramagnetic with a highly delocalized electronic structure. The spin resides in a nonbonding molecular orbital (NBMO) similar to that of the allyl radical in **Figure 2.1;**[30] thus the relationship to the electronic structure of graphene is clear. This state lies at the Fermi level in graphitic samples containing the hydrogen chemisorption defect and is observable in STM images as a threefold symmetric superlattice in the local density of states (LDOS) in both tunneling directions.[30,161]

Assuming that the first radical addition occurs in the A-sublattice as in **2**, two distinct electronic structures may result from the second radical addition process. In the presence of small substituents, thermodynamic considerations favor addition in the B-sublattice to give a diamagnetic product with an energy

gap,[162] as exemplified by **structure 3**; however, the steric bulk of the nitrophenyl group militates against the preferred 1,2- or 1,4-addition product and thus there is the possibility of structures such as **4,** which involves addition in the same sublattice. The spin count in the product increases with each radical functionalization process, which occurs in a given sublattice (without compensation by an accompanying radical addition in the other sublattice), and each spin resides in an NBMO; for biradical structures such as **4**, the simplest molecular analogue is trimethylenemethane (**Figure 2.1**).[163] Thus, at the very simplest level of tight binding HMO theory, the electronic structure of the various graphene open shell products is one in which the spins reside in NBMOs, which in the solid state lie at the Fermi level. More rigorous treatments modify this picture, but many of the qualitative conclusions remain valid; one of the more important theoretical results is the finding that the spins in these NBMOs couple ferromagnetically, because the unpaired electrons all lie in the same sublattice and this mode of coupling minimizes electron repulsion effects according to Hund's rule.[164,165]

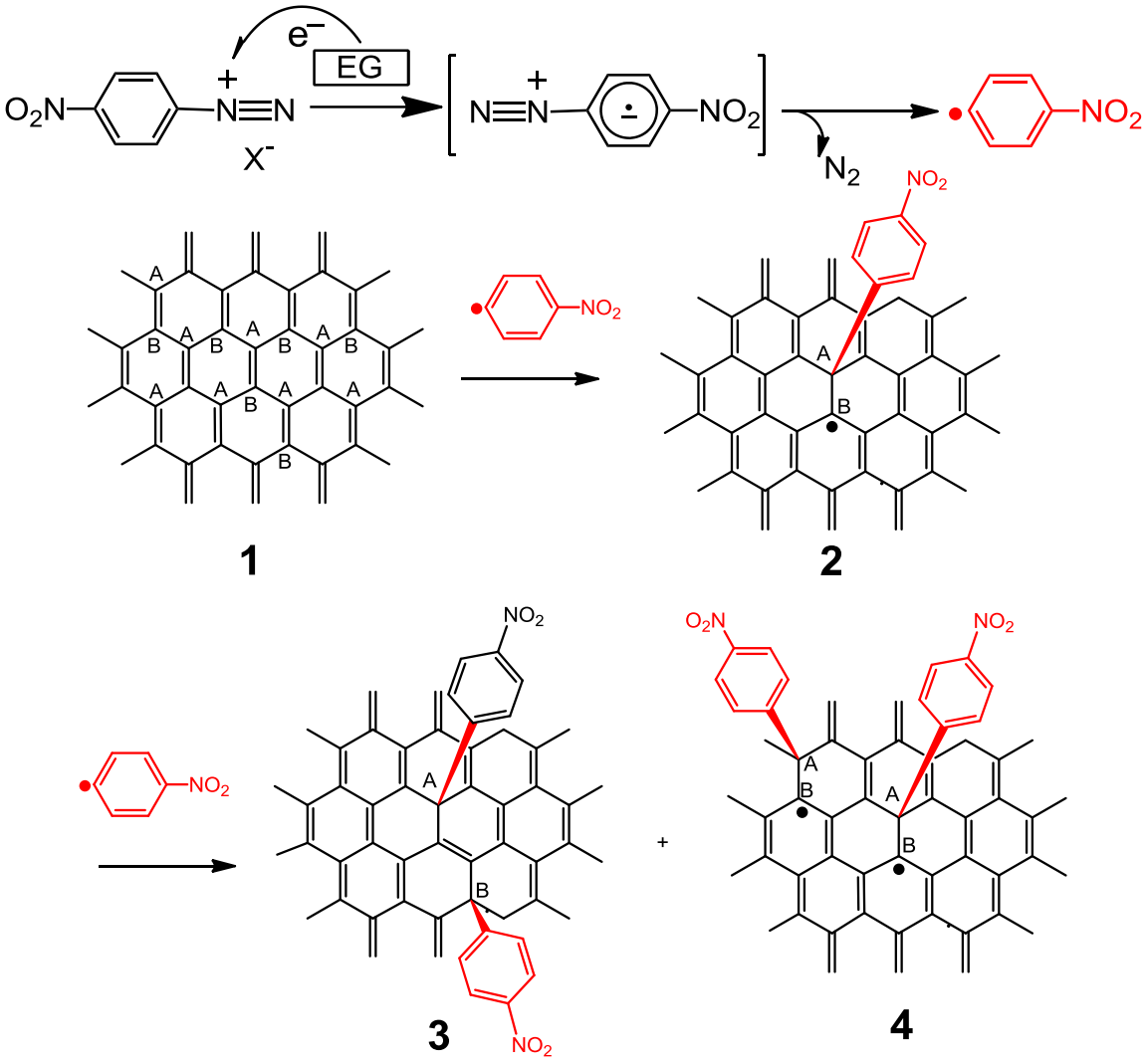

Figure 2.2. Schematics of spontaneous reduction of p-nitrophenyl (NP) diazonium salts on epitaxial graphene (EG) surfaces (**structure 1**) leading to covalent attachment of NP groups to graphene. The addition of the first radical leads to the **product 2**, which is expected to be paramagnetic, while the addition of a second NP radical may lead to either **product 3** (diamagnetic), and (or) **product 4** (biradical).[22,30]

Magnetic measurements showed a small magnetization in some of the pristine epitaxial graphene (EG) samples at all temperatures, which is attributed to either defects or impurities in the epitaxial graphene on SiC crystals.[29] Interestingly, the NP-EG samples show room-temperature ferromagnetism (ferrimagnetism) and superparamagnetism.[26,29-32]

2.2.2. BAND GAP ENGINEERING BY RADICAL ADDITION TO GRAPHENE

Covalent nitrophenyl radical addition chemistry carried out on epitaxial graphene[12,26,30,91,112] and exfoliated SLG (suspended film)[20] by use of simple solution chemistry suggests the applicability of this technique to the band-gap engineering of graphene devices. Theoretical calculations on fully hydrogenated graphene [graphane, $(CH)_n$], which requires the conversion of all sp^2 carbons of graphene to $C(sp^3)$–H bonds, indicate a band gap of 3 eV,[100,166] and 5.4 eV.[167] Similarly, the widely-studied stoichiometric fluorinated derivative of graphene (fluorographene), which is a thermally stable alternative to graphane, is an insulator with an optical gap close to 3 eV.[168,169] Steric considerations and the single-sided functionalization process of non-suspended SLG preclude high coverage with NP groups, and even the 25% coverage model shown in **Figure 2.3(a)**, is not attainable; and electrochemistry experiments indicate a coverage of 10-20%.[26,170]

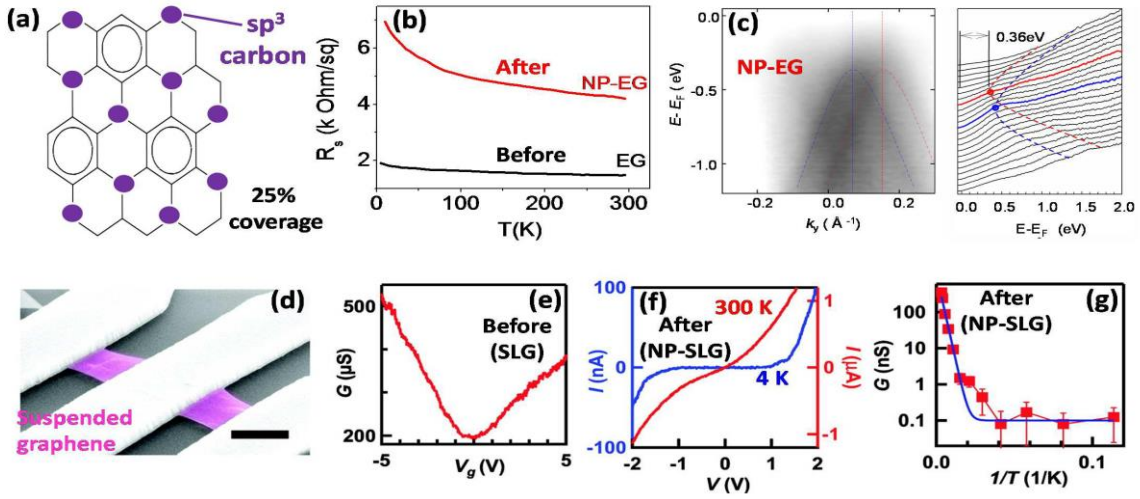

Figure 2.3. Effect of covalent chemistry on transport properties of graphene. (a) Schematics of a model radical addition process on the graphene lattice, which gives 25% coverage.[26] (b) Change in resistance and its temperature dependence after NP functionalization of EG.[12,112] Reprinted with permission from ref[112](Copyright © 2009 American Chemical Society). (c) Angle-resolved photoelectron emission spectroscopy (ARPES) of NP functionalized EG (NP-EG) showing two diffuse bands highlighted by the dashed lines, corresponding to Dirac cones with a band edge 0.36 eV below the Fermi level.[30,91] Adapted with permission from ref[91] (Copyright © 2010 American Chemical Society). (d) False-color SEM image of a suspended graphene device. (e) $G(V_g)$ of a typical suspended device before functionalization (pristine EG). Scale bar: 1 μm. (f) I–V curves of a suspended functionalized device (NP-EG) at $V_g = 0$ and T = 300 K (red curve, right axis) and 4 K (blue curve, left axis), respectively. (g) Linear response G vs $1/T$. The solid line is the best-fit to $G(T) = G_0 + A \exp(-E_A/k_BT)$, where $E_A \sim 40$ meV. Reprinted with permission from ref[20] (Copyright © 2011 American Chemical Society).

The NP radical addition chemistry has a pronounced effect on the transport properties of graphene and the resistance of pristine EG and NP-EG as a function of temperature is shown in **Figure 2.3(b)**.[112] The pristine EG (5-7 graphene layers) shows ideal semimetallic behavior with zero or small energy gap; the increase in resistance with decreasing temperature is attributed to the decreasing carrier density as has been previously reported for sub-10 nm thick graphite samples.[171-173] The NP functionalization of EG results in an increase in the room-temperature resistance from 1.5 to 4.2 kΩ/square, and a more pronounced temperature dependence; the semiconducting nature of the NP-EG is supported by the observation of a band gap of 0.36 eV in angle-resolved photoelectron emission spectroscopy (ARPES) measurements.[91] This study suggests that surface covalent functionalization of the top layer of epitaxial graphene is capable of influencing the bulk properties of the EG sample.

The ARPES measurements in **Figure 2.3(c)** show the modified band structure of graphene at the K point;[91] in NP- EG the linear bands of EG are transformed into massive bands shifted ~0.36 eV below the Fermi level and constant energy cuts (**Figure 2.3(c)**, right-hand figure) show that an energy-gap has opened in NP-EG.[26]

In contrast to the EG substrates (EG/SiC), which allow only one-sided functionalization of the topmost graphene layer, the suspended graphene (SG)

films (**Figure 2.3(d)**) provide the opportunity for double-sided covalent functionalization which is shown to produce a granular metal at low NP coverage, and a gapped semiconductor at high NP coverage.[20] The pristine free-standing graphene (SG) membranes typically show a mobility of 5,000-15,000 $cm^2 V^{-1}s^{-1}$ (**Figure 2.3(e)**).[20] After NP functionalization of suspended graphene (SG), the mobility decreased to 50–200 $cm^2V^{-1}s^{-1}$, the I–V curves are seen to be non-linear even at 300 K, and at 4 K the conductance is effectively zero (**Figure 2.3(f)**). In **Figure 2.3(g)** it can be seen that the zero-bias conductance [$G(V_g = 0\ V)$] decreases exponentially with 1/T at high temperature and crosses over to a constant value for T < 30 K. The data in **Fig. 2.3(g)** can be fit to the equation: $G(T) = G_0 + A\ \exp(-E_A/k_BT)$, where the activation energy, $E_A \sim 39 \pm 10$ meV, and G_0 is the background conductance; thus for double-sided NP addition to SG the energy gap is estimated as $2E_A \sim 80$ meV at room temperature.[20] Thus the surface density of the covalently linked functional groups is able to change graphene from a gapless semimetal, to a granular metal, which displays variable range hopping with a low temperature localization-induced gap, to a semiconductor with a transport gap.[20]

Despite the opportunities afforded by nitrophenyl radical addition to graphene, the highly reactive nature of the nitrophenyl (NP) radicals makes the reaction difficult to control and can sometimes lead to the formation of oligomers on the graphene surface (via radical coupling reactions).[30] In

contrast, the α-naphthylmethyl (α-NM) radicals are resonance stabilized and can lead to thermodynamically controlled products,[15] with the possibility to form well-ordered structural packing on graphene surfaces and the chemistry can be reversed under oxidative electrochemical conditions.[156] We, therefore, focus our attention on the α-naphthylmethyl (α-NM) radicals addition to graphene. We choose α-naphthylacetate as a precursor to α-NM radicals, which can be conveniently generated by Kolbe electro-oxidation, as shown below in **Scheme 2.1**.

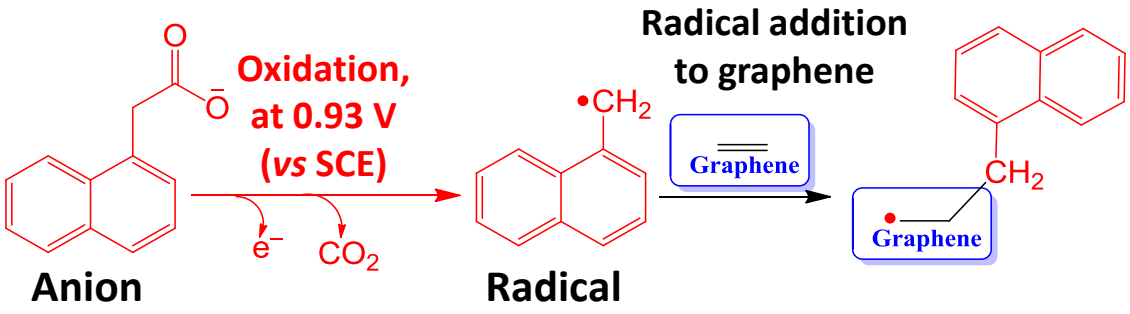

Scheme 2.1. Kolbe electrochemical oxidation of α-naphthylacetates to α-naphthylmethyl radicals and subsequent grafting of radicals to graphene.

2.3. EXPERIMENTS

Epitaxial graphene (EG) samples, grown on single crystal SiC (0001) by vacuum graphitization, were provided by Professor Walt de Heer (Georgia

Institute of Technology). All experiments were performed on the C-face of the EG. HOPG samples were obtained from Union Carbide Corporation. α-Naphthylacetic acid (FW = 186.21), tetrabutylammonium hexafluorophosphate (*n*-Bu_4NPF_6, FW = 387.43), tetrabutyl-ammonium hydroxide 30-hydrate (*n*-$Bu_4N^+OH^-.30H_2O$, FW = 259.47) and acetonitrile (anhydrous, 99.9 %) were obtained from Sigma-Aldrich. Electrochemical experiments were carried out with a computer-controlled CH Instruments Electrochemical Analyzer. Raman spectra were collected with a Nicolet Almega XR Dispersive Raman microscope with a 0.7 μm spot size and 532 nm laser excitation. The ATR-IR spectra were taken using a Thermo Nicolet Nexus 670 FTIR instrument, equipped with an ATR sampling accessory.

The EG and HOPG samples for electrochemical reactions were fixed on a glass substrate with pre-patterned gold contacts. The graphene samples were electrically contacted with silver paint and the contacts were isolated with epoxy resin (**Figure 2.4-a,b**). The EG (or HOPG) substrate served as the working electrode, while the platinum (Pt) wire and saturated calomel electrode (SCE) were used as counter and reference electrodes, respectively (**Figure 2.4-c**). The solutions of α-naphthylacetate were prepared in a glove box. The electrochemical cell with the substrate and solution was purged with argon prior to use.

The grafting of α-NM groups to the EG surface was performed by anodic oxidation of α-naphthylacetate (**Figure 2.5-a**, process **1** in **Scheme 2.2**); this process produces α-naphthylmethyl (α-NM) radicals in the vicinity of the graphene surface, which rapidly leads to the covalent attachment of the α-NM functionality to the graphene lattice via the formation of C–C bond and subsequent creation of an sp^3 carbon centre in the graphene lattice (processes **2** and **3** in **Scheme 2.2**).[15]

The experiments were performed using a 4.5 × 3.5 mm^2 EG wafer as the working electrode immersed in a solution of α-naphthylacetic acid and *n*-Bu_4NOH in acetonitrile, to which ~0.1 M *n*-Bu_4NPF_6 was added as an electrolyte.

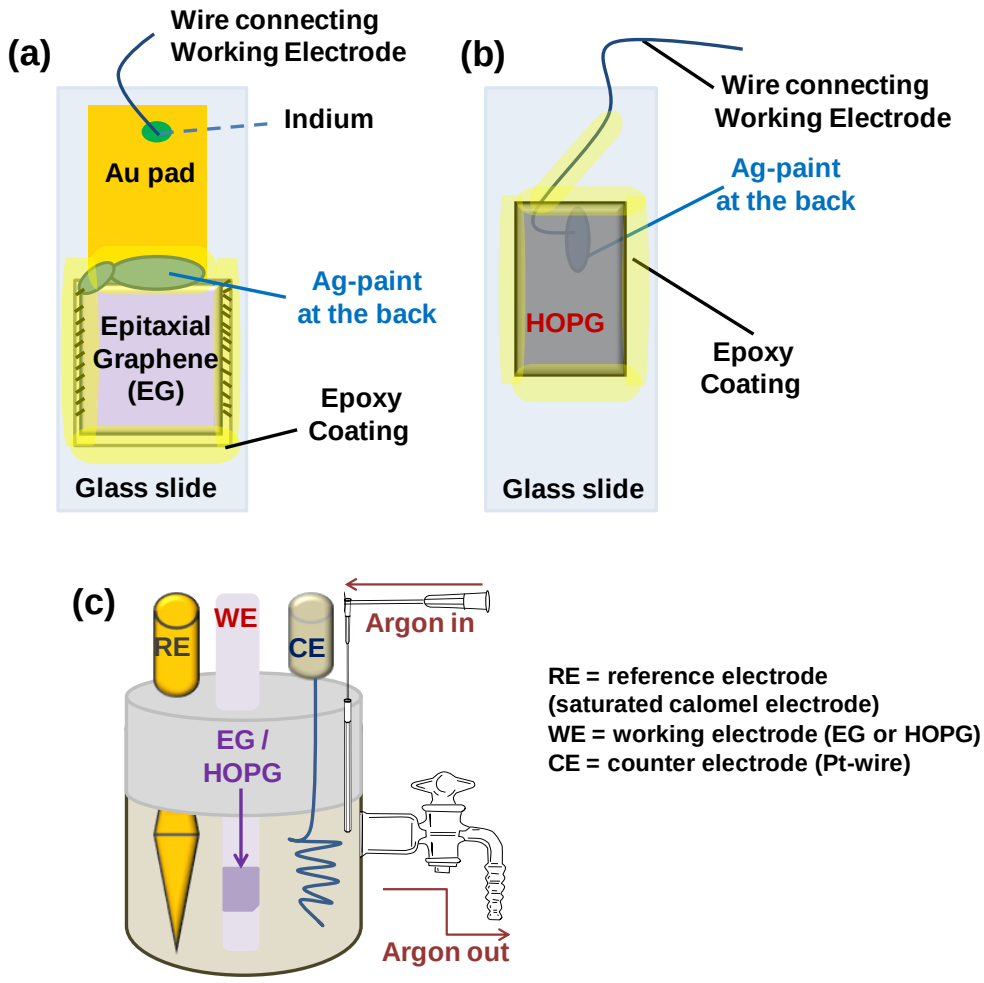

Figure 2.4. Sample preparation for electrochemical functionalization of (a) epitaxial graphene and (b) HOPG mounted on a glass substrate using Ag-paint. (c) Typical configuration of the electrochemical cell used for the generation and electro-grafting of α-naphthylmethyl radicals to epitaxial graphene and HOPG. Reprinted with permission from ref.[15] (Sarkar, S. et al. *Angew. Chem. Int. Ed.* **2012**, *51*, 4901-4904; Copyright © 2012 WILEY-VCH Verlag GmbH & Co. KGaA, Weinheim).

2.4. RESULTS AND DISCUSSIONS

2.4.1. FUNCTIONALIZATION by KOLBE ELECTROCHEMISTRY

Kolbe reaction involves electrochemical oxidation of carboxylates (anions) to generate the corresponding carbon radicals. We have observed that during the derivatization of epitaxial graphene (EG) with α-NM groups the anodic current (oxidation peak) in the cyclic voltammetry curve vanishes almost completely after the first scan (**Figure 2.5-b**, scan rate = 0.2 $V.s^{-1}$), irrespective of the concentration of the α-naphthylacetate solution, indicating complete passivation of the EG surface due to the attached α-NM functionality.[15]

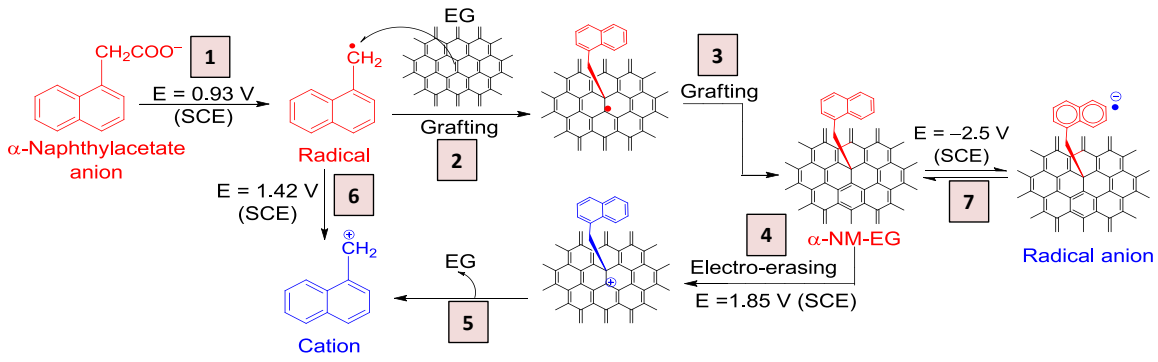

Scheme 2.2. Mechanistic pathways associated with the grafting of α-naphthylmethyl (α-NM) groups to epitaxial graphene (EG).[15]

The efficient passivation of EG is in contrast to the passivation of HOPG, which occurs progressively and depends on the concentration of the arylacetate as illustrated in **Figures 2.5-c** and **2.5-d**. Thus, in case of a 2 mM α-

naphthylacetate solution the number of cycles required for the passivation of the HOPG electrode at a scan rate of 0.2 $V.s^{-1}$ was 11 (**Figure 2.5-c**), whereas 4 cycles were necessary when a 4 mM solution was used (**Figure 2.5-d**).[15] This phenomenon is attributed to the competing dimerization of the α-NM radicals, which is operative only in the presence of the less reactive graphite (HOPG) surface, and not on the graphene (EG) surface.[98,104,150]

2.4.2. RAMAN SPECTROSCOPY OF FUNCTIONALIZED GRAPHENE

The covalent attachment of the α-NM radical to the epitaxial graphene (processes **2** and **3** in **Scheme 2.2**) creates a new sp^3 carbon center in place of an sp^2 carbon atom in the graphene lattice and this is readily detected by Raman spectroscopy with the development of a D-band at ~1345 cm^{-1} as shown in **Figure 2.6-a**.[15] The Raman spectrum of the pristine EG sample shows the characteristic G, G', 2D and 2D' bands (**Figure 2.6-a**), whereas the D, D* and D+D' bands appear in the spectra of the α-NM-EG product; the intensity of the 2D band is reduced by functionalization as observed in the addition of nitrophenyl groups to graphene.[30,91] The Raman intensity map of the D-band in the graphene samples is shown in **Figure 2.6**; the map of pristine EG (**Figure 2.6-b**) shows that the selected area of the wafer is defect-free, whereas covalent functionalization of the same EG surface leads to the appearance of a prominent D-peak (**Figure 2.6-c**).[15]

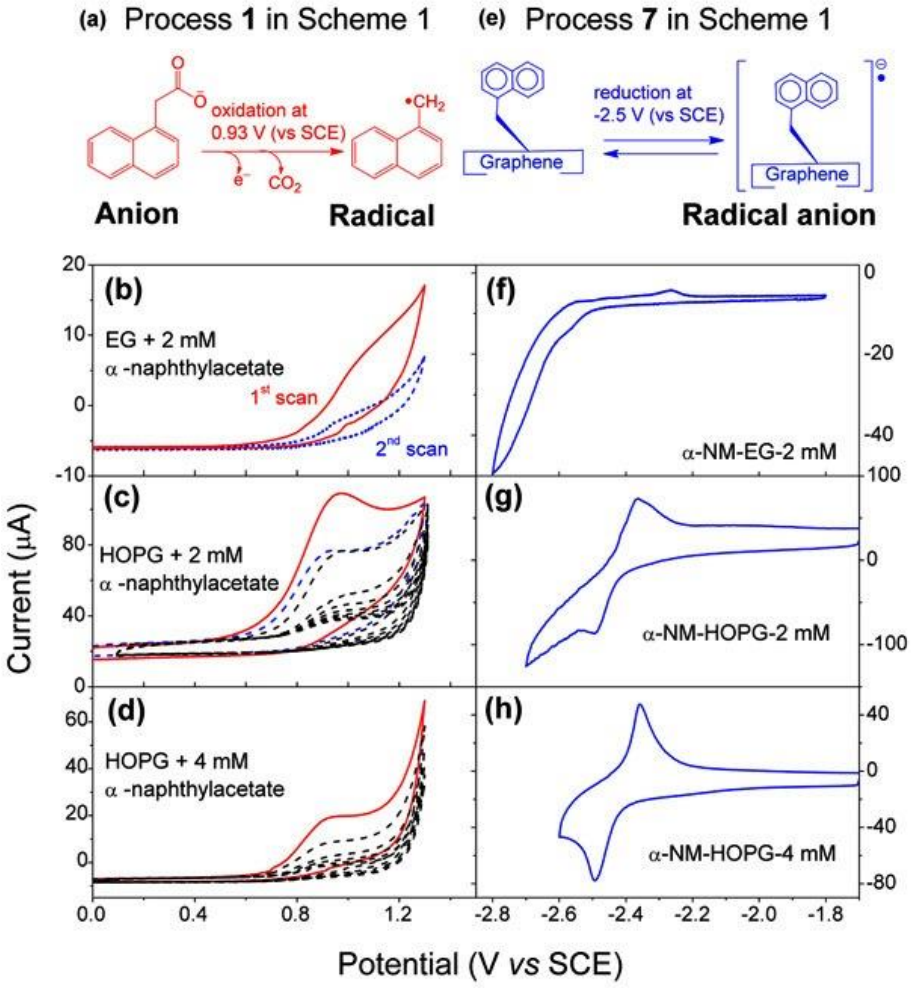

Figure 2.5. (a) Generation of an α-naphthylmethyl radical by oxidation of α-naphthylacetate. Oxidative cyclic voltammetry of (b) EG-electrode in 2 mM α-naphthylacetic acid (α-NAA), (c) HOPG in ~2 mM α-NAA, and (d) HOPG in ~4 mM α-NAA; the solutions were prepared with CH_3CN and contained *n*-Bu_4NOH and ~0.1 M *n*-Bu_4NPF_6. Solid line: first scan, dotted line: sucessive scans; scan rate = 0.2 Vs^{-1}. (e) Reduction of the α-naphthylmethyl group attached to graphene. Reductive cyclic voltammetry of (f) α-NM-EG and (g, h) α-NM-HOPG electrodes (derivatized using the electrochemical processes in the left frames) with ~0.1 M n-Bu_4NPF_6 in CH_3CN. Reprinted with permission from ref.[15] (Sarkar, S. et al. *Angew. Chem. Int. Ed.* **2012**, *51*, 4901-4904; Copyright © 2012 WILEY-VCH Verlag GmbH & Co. KGaA, Weinheim).

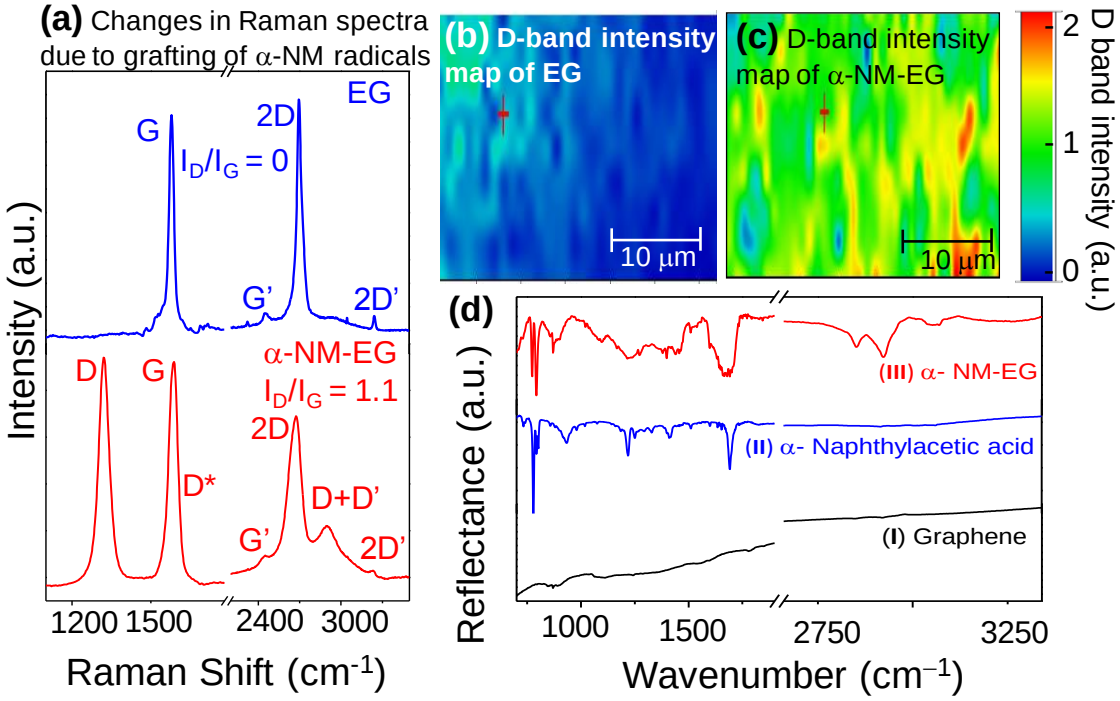

Figure 2.6. (a) Raman spectra (excitation wavelength, λ_{ex} = 532 nm) before (EG) and after electrochemical grafting of α-naphthylmethyl group to EG (α–NM-EG). α–NM-EG was prepared by complete passivation as shown in Figure 1b. Raman intensity map of the D-band in (b) pristine EG and (c) α–NM-EG for a selected area of the wafer; (d) ATR-IR spectra of (I) pristine EG, (II) α-naphthylacetic acid, and (III) α-NM-EG. Reprinted with permission from ref.[15] (Sarkar, S. et al. *Angew. Chem. Int. Ed.* **2012**, *51*, 4901-4904; Copyright © 2012 WILEY-VCH Verlag GmbH & Co. KGaA, Weinheim).

2.4.3. INFRARED SPECTRSOCOPY OF FUNCTIONALIZED GRAPHENE

The presence of α-NM group to EG was further confirmed by ATR-IR spectroscopy (**Figure 2.6-d**);[15] the spectrum of α-NM-EG shows the characteristic intense band at ~792 cm^{-1}, which is ascribed to the in-phase C–H

wagging vibrations of aryl groups and similar peaks in α-naphthylacetic acid and naphthalene appear at ~779 and 774 cm^{-1} respectively (**Figure 2.7**).[174,175]

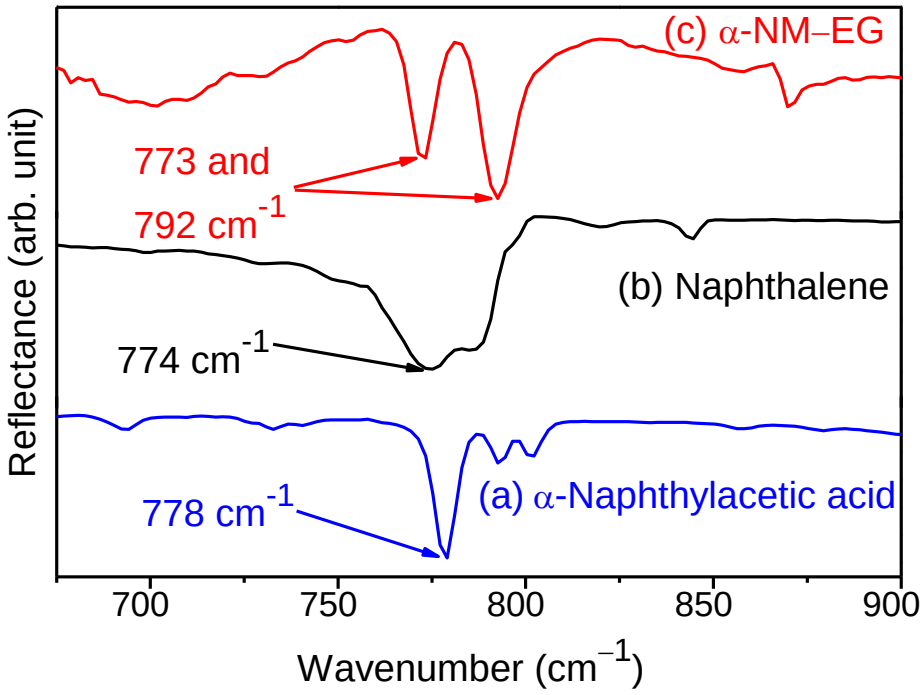

Figure 2.7. Low-frequency ATR-IR spectroscopy of (a) α-naphthylacetic acid, (b) naphthalene, and (c) α-naphthylmethyl (NM) grafted EG, showing the aryl C–H wagging bands. Reprinted with permission from ref.[15] (Sarkar, S. et al. *Angew. Chem. Int. Ed.* **2012**, *51*, 4901-4904; Copyright © 2012 WILEY-VCH Verlag GmbH & Co. KGaA, Weinheim).

2.4.4. CALCULATION OF SURFACE COVERAGE BY ELECTROCHEMISTRY

The epitaxial graphene surfaces thus derivatized with α-NM groups were further characterized by analyzing the reductive cyclic voltammetry, which was conducted in a pure electrolyte solution.[15] The one-electron reduction of the attached α-NM groups (**Figure 2.5-e**, process **7** in **Scheme 2.2**) gives rise to a reduction wave (**Figure 2.5-f-h**) and the surface coverage (Γ) of the α-NM groups can be estimated from the charge using the formula: $\Gamma = Q/nFA$, where Q is the integrated area of the reduction peak (Coulombs of charge), n is the number of electrons (n=1), F is the Faraday constant (9.648×10^4 C.mol^{-1}), and A is the area of the electrode. The functionalized α-NM-EG samples, obtained by complete passivation of the EG surface in a α-naphthylacetate solution (as illustrated in **Figure 2.5-b**), were found to have an approximate surface coverage of 10×10^{-10} mol.cm^{-2} (**Figure 2.5-f**), which corresponds to a densely packed layer of α-NM groups. Corresponding reductive CV for the derivatized samples using 4 mM α–naphthylacetate until complete passivation of the electrode are shown in **Figure 2.8** and were used for surface coverage calculations. For the EG substrate the surface coverage was found to be independent of the concentration of the α-naphthylacetate, while for the HOPG functionalization the surface coverage was found to be: 4.5×10^{-10} mol.cm^{-2} (**Figure 2.5-g**, 2 mM), and 9.5×10^{-10} mol.cm^{-2} (**Figure 2.5-h**, 4 mM).[98,104]

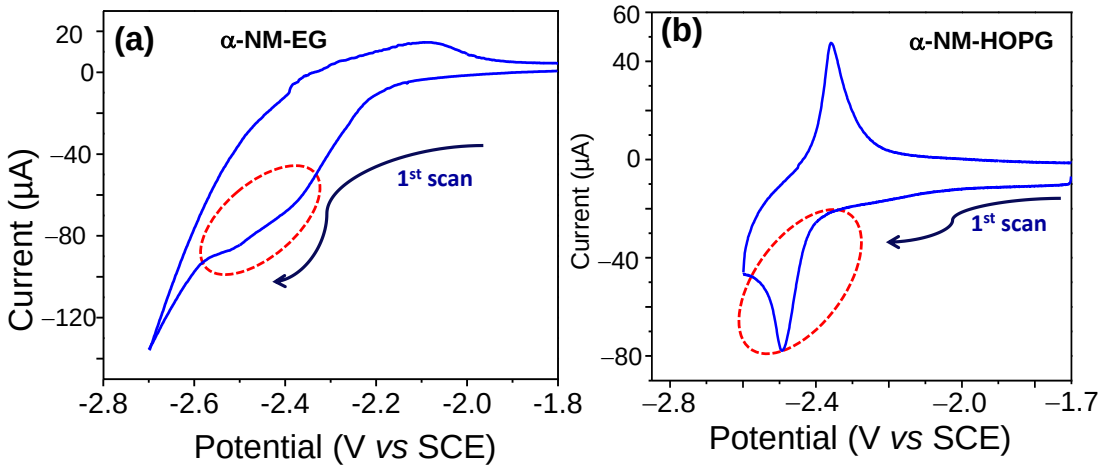

Figure 2.8. Reductive cyclic voltammograms of α–NM grafted (a) epitaxial graphene (α–NM-EG) and (b) HOPG (α–NM-EG) electrodes (derivatized using 4 mM α–naphthylacetate until complete passivation of the electrode) in pure electrolyte (~0.1 M *n*-Bu_4NPF_6 in acetonitrile) solution. Reprinted with permission from ref.[15] (Sarkar, S. et al. *Angew. Chem. Int. Ed.* **2012**, *51*, 4901-4904; Copyright © 2012 WILEY-VCH Verlag GmbH & Co. KGaA, Weinheim).

2.4.5. CONTROL OF ELECTROCHEMICAL FUNCTIONALIZATION

Electrochemical conditions to functionalize EG by method **Figure 2.5-b** lead to completely passivated surfaces with surface coverage of ~10×10^{-10} mol.cm^{-2} and the atomic force microscopy (AFM) image (shown in **Figure 2.10-b**) confirms densely-packed EG surface with α-NM groups.

In order to control the extent of electrochemical functionalization and prepare α-NM-EG substrates with low surface coverage of the α-naphthylmethyl groups, we conducted a potentiostatic electrolysis of the EG electrode for 2.5 seconds at 0.8 V vs SCE (**Figure 2.9-a**) in presence of ~2.0 mM α-naphthylacetate (with ~0.1 M *n*-Bu_4NPF_6 in CH_3CN). The subsequently recorded reductive cyclic voltammogram shows the reduction peak at potential –2.5 V vs SCE. (**Figure 2.9-c**, after transferring the cleaned α-NM-EG to a pure electrolyte solution of ~0.1 M *n*-Bu_4NPF_6 in CH_3CN). The integrated area (**Figure 2.9-d**) of this reduction peak corresponds to a charge, Q = 7.62×10^{-7} Coulombs. This corresponds to a surface coverage of ~0.49×10^{-10} mol.cm^{-2}, and AFM imaging of the derivatized sample shows sparsely functionalized graphene (**Figure 2.10-c**). A series of control experiments on HOPG substrates showed that the film thickness can be controlled by the applied potential and the scan duration.[15]

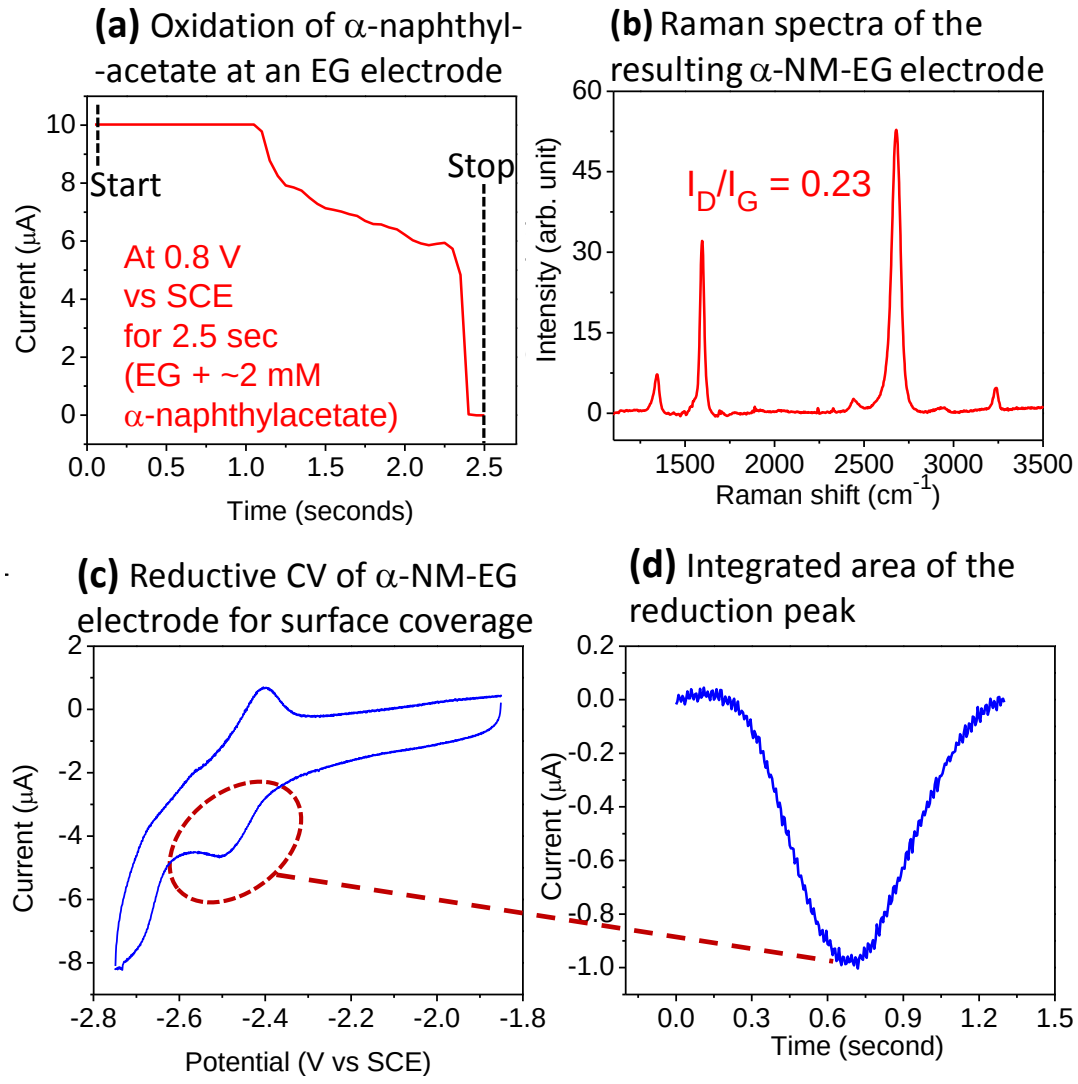

Figure 2.9. (a) Potentiostatic electrolysis of ~2 mM α-naphthylacetate at 0.8 V vs SCE on a pristine EG (working electrode) in ~0.1 M *n*-Bu_4NPF_6 in CH_3CN for 2.5 seconds at a scan rate of 0.2 $V.s^{-1}$. (b) Raman spectra (λ_{ex} = 532 nm), which shows the evolution of the weak D-band at about 1345 cm^{-1} (with I_D/I_G = 0.23) in the resulting α-NM-EG electrode, derivatized using the above method. (c) Reductive CV of α-NM-EG in a 0.1 M acetonitrile solution of *n*-Bu_4NPF_6, and (d) baseline corrected reduction peak of α-NM-EG at –2.5 eV *vs* SCE. Reprinted with permission from ref.[15] (Sarkar, S. et al. *Angew. Chem. Int. Ed.*

2012, *51*, 4901-4904; Copyright © 2012 WILEY-VCH Verlag GmbH & Co. KGaA, Weinheim).

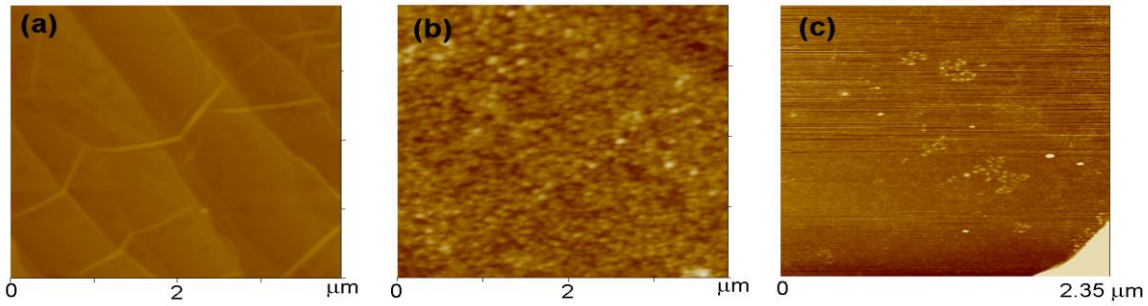

Figure 2.10. AFM images of (a) pristine EG, (b) completely passivated α-NM-EG obtained by oxidative CV runs in 2 mM α-naphthylmetyl acetate between 0 and 1.3 V vs SCE, and (c) sparsely functionalized α-NM-EG obtained by controlled potentiostatic electrolysis of 2 mM α-naphthyl acetate at 0.8 V vs SCE for 2.5 seconds. Reprinted with permission from ref.[15] (Sarkar, S. et al. *Angew. Chem. Int. Ed.* **2012**, *51*, 4901-4904; Copyright © 2012 WILEY-VCH Verlag GmbH & Co. KGaA, Weinheim).

2.4.6. FORMATION OF CLOSED PACKED LAYERED STRUCTURES AND EASE OF COMPLETE PASSIVATION OF EPITAXIAL GRAPHENE

The formation of more compact (closely packed) layer of α–NM groups over an epitaxial graphene (EG) surface and ease of complete electrochemical passivation of the EG surface just after two cyclic voltammetric cycles (which was found to be independent of the concentration of α-naphthylacetate) can be

rationalized based on the fact that graphene is much more reactive than graphite.[18,150] The epitaxial graphene sample contains an inhomogeneous fraction of single- and few-layers of graphene (which are rotationally disordered and thus are electronically decoupled).[176] Furthermore, given that single-layer graphene (SLG)[150] is ~14 times more reactive[105,106] than double layer graphene (2LG)[104] and that the edge carbons are more reactive than basal plane carbons towards grafting,[156] the exact theoretical surface concentration for monolayer coverage of α-naphthylmethyl group on an epitaxial graphene sample of given surface area could not be estimated accurately. Additionally, the reactivity of graphene increases as more defect sites (sp^3 carbon centers) are formed[104] during the electrochemical grafting of α-NM groups. Consequently, in epitaxial graphene, a more dense coverage of functional groups could be obtained, and this might vary significantly from sample to sample depending on the population of SLG and distribution of edge carbon atoms in different samples.

Reported values of surface coverage in α-NM-HOPG, Γ_{HOPG} = 0.5 × 10^{-10} moles.cm^{-2} = 3.03 × 10^{13} molecules.cm^{-2} and on glassy carbon (GC) electrode, α-NM-GC, τ_{GC} = 1.5 × 10^{-10} moles.cm^{-2} = 9.1 × 10^{13} molecules.cm^{-2} (Note that surface coverage in α-NM-GC is three times higher than α-NM-HOPG surfaces, which is rationalized based on surface roughness and the difficulty in estimating accurate geometrical area of GC electrodes).[156]

The maximum surface coverage that can be achieved on a graphene surface can be rationalized based on the reported distances between the anchoring groups (from STM experiments on α-NM-HOPG samples), reported surface coverage on α-NM-HOPG surface (0.5×10^{-10} mol/cm^2),[156] and calculated area occupied by each functional groups. The distance between the anchoring points of α–NM groups on a graphitic surface based on scanning tunneling microscopy (STM) imaging has been given by Saveant;[156] the parallelogram model gives an area defined by four anchoring groups of 281.8 Å^2 (**Figure 2.11-a**), whereas the area occupied by each α-NM group is given as 30.5 Å^2 (**Figure 2.11-b**). Therefore a close packing (cp) structure would give about (281.8/30.5) = 9.24 times higher coverage than reported for α-NM-HOPG ($\Gamma_{HOPG} = 0.5 \times 10^{-10}$ moles.cm^{-2} = 3.03×10^{13} molecules.cm^{-2}). This corresponds to a surface coverage, $\Gamma_{cp\text{-}HOPG} = [9.24 \times \Gamma_{HOPG}] = 2.8 \times 10^{14}$ molecules/cm^{2,} while for a closest packed structure on α-NM-GC surface, $\Gamma_{cp\text{-}GC} = [9.24 \times \Gamma_{GC}] = = 8.4 \times 10^{14}$ molecules/cm^2.

Our present experiment on epitaxial graphene functionalization gives the highest surface coverage for α-NM-EG as 9.4×10^{-10} moles.cm^{-2} = 5.7×10^{14} molecules.cm^{-2} = $2\Gamma_{cp\text{-}HOPG}$ or = 0.68 Γ_{cp} on α-NM-GC. Therefore our surface functional group densities values are more comparable (68% of $\Gamma_{cp\text{-}GC}$) to

closest packed structures on GC surfaces, but twice higher than a close packed arrangement on HOPG surfaces ($2\Gamma_{cp\text{-}HOPG}$).

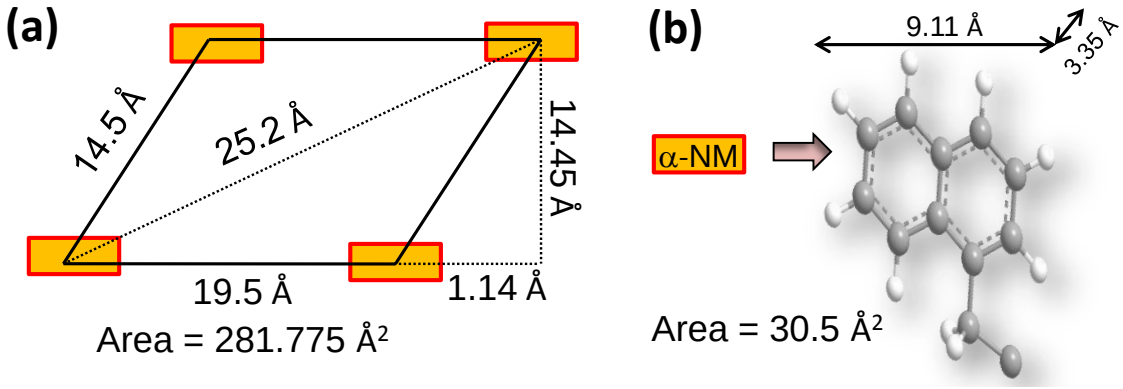

Figure 2.11. (a) Parallelogram model of anchoring points of α–NM functional groups over graphite surface, as measured by scanning tunneling microscopy (STM) and calculated area covered by functional groups.[156] (b) Calculated area of the α-NM groups based on the C–C and C–H bond distances.

2.4.7. ELECTRO-ERASING OF THE FUNCTIONAL GROUPS

The oxidation waves of the grafted groups (process **4** in **Scheme 2.2**) were irreversible at low scan rates in a pure electrolyte solution, and these waves disappeared after the second anodic scan (**Figure 2.12-a** and **2.12-b**), showing the erasure of the grafted functionalities under electro-oxidative conditions (process **5** in **Scheme 2.1**). Thus, electro-erasing of the α-NM-EG films was achieved by running two cycles of an oxidative CV between 1 and 2.5

V vs SCE and this is illustrated in **Figure 2.12-a** for α-NM-EG and Figure **2.12-b** for α-NM-HOPG.

After electrochemical erasure, the resulting EG or HOPG electrode behaved like a clean EG or HOPG electrode as may be seen by running the reductive cyclic voltammetry of the electro-erased electrodes, which are essentially featureless (**Figures 2.12-c** and **2.12-d**). After electro-erasing of the α-NM-groups from the α-NM-EG electrode, the surface can be re-functionalized under the oxidative CV conditions shown in **Figure 2.5-b**, and the electrode exhibited the same behaviour towards passivation by α-naphthylacetate as the pristine EG-electrode.[15]

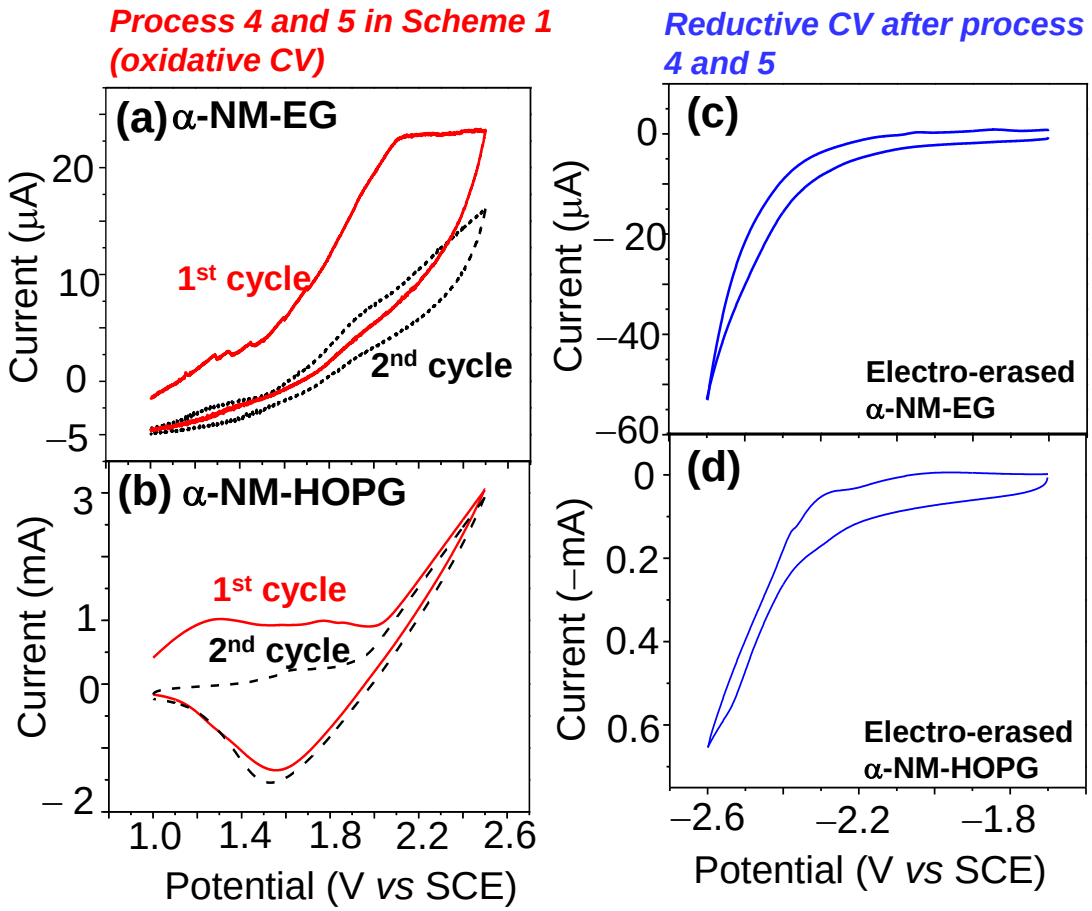

Figure 2.12. Electrochemical erasure of the α-NM-groups from (a) α-NM-EG electrode and (b) α-NM-HOPG electrode by oxidative cleavage. Reductive cyclic voltammetry of electro-erased (c) α-NM-EG and (d) α-NM-HOPG electrodes (scan rate = 0.2 Vs-1). Reprinted with permission from ref.[15] (Sarkar, S. et al. *Angew. Chem. Int. Ed.* **2012**, *51*, 4901-4904; Copyright © 2012 WILEY-VCH Verlag GmbH & Co. KGaA, Weinheim).

The fidelity of the electro-grafting (process **2, 3**) and -erasing (process **4**, **5**) steps is apparent in the evolution of the D-band in the Raman spectrum as a function of the electrochemical treatment (**Figure 2.13**).

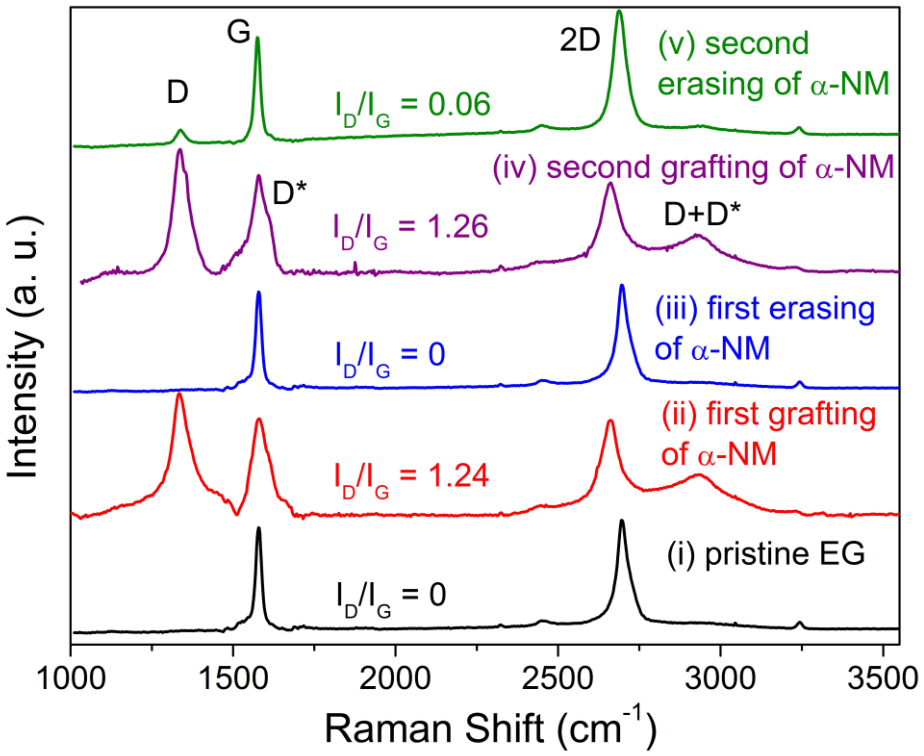

Figure 2.13. Evolution of the EG Raman spectrum (excitation wavelength, λex = 532 nm) following multiple electrochemical grafting and erasing steps of the α-naphthylmethyl group: (i) pristine EG, (ii) after first grafting of α-NM (α-NM-EG), (iii) after first electrochemical erasing of α-NM functional group from α-NM-EG, (iv) after second grafting of α-NM to electro-erased α-NM-EG, and (v) second electrochemical erasing. Reprinted with permission from ref.[15] (Sarkar, S. et al. *Angew. Chem. Int. Ed.* **2012**, *51*, 4901-4904; Copyright © 2012 WILEY-VCH Verlag GmbH & Co. KGaA, Weinheim).

Alternatively, the α-NM groups can be electrochemically erased by transferring the α-NM–EG electrode to a pure electrolyte solution and setting the potential at the level of the oxidation wave. Thus potentiostatic electrolysis of the α-NM-EG electrode at 1.85 V vs SCE for 240 s in a pure electrolyte solution produces a subsequent CV which is essentially featureless, suggesting the efficient erasure of the grafted functionality and the restoration of the initial structure of the epitaxial graphene.[15]

2.5. CONCLUSION

Our present work demonstrates that arylmethyl groups can be grafted electrochemically to the surface of epitaxial graphene. The surface coverage of naphthylmethyl groups can be controlled from densely-packed (ideal as organic dielectrics) to sparsely functionalized surface (ideal for introducing a reasonable band gap in graphene) with well-ordered structural patterning of the functional groups on EG surface by adjustment of electrochemical conditions.[15] The control of the layer structure and packing of the functional groups over the graphene surface is an essential issue in the development of graphene chemistry.[13,14,26] The functionalization is readily reversed and may be repeated in a simple, efficient and reproducible manner suggesting the potential of this approach for reversible engineering of the band structure and conductivity.

CHAPTER 3. Diels-Alder Chemistry of Graphene

3.1. INTRODUCTION

The Diels-Alder (DA) transformation is one of the most powerful and elegant reactions in organic chemistry.[177] The prototypical Diels-Alder [4+2] pericyclic reaction process involves the reaction between a diene (generally a 4π electron system, such as 1,3-butadiene) and a dienophile (generally a 2π electron system, such as ethylene) leading to the formation of a cyclohexene ring system (**Figure 3.1-a**). This chemistry has been extensively used in carbon materials in order to tailor their physical and chemical properties for various applications.

The Diels–Alder reaction chemistry of fullerene and carbon nanotubes is well documented (**Scheme 3.1**). Fullerenes are excellent dienophiles due to the [6,6] double bonds of C_{60} and consequently fullerenes react with various dienes [178-180] including anthracene[179,181] and its derivatives,[179,182] anthraquinone dienes,[183] and o-quinodimethanes.[184] Microwave irradiation helps to avoid the retro-Diels–Alder reaction and improve the yield by shortening the reaction time.[185,186] Although the Diels–Alder reaction is favored by the presence of electron rich substituents in the diene, C_{60} can also react with electron-deficient

dienes, as evidenced by the inverse electron demand Diels–Alder (DA) reaction to prepare fullerenopyridazine.[187]

The DA reaction of single–walled carbon nanotubes (SWNT) has been predicted to be favorable[188] and this has recently been experimentally validated; microwave irradiation of o-quinodimethane with soluble SWNTs,[189] cycloaddition of dienes to fluorinated SWNTs,[190] the application of high pressure in presence of $Cr(CO)_6$,[191] and functionalization of pristine SWNT and MWNT[192] have all been reported to give rise to Diels–Alder chemistry. The Diels–Alder reaction chemistry of pristine HiPCO SWNTs towards fluorinated olefins was proposed to proceed by a [2+2] cycloaddition;[193] this chemistry was able to eliminate or completely transform metallic carbon nanotubes into semiconductors, thereby resulting in field effect transistors with reasonable on-off ratios (1: 100, 000) while retaining high mobilities (~100 $cm^2V^{-1}s^{-1}$) in these devices.

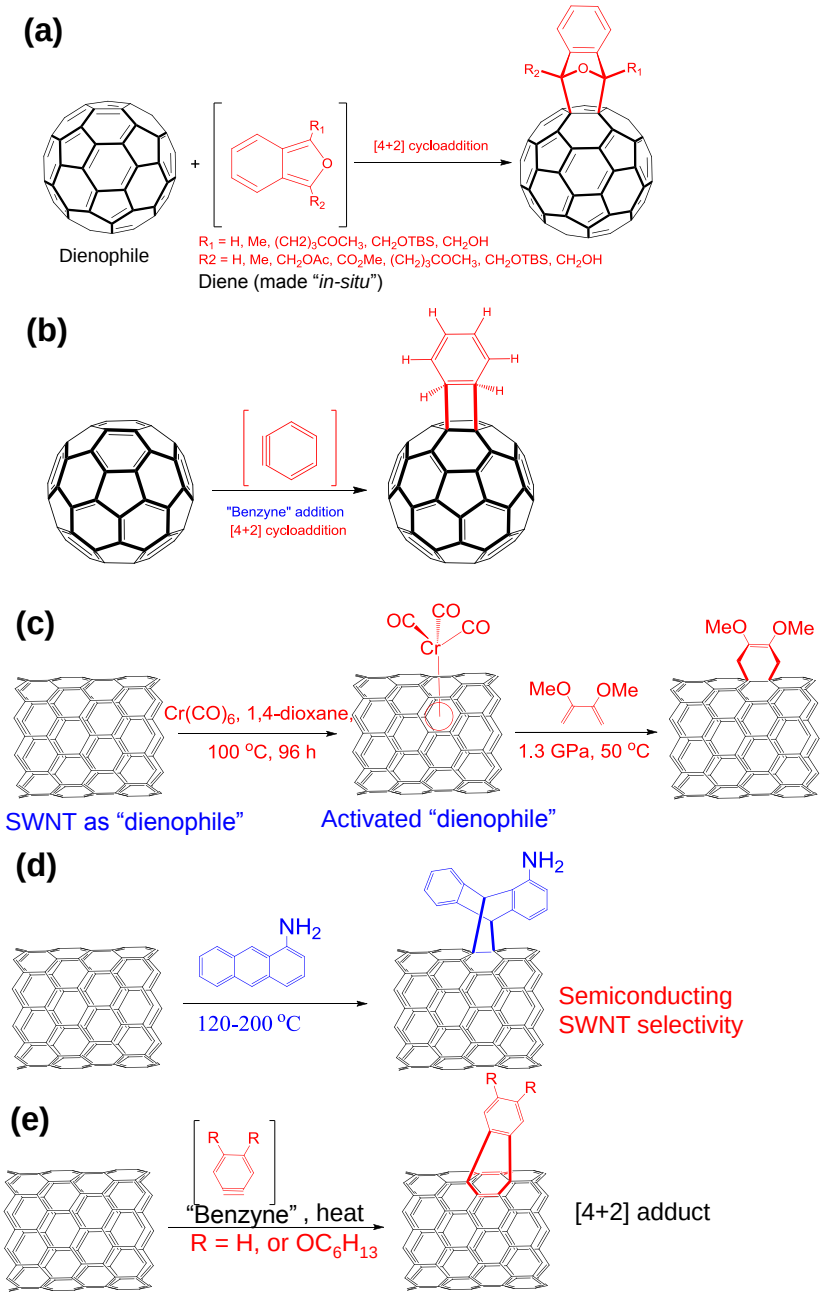

Scheme 3.1. Diels-Alder reactivity of fullerene and pristine SWNTs. (a) [4+2] cycloaddition of fullerene (dienophile) with an 'in-situ" prepared benzofuran (diene) reactant.[194] (b) [2+2] cycloaddition of fullerene with an "in-situ" prepared benzyne reactive intermediate.[195] (c) Activation of SWNTs using chromium hexacarbonyl and subsequent reaction with an electron-rich diene, 2,3-

dimethoxy-1,3-butadiene.[191] (d) Preferential reactivity of 1-aminoanthracene towards semiconducting-SWNTs.[196] (e) Benzyne addition reactions of graphene towards SWNTs.[197]

Recently, the Diels–Alder chemistry between single–walled carbon nanotubes (SWNTs) and an electron-rich diene (1-aminoanthracene) was suggested to be selective towards semiconducting carbon nanotubes, suggesting the initial applications of this chemistry in the separation of metallic (M)- and semiconducting (SC)- single–walled carbon nanotubes.[196] The addition of benzyne to carbon nanotubes has been reported to occur preferentially with larger diameter SWNTs as a result of the more favorable electronic structure (lower band gap).[197] Diels–Alder chemistry has also been suggested to play a role in the polymerization of small molecules to produce single-walled carbon nanotube by rational synthesis.[198]

Graphene, a two-dimensional sp^2-carbon crystal of atomic thickness, has garnered tremendous attention among both physicists and chemists. Most molecules that participate in the Diels–Alder reaction do so as either diene or dienophile (**Figure 3.1-a**), although there are exceptions to this generalization.[192] Furthermore graphene is often considered to be highly aromatic and chemically stable, and aromatic molecules do not usually participate in thermal (ground state) Diels–Alder reactions. We reported a

series of facile Diels-Alder reactions in which graphene can function either as a diene when paired with appropriate dienophiles (e.g. maleic anhydride, tetracyanoethylene) or as a dienophile when paired with appropriate dienes (e.g. 2,3-dimethoxy-1,3-butadiene, 9-methylanthracene) and thereby established graphene as a solid-state counterpart of classical small molecule electrocyclic organic reactions.[18,21] We attributed this dual nature of reactivity of graphene in DA reaction to the absence of an energy gap (the valence and conduction bands touch at the Dirac point), which makes available a number of canonical structures (**Figure 3.1-b**), thereby motivating its DA reactivity as both diene and dienophile. [18] The principles of orbital symmetry and the frontier molecular orbital (FMO) theory can be applied to explain the unique Diels-Alder reactivity of graphene.[21]

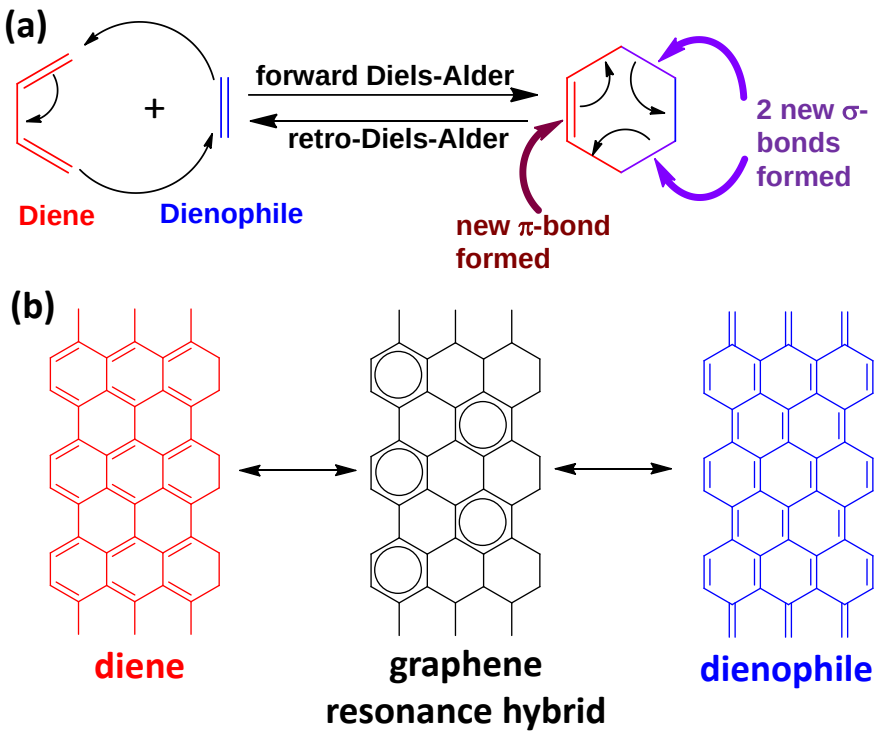

Figure 3.1. (a) Schematic illustration of the Diels-Alder [4+2] cycloaddition between 1,3-butadiene (diene) and ethylene (dienophile). (b) Canonical resonance structures of graphene: diene and dienophile.

The choice of the Diels-Alder (DA) chemistry in modifying graphene is motivated by our recent discovery of the DA reactivity of graphene[18,21] as well as due to the several advantages this chemistry offers: (i) very simple to perform and highly efficient under mild reaction conditions, (ii) catalysts are not required, (iii) leads to simultaneous formation of a pair of sp^3 carbon centers (spin-paired Kekule structures) in graphene lattice, (iv) reactive towards graphene edges leading to elongation and quenching of graphene edges (can

quench dangling bonds and can repair the defective edges), (v) exclusion of possibility of generating conjugated π-radicals, (vi) does not produce by-products, and (vii) availability of simple thermal retro-DA reactions offers the easy regeneration of starting materials.[26] The retro-Diels–Alder reactions of the adducts offer another dimension in making the system reversible, where the electronic and phonon properties of graphene could be thermally switched back to its pristine state in a very simple, reproducible and efficient manner.

Several other research groups have investigated this Diels-Alder chemistry of graphene from both theoretical and experimental viewpoint. The chemistry was employed in one-step functionalization of graphene with cyclopentadienyl-capped macromolecules,[114] in covalently patterning graphene surfaces (by force-accelerated Diels-Alder reaction between graphene and cyclopentadienes),[115] in producing graphene nanoplatelets (by mechanochemically driven solid-state Diels-Alder chemistry of graphite),[116] while the computational studies on the Diels-Alder adduct formation on graphene by using density functional theory (DFT) calculations have been reported to be highly endothermic.[199,200] The calculations from Houk and co-workers and Denis indicate that graphene edges may be functionalized by Diels-Alder cycloadditions, while interior regions are unreactive towards the cycloaddition due to high reaction enthalpies and loss of aromaticity.[199,200]

3.2. EXPERIMENTS: THE DIELS-ALDER REACTIONS OF GRAPHENE

3.2.1. Characterization Techniques

Infra-red ATR spectra were taken using a Thermo Nicolet Nexus 670 FTIR instrument, equipped with an ATR sampling accessory. Raman spectra were acquired in a Nicolet Almega XR Dispersive Raman spectrometer with 532 nm laser excitation. Raman spectroscopy was employed to monitor the changes induced by the Diels–Alder cycloaddition reaction chemistry on graphite (HOPG and μG) and graphene (exfoliated graphene and epitaxial graphene) and the retro-Diels–Alder reaction chemistry of the derived Diels-Alder adducts. In the Raman spectroscopy of graphene and its derivatives,[91,92] the G peak (at ~1580 cm^{-1}) originates from the optical E_{2g} phonons at the Brillouin zone center, whereas the D peak (at ~1340 cm^{-1}), which requires a defect for its activation via an intervalley double-resonance Raman process,[88] is caused by breathing modes (corresponding to the transverse optical phonons near the K point of the Brillouin zone).[119] The intensity of the D peak is sensitive to the degree of disorder or functionalization in the graphene macromolecular sp^2 backbone, and therefore provides a convenient index for the degree of reaction achieved in the Diels-Alder chemistry, as measured by the ratio of the intensities of the D- and G-bands (I_D/I_G).[89,91,93,201] It should be mentioned that the 2D peak (at ~2680 cm^{-1}), being the sum of two phonons with opposite

momentum, is always present even in the absence of any defects (even in pristine epitaxial graphene). On the other hand the D′ peak (located at ~1610 cm^{-1} in case of MA–EG adduct) occurs via an intravalley double-resonance process and is observed only in the presence of defects.

3.2.2. Liquid Phase Exfoliation of Graphite to Graphene (XG_{sol})

Microcrystalline graphite (μG, 1-2 μm, 50 mg, synthetic, Aldrich) was probe sonicated in o-dichlorobenzene (~20 mL ODCB) for 1 h using an ultrasonic processor (Cole-Parmer) at 40% amplitude. The slurry was centrifuged at 4400 rpm for 30 min. The resulting supernatant, which yielded dispersions of graphene in ODCB,[202] was collected and concentrated under vacuum (12 mg). The powdered exfoliated graphene was dried in vacuum overnight and used in subsequent reactions after re-dispersion in anhydrous *p*-xylene. In some cases the ODCB-dispersions of graphene were used directly. This procedure has been shown to produce graphene flakes in high yield;[202] these graphene flakes consisted mainly of four to five layers of graphene and thin graphite, as indicated by Raman spectroscopy and atomic force microscopy.[104]

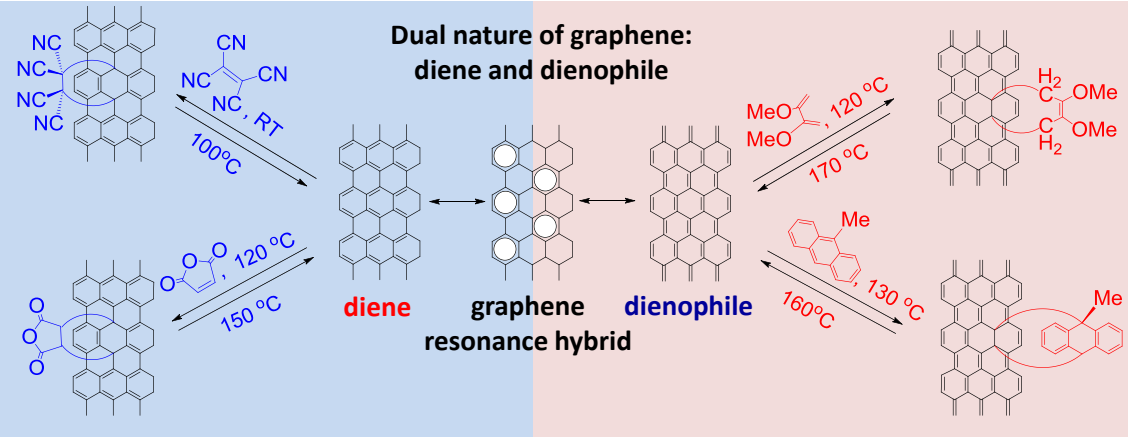

Scheme 3.2. Dual nature of reactivity of graphene in Diels–Alder chemistry. Diene character of graphene (left), shown by its reactions with electron-deficient dienophiles (tetracyanoethylene and maleic anhydride), dieneophile character of graphene (right), demonstrated by its reactivity towards electron-rich dienes (2,3-dimethoxy-1.3-butadiene and 9-methylanthracene).[21]

3.2.3. Diels–Alder Chemistry of Graphene (Diene) with Tetracyanoethylene (Dienophile)

In a typical reaction TCNE (100.0 mg, 0.78 mmol, ~0.13 M) was dissolved in the absence of light in anhydrous dichloromethane (~2 mL) to obtain a clear solution; the TCNE solution was added to a suspension of solution-exfoliated graphene (XG_{sol}) in 1,4-dioxane (~4 mL). The solution was stirred at room temperature for 3 h and the resulting Diels–Alder adduct was

washed with acetone, warm ethanol and finally with acetone; dried under vacuum overnight.

3.2.4. Diels–Alder Chemistry of Graphene (Diene) with Maleic Anhydride (Dienophile)

In a typical reaction maleic anhydride (50 mg, 0.5 mmol) was added to a solution of exfoliated graphene (5 mL XG_{sol} in ODCB) and stirred at 130 °C for ~3 h. The reaction mixture was allowed to cool to room temperature, and then filtered through a 0.1 μm PTFE filter paper, washed thoroughly with warm ethanol and acetone and then dried under vacuum overnight.

In the case of the reactions with EG (C-face surface of area 0.18 cm^2) or HOPG, the wafers were heated in ~0.13 M solution of maleic anhydride in *p*-xylene (50 mg, 0.5 mmol, 4 mL p-xylene) at the specified temperature for 3 hours. In the case of HOPG, the best results were obtained at 120°C; in case of epitaxial graphene (EG), the optimum temperature was found to be 70°C. Raman spectroscopy was used to monitor the changes induced by the chemistry and to optimize the reaction parameters (temperature and reaction time). Based on the optimized reaction conditions, we observed that HOPG and XG_{sol} undergo cycloaddition in the presence of ~0.15 M maleic anhydride in *p*-xylene (for 3 h) at 120 °C and 130 °C respectively.

3.2.5. Diels–Alder Chemistry of Graphene (Dienophile) with 9-Methylanthracene (Diene)

Based on our optimized reaction conditions, we observed that the cycloaddition adducts, could be obtained by stirring a suspension of microcrystalline graphite (or exfoliated graphene) in ~0.1 M solution of 9-methylanthracene in *p*-xylene at 130°C for 12 h under a argon.

In a typical reaction 9-methylanthracene (100.0 mg, 0.52 mmol) was added to a dispersion of exfoliated graphene XG_{sol} in ODCB (~5 ML) and the reaction mixture was stirred at 130°C in absence of light for 12 h and then filtered through a 0.2 µm PTFE membrane. The filter cake was washed with warm ethanol and then with acetone to remove any unreacted reagent and the product was dried under vacuum overnight.

3.2.6. Diels–Alder Chemistry of Graphene (Dienophile) with 2,3-Dimethoxy-1,3-butadiene (Diene)

In a typical reaction, 2,3-dimethoxy-1,3-butadiene (100 mg, 0.88 mmol, FW = 114.07) was added to a suspension of microcrystalline graphite (µG, 50 mg, 4.2 mmol carbon atoms) (or exfoliated graphite, XG_{sol}) in anhydrous *p*-

xylene (6 mL) under argon. The suspension was stirred overnight under a positive pressure of argon at 120°C. The reaction mixture was filtered using a 0.2 µm PTFE membrane and the solid product washed with warm ethanol and acetone to remove unreacted reagent and finally dried under vacuum overnight.

For the reactions of EG and HOPG with 2,3-dimethoxy-1,3-butadiene, the EG or HOPG wafers were heated overnight at 120 °C in a solution of ~0.15 M 2,3-dimethoxy-1,3-butadiene (DMBD) in *p*-xylene under argon. After the reaction the EG or HOPG substrates were washed repeatedly with acetone and dried with a gentle flow of argon, then under vacuum for 2 h. In the case of the reaction between epitaxial graphene and DMBD, the best results are obtained by heating the wafer at 50°C with the neat reagent in an argon atmosphere for 3 h.

The ATR spectra of the DMBD–graphene showed the following characteristic peaks at: 823, 869, 1100 (CH_2 wag), 1148, 1262 (CH_2 rock), 1344, 1600 (C=C stretch, graphene), 1642 (C=C stretch), 1660, 1670, 2843 (C_{sp3}–H asymmetric stretch) and 2921 (C_{sp3}–H asymmetric stretch) cm^{-1}. The reagent, 2,3-dimethoxy-1,3-butadiene shows the following characteristic peaks: 774, 810, 913, 1000, 1036, 1116 (CH_2 wag), 1218, 1254 (CH_2 rock), 1318, 1424, 1493 (CH_2 scissor), 1530, 1650 (C=C stretch), 1713, 2131 (C=C

symmetric stretch), 2500, 2565, 2641, 2728 (CH_2 symmetric stretch), 2847 (CH_2 asymmetric stretch), 2940 and 3007 (C_{sp2}–H stretch of $=CH_2$) cm^{-1}.[175]

3.2.7. Retro-Diels–Alder Reaction of TCNE–HOPG and TCNE–Graphene Adducts

It was observed that when the TCNE–HOPG or TCNE–graphene adducts were heated in *p*-xylene at ~100 °C or if the reaction with TCNE (~0.15 M in 1,4-dioxane/dichloromethane) was performed at 100 °C, no detectable D peaks were observed in the Raman spectra of the derived materials, indicating that the cycloreversion (retro-Diels–Alder reaction) is dominant at high temperatures.

3.3. THEORETICAL RATIONALIZATION OF THE DIELS-ALDER REACTIVITY OF GRAPHENE

Here we examine the experimentally observed dual nature of Diels-Alder reactivity of graphene from the standpoint of orbital symmetry[23] and frontier molecular orbital (FMO) theory[24] which together provide the key concepts for analyzing pericyclic reactions. As an introduction to this analysis we first examine some simple, well known DA reactions which have received detailed

theoretical examination and which now may be used to instruct the basic theoretical concepts which come into play in assessing the DA reactivity of graphene.

Chemistry at the Dirac Point: Diels-Alder Reactivity of Graphene

The unique Diels-Alder reactivity of graphene and its dual behavior as both diene and dienophile can be rationalized using simple arguments based considerations of the zero-band-gap electronic structure (degenerate HOMO and LUMO, as shown in **Figure 3.2**), frontier molecular orbitals (FMOs) and Woodward-Hoffmann principles of conservation of orbital symmetry.

The energy-gap between the HOMO of the diene and LUMO of the dienophile is a key factor in determining the reactivity of the Diels-Alder partners in cycloaddition chemistry according to the frontier molecular orbital (FMO) theory.[23,24,203,204] It has been suggested that as the CNT structure elongates, the activation energies for the DA reaction decreases.[198] The extreme example of this behavior is graphene, with its flat two-dimensional infinite framework of sp^2-bonded carbon atoms with valence and conducting bands touching at the Fermi level (Dirac point). Consequently, graphene, with no energy gap between HOMO and LUMO (**Figure 3.2**), shows dual nature of reactivity as diene and dienophile and is therefore found to be a versatile Diels-Alder substrate.[18] This chemistry establishes the importance of the HOMO-LUMO energy gap in the

DA cycloaddition quite apart from the conventional curvature-dependent reactivity (based on the carbon pyramidalization angle, θ_p),[36] which is operative in fullerenes and carbon nanotubes.

The band structure of graphene at the level of tight binding theory with transfer integral **t** (resonance integral **β**, equivalent to the Huckel molecular orbital theory), was solved in 1947 by Wallace[54] (**Figure 3.2-b**). Two of the points at the corners of the Brillouin zone are distinct and are labeled as K and K', whereas the other points are related to them by symmetry. As may be seen in **Figure 3.2**, the K points are particularly important because this is where the valence and conduction bands meet and cross. Importantly, the bands touch at a single point in **k** space (the Dirac point) due to the crossing of valence and conduction bands; as a consequence graphene is a zero-band-gap semiconductor, and the density of states at the Fermi level is zero (at the absolute zero of temperature).

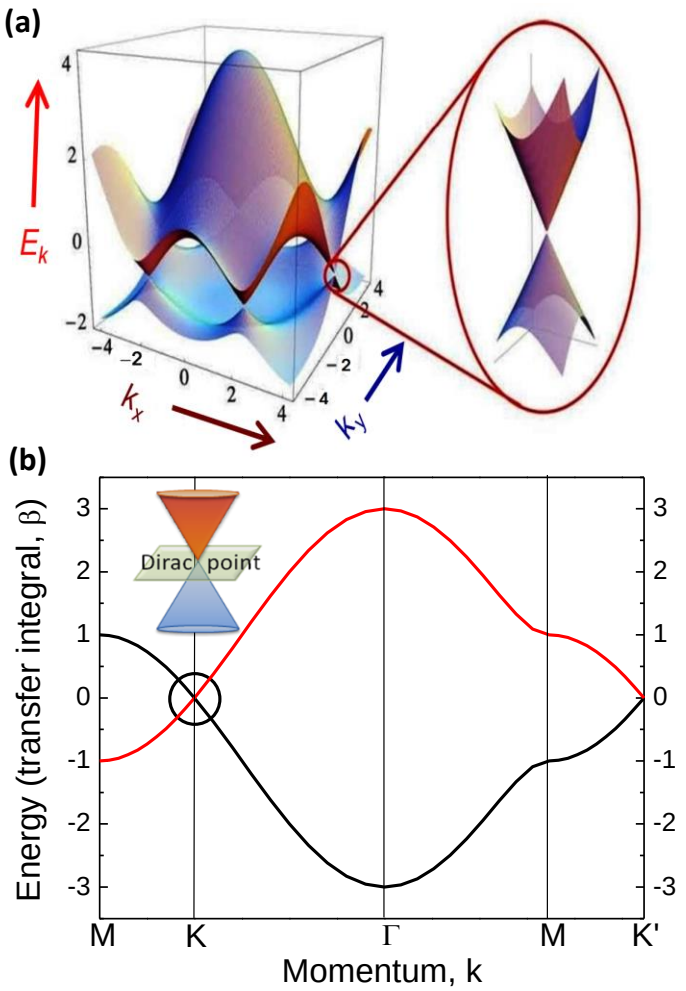

Figure 3.2. (a) Electronic band dispersion in the graphene honeycomb lattice. Left: energy spectrum (in units of *t*), with *t* = 2.7 eV and *t*'= −0.2*t*. Right: expanded view of energy bands close to one of the Dirac points.[17] (b) Dispersion of the graphene energy band in momentum space within simple tight-binding (HMO) theory as a function of the resonance or transfer integral (β, t ~ 3 eV).[21] Reprinted with permission from ref.[21] (Sarkar, S. et al. *Acc. Chem. Res.* **2012**, 45, 673-682; Copyright © 2012 American Chemical Society).

The orbital interactions in most pericyclic reactions may be analyzed from the standpoint of orbital symmetry and correlation diagrams between reactants and products or by consideration of frontier molecular orbitals (HOMOs and LUMOs) of the reactants and their relative energies. This is illustrated **in Figure 3.3** in the classic reaction between butadiene (diene) and ethylene (dienophile) [**Figure 3.1-a**]. From the standpoint of the correlation diagram it may be seen that the orbital symmetries in reactant and product allow smooth evolution of the electronic structure of the reaction complex along the reaction pathway. While the energy gap between the reactant HOMOs and LUMOs narrows in the transition state, detailed calculations show that these orbitals do not cross along the reaction coordinate, and thus the orbital symmetries are rigorously maintained in throughout the transformation between reactants and products.

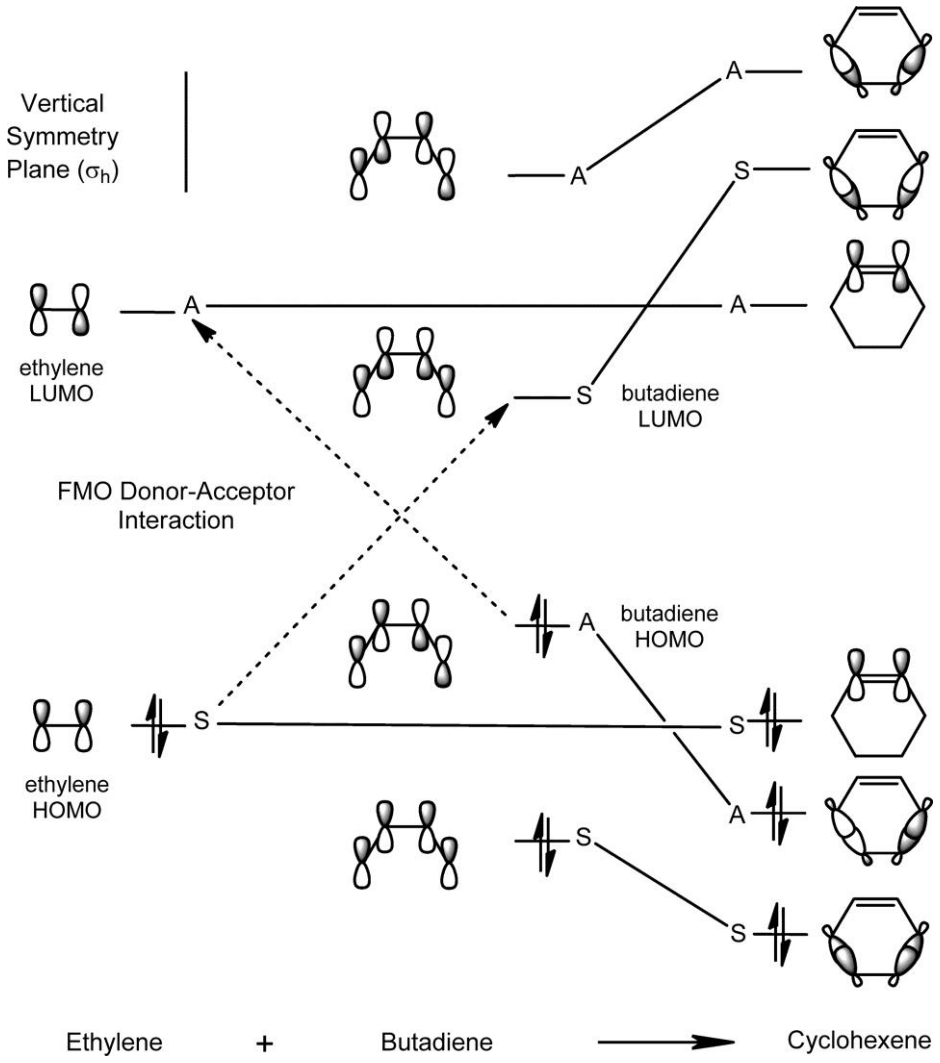

Figure 3.3. Diels–Alder orbital symmetry correlation diagram for the reaction of ethylene with butadiene, together with frontier molecular orbital (FMO) interactions. The orbitals are classified as either symmetric (S) or antisymmetirc (A) with respect to the vertical symmetry plane shown in the diagram.[21] Reprinted with permission from ref.[21] (Sarkar, S. et al. *Acc. Chem. Res.* **2012**, 45, 673-682; Copyright © 2012 American Chemical Society).

The FMO theory considers only the reactant orbitals and analyzes the HOMO-LUMO interactions between reactants. In principle, for the DA reaction, this involves two pairs of HOMO-LUMO interactions, but because the FMO theory focuses on the energy separation between the interacting orbitals, it is often sufficient to consider a single HOMO-LUMO reactant interaction.

The FMO analysis of the Diels–Alder reaction between butadiene and ethylene is shown on the left side of **Figure 3.3**; typically such an analysis is focused on the interaction between the butadiene (diene) HOMO and the ethylene (dienophile) LUMO, although reactions involving the converse situation (inverse electron demand) have been reported, and it is clear that both HOMO-LUMO interactions are operative to some degree in the Diels-Alder reaction. Implicit in the FMO treatment is the concept of charge transfer between reactants; that is electron density is transferred from an occupied orbital (often the HOMO) of one reactant to a vacant orbital (often the LUMO) of the other reactant and in this sense the FMO theory implies an orbital crossing which at first sight seems to be at odds with the correlation diagram in **Figure 3.3** and the results of detailed calculations.[205] The resolution of this difficulty is made clear if we consider the energy change (ΔE) which accompanies the interaction between the frontier orbitals from the standpoint of second-order perturbation theory

$$\Delta E = \frac{[H_{(HOMO-ethylene),(LUMO-butadiene)}]^2}{\varepsilon_{HOMO-ethylene} - \varepsilon_{LUMO-butadiene}} + \frac{[H_{(HOMO-butadiene),(LUMO-ethylene)}]^2}{\varepsilon_{HOMO-butadiene} - \varepsilon_{LUMO-ethylene}} \quad (3.1)$$

where the matrix elements in the numerators depend on the overlap and symmetry of the frontier orbitals of the two reactant molecules (exemplified here by ethylene and butadiene), and the denominators are the differences between the orbital energies of the frontier orbitals.[24,25]

In fact the FMO analysis may be recast in terms of a theory for the inclusion of configuration interaction in the wave function, which allows the admixture of excited states into the ground state of the reaction complex according to eq (3.1). In this way the interactions between HOMOs and LUMOs in the reactants are understood to evolve along the reaction coordinate in the form of configurational mixing, and the intended correlations and charge transfer processes are therefore not rigorous in the same way as the orbitals involved in the construction of the correlation diagram.

The FMO theory is particularly convenient in the present context because its application is confined to a consideration of the orbitals of the reactants and their energies. Graphene possesses high-lying HOMO (low ionization potential and the energy of which is taken as: $E_{HOMO} = -IP$) and low-lying LUMO (high

electron affinity, and the energy of which is taken as: $E_{LUMO} = -EA$).[21] The work-function (W) of graphene ($E_{HOMO} = E_{LUMO} = -W = -4.6$ eV) is defined by the crossing of valence (HOMO) and conduction (LUMO) bands in graphene. The FMO theory suggests that the appropriate HOMO-LUMO gap(s) ($E_{H-L} = IP-EA$) can provide an excellent inverse index of chemical reactivity,[24,25,203,206] and the larger the gap lower is the reactivity. As is obvious from **Figure 3.4** from the comparison of energy gaps between graphene and few representative dienes and dienophiles, graphene is located in between their HOMOs and LUMOs. When we consider the DA reactivity of graphene (as a diene) with tetracyanoethylene (TCNE), the energy gap, $E_{H-L} = 1.7$ eV (very low value), and with maleic anhydride (MA), $E_{H-L} = 3.4$ eV. This theoretical consideration conforms very well to the experiment; TCNE reacts with graphene at room-temperature, while the reaction of graphene with MA requires about 120 ^{o}C.

In the study by Houk of the rates of DA cycloadditions of dienes with cyanoalkenes referred to above,[25] the highest rates were found in the reaction between 9,10-dimethylanthracene (DMA, IP = 7.1 eV) and tetracyanoethylene (TCNE, EA = 2.9 eV), for which $E_{H-L} = IP - EA = 4.2$ eV; whereas the DA reaction between graphene and TCNE has $E_{H-L} = 1.7$ eV and between DMA and graphene $E_{H-L} = 2.5$ eV.

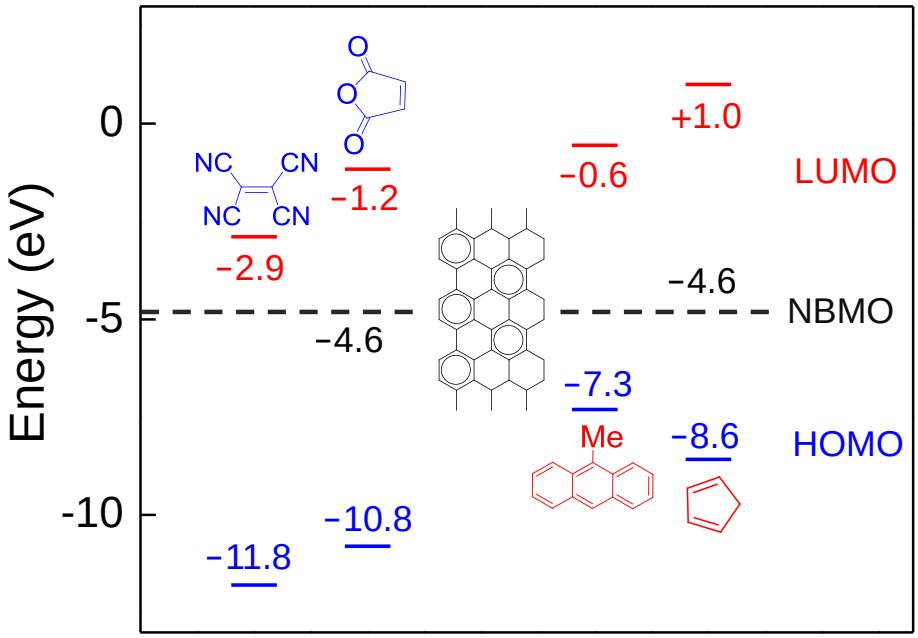

Figure 3.4. Orbital energies of selected dienes and dienophiles as obtained from ionization potentials (HOMO, –IP), electron affinities (LUMO, –EA), and the work function of graphene (W = 4.6 eV). The neutrality point in graphene corresponds to the energy of the carbon-based nonbonding molecular orbital (NBMO).[21] Reprinted with permission from ref.[21] (Sarkar, S. et al. *Acc. Chem. Res.* **2012**, 45, 673-682; Copyright © 2012 American Chemical Society).

Hence from a consideration of the orbital energies it is expected that graphene will be an extremely reactive DA partner, but in order to complete the analysis it is now necessary to examine the symmetries of the graphene orbitals which might be involved and to delineate their role in DA chemistry based on their ability to function as donor and/or acceptor according to FMO theory. Thus

we require knowledge of the FMO orbitals of graphene, that is, those orbitals which are most proximate to the Fermi level; in the case of graphene we have orbitals which cross at the Dirac point, the K point in momentum space (k) (**Figure 3.2**).

The orbitals at the Dirac point of graphene (FMOs) bear a direct relationship to the HOMOs and LUMOs of benzene as depicted in **Figure 3.5**. These orbitals comprise the FMOs of graphene and are argued to dictate the Diels-Alder reactivity of graphene. Because the e_{2u} benzene LUMO is placed in the lattice in a bonding configuration with nearest neighbors, while the e_{1g} benzene HOMO enters the lattice in antibonding relationships with nearest neighbors, they result in a pair of degenerate orbitals at the NBMO level [Dirac point K, as in **Figure 3.2-b**]. Furthermore these FMOs map directly onto the Clar representation of graphene and clearly motivates its chemical reactivity.[27]

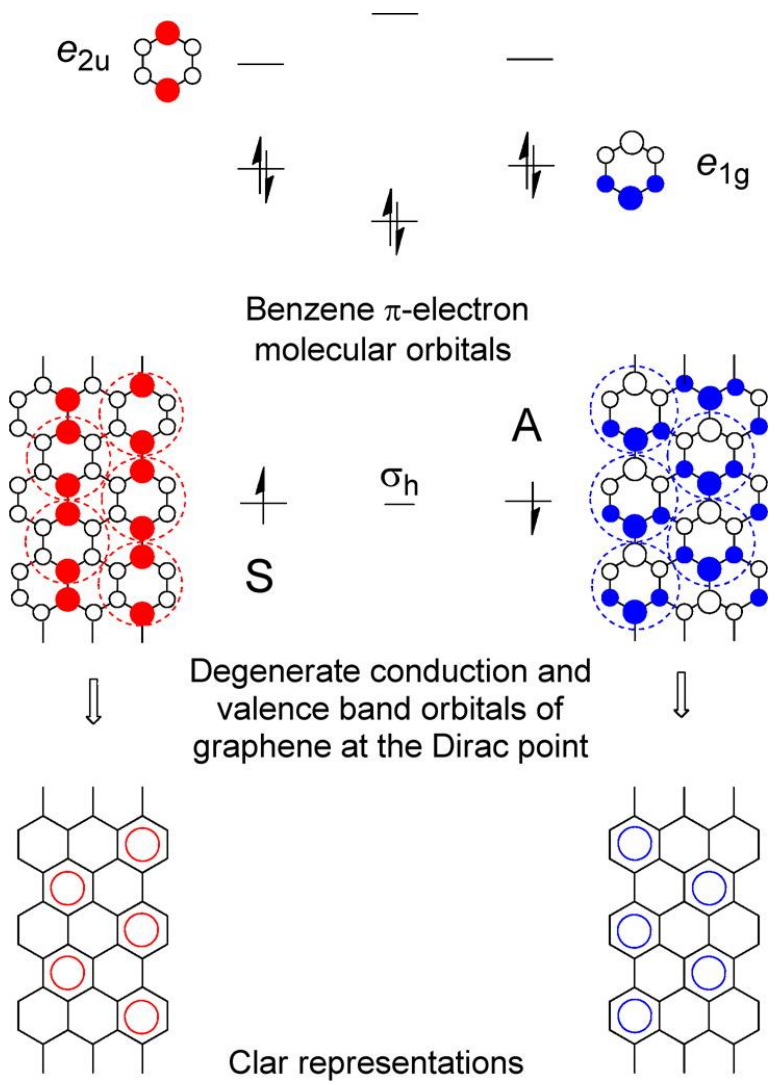

Figure 3.5. HMO energy levels of benzene and their symmetry, together with the orbital coefficients of HOMO and LUMO that map onto the degenerate conduction and valence bands of graphene at the Dirac point. These orbitals comprise the FMOs of graphene, and because the e_{2u} benzene LUMO is placed in the lattice in a bonding configuration with nearest neighbors, while the e_{1g} benzene HOMO enters the lattice in an antibonding relationship with nearest neighbors, they result in a pair of degenerate orbitals at the NBMO level [Dirac point (*K*)]. Furthermore, these FMOs map directly onto the Clar representation of graphene and clearly motivate its chemical reactivity.[21] Reprinted with

permission from ref.[21] (Sarkar, S. et al. *Acc. Chem. Res.* **2012**, 45, 673-682; Copyright © 2012 American Chemical Society).

The orbital correlation diagram (**Figure 3.6**) includes a number of unique features mainly related to the twofold degeneracy at the Dirac point; because of the degeneracy and the fact that this pair of orbitals is half-filled there is a choice in the electronic configuration, and thus the electron pair may be accommodated in either the antisymmetric (A) graphene orbital (**Figure 3.6-a**) or the symmetric (S) graphene orbital (**Figure 3.6-b**), and this allows graphene to function as both donor and acceptor within FMO theory by matching the S or A orbital symmetries of its DA partner.[23,24] In the case of ethylene the A graphene orbital donates electron density to ethylene, whereas the S orbital of graphene functions as an acceptor; the traditional picture would emphasize the former interaction.[25] Likewise, butadiene donates electron density into the empty A orbital of graphene and acts as acceptor from the S graphene orbital. Note that the orbital correlation diagram does not place any restrictions on the mode of pericyclic addition, and 1,2- and 1,4-cyclizations are allowed with both ethylene and butadiene; based on FMO theory,[24,25] the reactant atoms in graphene with the largest FMO coefficients should constitute the preferred sites of reaction. Thus according to this picture, graphene can function as diene or dienophile with equal ease; in practice graphene DA reaction preferences will depend on the orbital energies of the reacting partner, steric factors and

electron repulsion effects which are not taken into account during discussion in this chapter.

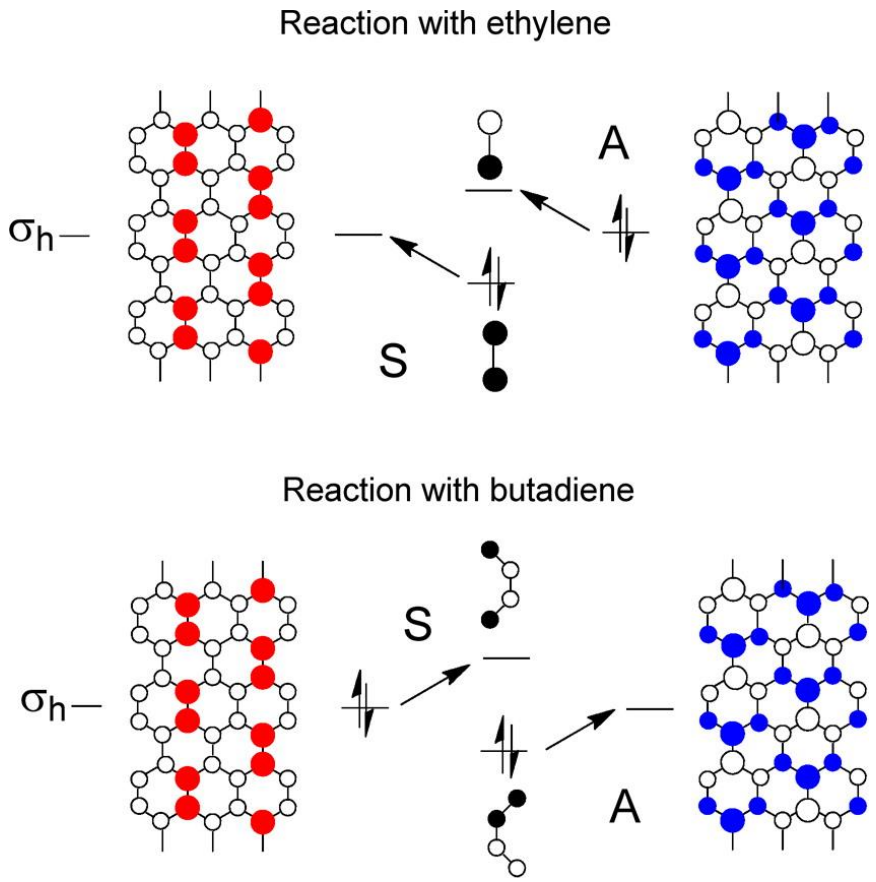

Figure 3.6. Orbital symmetry correlation diagram for the Diels–Alder reaction of ethylene and butadiene with graphene (FMOs taken from the band structure of graphene at the Dirac point) where the signs of the lobes of the p orbitals above the plane are given by open and solid circles. The symmetry classification is based on the (σ_h) vertical symmetry plane; note that this symmetry plane is rotated by 90° from that used in Figure 3.3. Reprinted with permission from ref.[21] (Sarkar, S. et al. *Acc. Chem. Res.* **2012**, 45, 673-682; Copyright © 2012 American Chemical Society).

3.4. EXPERIMENTAL RESULTS AND DISCUSSIONS

Graphene is available in various forms, and there is already strong evidence that the chemical and physical properties of the material are sensitive to the particular environment of the graphene sheet. Microcrystalline natural graphite (μG) is the most readily available commercial precursor for the generation of exfoliated graphenes;[3] single layer (SLG) and few layer graphenes (FLG) are typically obtained by exfoliation of natural graphite and studied as dispersions (XG_{sol}) or flakes (XG_{flake}), usually on a silicon dioxide substrate. Epitaxial graphene (EG) is typically grown on SiC by thermal desorption of Si above 1000 ^{o}C in vacuum or in an inert gas environment and is usually made available as rotationally disordered multilayer epitaxial graphene.[2,10] The interface layer has an energy gap and a rather complicated electronic structure that includes the presence of covalent bonds between the graphene sheet and the underlying SiC, which induces variations in the carrier concentration (doping), the work function and the graphene band structure near the Fermi level.[30,207] The enhanced reactivity of (multilayer) EG with respect to the Bernal-stacked graphite (μG and HOPG) discussed below, is of interest with respect to previous studies of the reactivity of the various forms of graphene;[98,104,150] apart from the differences discussed above, an obvious distinction is the splitting that occurs at the K point in graphene as a result of the interlayer interaction.[42] At the level of simple tight binding theory, allowance for additional transfer integrals to describe the various interactions in the 3-D

graphite lattice leads to a bandwidth of ~1.5ev at the K points and the material becomes a semimetal with a band overlap of ~0.1ev.[42]

The conversion of sp^2 to sp^3 carbon atoms due to chemical reaction leads to distinct changes in the Raman spectra of graphene,[91,150] and the presence of a D-band in the Raman spectrum of functionalized graphene is routinely used as evidence for covalent bond formation.[13,18,91,106,119,150,208]

Our current experimental findings are summarized in **Scheme 3.2**, and it is apparent that graphene reversibly undergoes DA reactions with various reaction partners and is able to function as diene or dienophile as suggested by the foregoing analysis (**Figures 3.3-3.6**). We have found that the DA reaction is highly sensitive to the nature of graphene, the substrate on which graphene is placed (e.g. SiO_2, *h*-BN, SiC, Cu etc.), reaction temperature, solvent, doping etc.. The Diels-Alder reactions of graphene are demonstrated below in details.

3.5. GRAPHENE AS A DIENE

Graphene was found to be very reactive toward tetracyanoethylene (TCNE), and the reactions proceed at room temperature;[18] (in agreement with the very low value of E_{H-L} = 1.7 eV calculated for this reaction),[21] whereas functionalization with maleic anhydride (MA), required a reaction temperature of about 120 ^{o}C, presumably as a result of the higher value of E_{H-L} = 3.4 eV

calculated for this reaction. There is already strong evidence for doping reaction channels (electron transfer processes) which compete with covalent functionalization reactions in graphene chemistry,[30,209] and we also observed the occurrence of p-type doping (oxidation) by the highly electron-deficient reagent, tetracyanoethylene (TCNE, electron affinity = 2.88 eV)[25] in preference to the simple Diels–Alder reaction. Formation of charge transfer (CT) complex between graphene (electron donor) and TCNE (electron acceptor) in solution phase was previously reported by Rao and co-workers in 2008; the formation of such CT complexes was observed by Raman and solution UV-vis spectroscopy.[148]

3.5.1. Reactions with Tetracyanoethylene (TCNE)

The chemical behaviour of graphene as a diene is illustrated in **Figure 3.7** by its reactivity with the electron-withdrawing dienophile, tetracyanoethylene (TCNE). Raman spectroscopy is employed to monitor the progress of the reaction and to track the differential reactivity of SLG, FLG, and HOPG; **Fig. 3.7c** shows an increase of I_D/I_G ratio in the TCNE-SLG adduct to 2.53 from 0.03 in pristine SLG, while the I_D/I_G ratio is 0.28 in TCNE-FLG and 0.17 in TCNE-HOPG for reactions conducted under identical conditions.[18,21] The differential evolution of the D-band in the presence of the same DA chemistry suggests the following order of reactivity in DA chemistry: SLG >> FLG > HOPG.

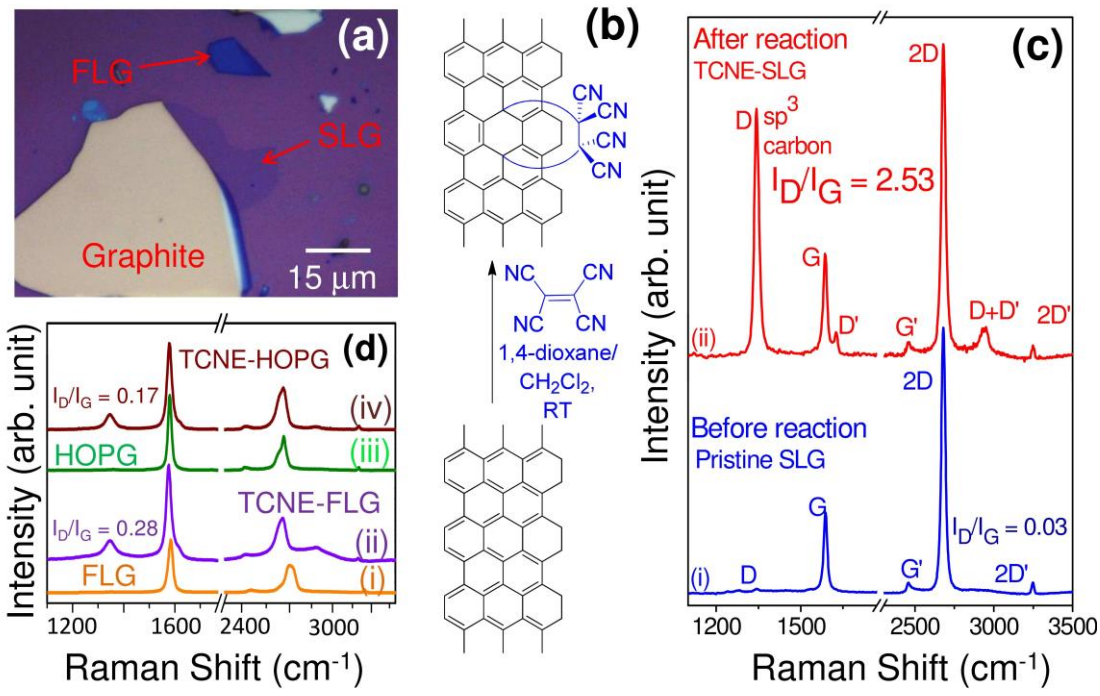

Figure 3.7. Graphene as diene: (a) optical micrograph of single-layer (SLG), few-layer graphene (FLG) and graphite (HOPG). Contrast in the image is increased by 30% to enhance clarity. (b) Schematics of the room-temperature reaction of graphene (as diene) with tetracyanoethylene (TCNE, dienophile). Differential reactivity of (c) SLG,[22] (d) FLG, and graphite (HOPG) in the Diels-Alder chemistry with TCNE is manifested by the evolution of the Raman D-band.

3.5.2. Reactions with Maleic Anhydride (MA)

It was observed that the reaction proceeds most effectively at 120 °C (**Figure 3.8-d**) and the product decomposes at higher temperature and at 150

^{o}C the product reverses to almost its pristine HOPG state, suggesting the operation of retro-Diels-Alder reactions at higher temperature. The Raman spectra of MA-HOPG adduct (**Figure 3.8-d**) shows a strong D band at ~1341 cm^{-1} with FWHM (full width at half maximum) of 50 cm^{-1} and I_D/I_G = 0.63; other peaks are observed at 1572 (G), 1614 (D'), 2445 (G'), 2691 (2D), 2936 (D+D'), 3236 (2D') cm^{-1}.

The formation of graphene adducts with maleic anhydride (MA) was found to be sensitive to the nature of the graphene sample and to the reaction temperature. Examination of a variety of reaction conditions in conjunction with Raman spectroscopy of the products, led to the following optimum temperatures for the MA reaction: HOPG (120 °C, **Figure 3.8**), XG_{sol} (130 °C) and EG (70 °C, **Figure 3.9**).

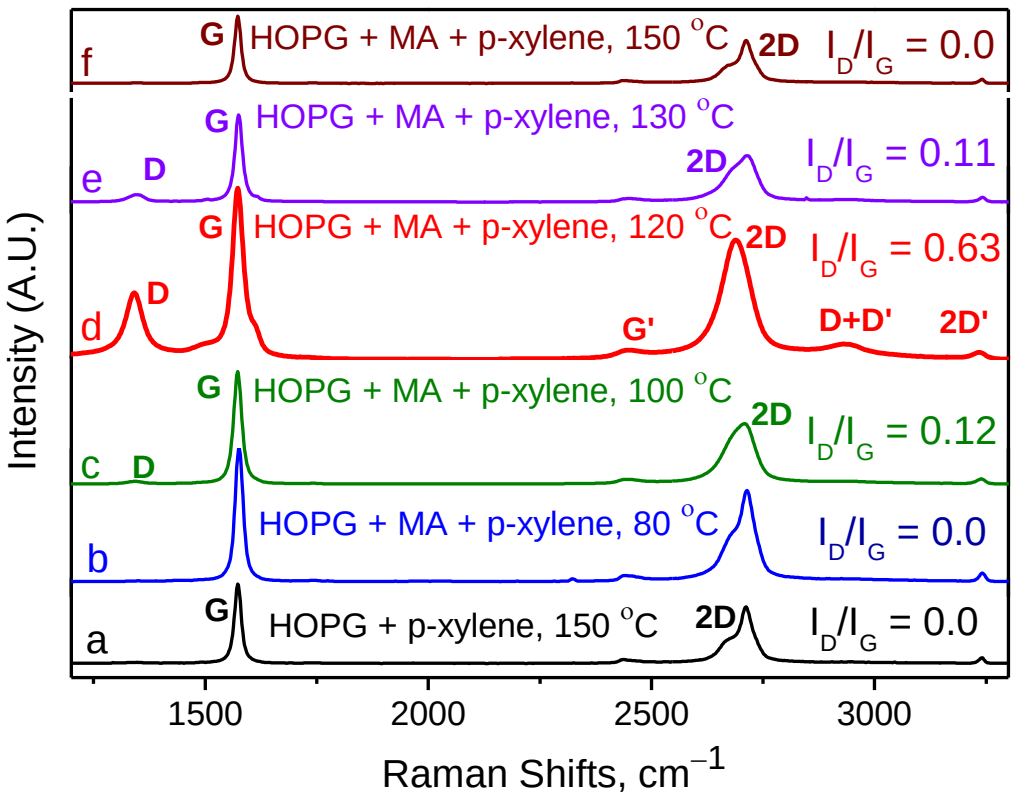

Figure 3.8. Raman spectra of the thermal Diels–Alder adducts MA-HOPG, obtained by reaction between HOPG (diene) and maleic anhydride (dienophile) at different temperatures: (a) HOPG and *p*-xylene (solvent) at 150°C, with no maleic anhydride (dienophile) added; HOPG, reacted with maleic anhydride in p-xylene at (b) 80°C: I_D/I_G = 0.0, (c) 100°C: I_D/I_G = 0.12, (d) 120°C: I_D/I_G = 0.63, (e) 130°C: I_D/I_G = 0.11 and (f) 150°C: I_D/I_G = 0.0.[18] Reprinted with permission from ref.[18] (Sarkar, S. et al. *J. Am. Chem. Soc.* **2011**, 133, 3324-3327; Copyright © 2011 American Chemical Society).

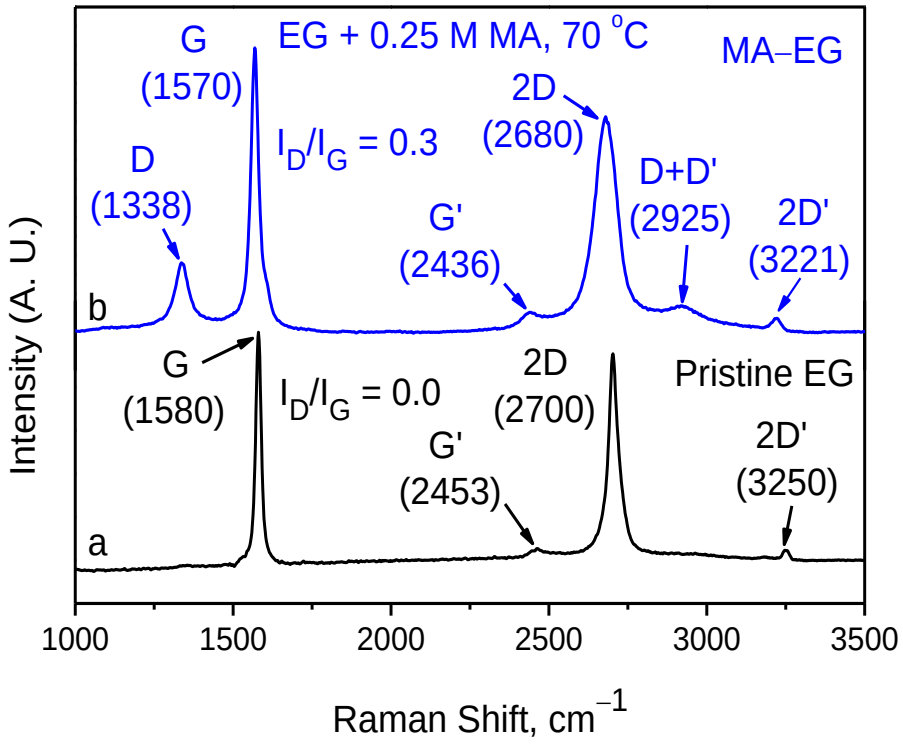

Figure 3.9. The Raman spectra of (a) pristine epitaxial graphene, EG (before functionalization), (b) after functionalization at 70 °C, MA-EG using ~0.25 M maleic anhydride in *p*-xylene.[18] Reprinted with permission from ref.[18] (Sarkar, S. et al. *J. Am. Chem. Soc.* **2011**, 133, 3324-3327; Copyright © 2011 American Chemical Society).

The presence of the maleic anhydride functionality in the MA-XG product obtained at 130 °C is also observed in the IR spectrum (**Figure 3.10**). The ATR spectrum of the MA-Graphene shows the following characteristic infrared features: 896 (C–C stretch), 1013, 1042, 1177, 1200, 1238 (C–H deformation), 1300 (C–O stretch), 1600 (C=C stretch), 1700 (symmetric C=O stretch,

–COOH, due to hydrolyzed maleic anhydride), 1775 (symmetric C=O stretch), 1860 (asymmetric C=O stretch), 2850 (C_{sp3}–H stretch) and 2925 (C_{sp3}–H stretch) cm^{-1}. For the maleic anhydride monomer[210] the observed infrared frequencies can be assigned as follows: 1057 (C–H deformation), 1240 (C–H deformation), 1289 (C–O stretch), 1594 (C=C stretch), 1775 (symmetric C=O stretch), 1855 (asymmetric C=O stretch), 3122 and 3187 (C-H stretch) cm^{-1}.

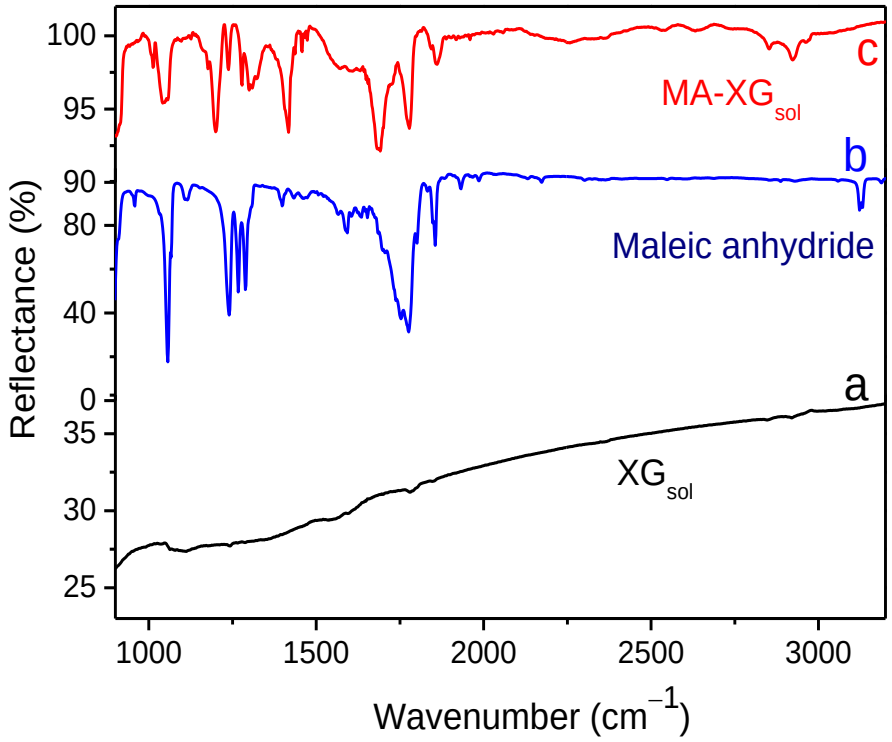

Figure 3.10. The ATR spectra of (a) exfoliated graphene (XG_{sol}), (b) maleic anhydride (MA), and (c) MA-XG_{sol}, the thermal Diels-Alder adduct, obtained by reaction of exfoliated graphene with maleic anhydride at 130°C in *p*-xylene.[18] Reprinted with permission from ref.[18] (Sarkar, S. et al. *J. Am. Chem. Soc.* **2011**, 133, 3324-3327; Copyright © 2011 American Chemical Society).

3.6. GRAPHENE AS A DIENOPHILE

3.6.1. Reactions with 9-Methylanthracene (MeA)

After optimization, we observed that 9-methylanthracene (MeA) cycloadducts (**Scheme 3.2**) could be obtained in high yield (I_D/I_G > 1), by treating HOPG, or XG_{sol} with a *p*-xylene solution of MeA at 130°C. The Raman spectra of MeA–XG_{sol} shows the following peaks: D (1337 cm^{-1}, with the FWHM = 70 cm^{-1}), G (1584 cm^{-1}), D' (1630 cm^{-1}), G' (2448 cm^{-1}), 2D (2677cm^{-1}), D+D' (2934 cm^{-1}), and 2D' (3236cm^{-1}).

The MeA-XG products were characterized with ATR-IR (**Figure 3.11-c**), which shows the following characteristic frequencies: 869 (in-phase C–H, wagging vibrations of aryls, most intense band), 1070 (C–H deformation), 1120, 1285 (C–H deformation), 1378, 1420 (C_{sp2}–H, bending, aromatic), 1437 (C_{sp3}–H bending), 1460 cm^{-1} (C_{sp3}–H, bending, of –CH_3), 1490 (asymmetric C_{sp3}–H bending), 1508 (in-plane C–H ring band), 1541 (C=C bending aromatic), 1600 (C=C, stretch, of graphene), 1735 (C=C, stretch, alkenyl), 2850 (symmetric C_{sp3}–H, stretch, –CH_3), 2917 (asymmetric C_{sp3}–H, stretch, –CH_3), and 2960 (C_{sp2}–H, stretch, aromatic). For 9-methylanthracene (**Figure 3.11-b**), the following characteristic infrared frequencies are observed: 780 (in-phase C–H wagging vibration of aryls), 885 (C–H deformation), 1350 (C–H bending of

–CH_3), 1622 (C=C stretch), 2850 (symmetric C_{sp3}–H stretch), 2930 (asymmetric C_{sp3}–H stretch), and 3050 (C_{sp2}–H stretch, aromatic) cm^{-1}.[174,175]

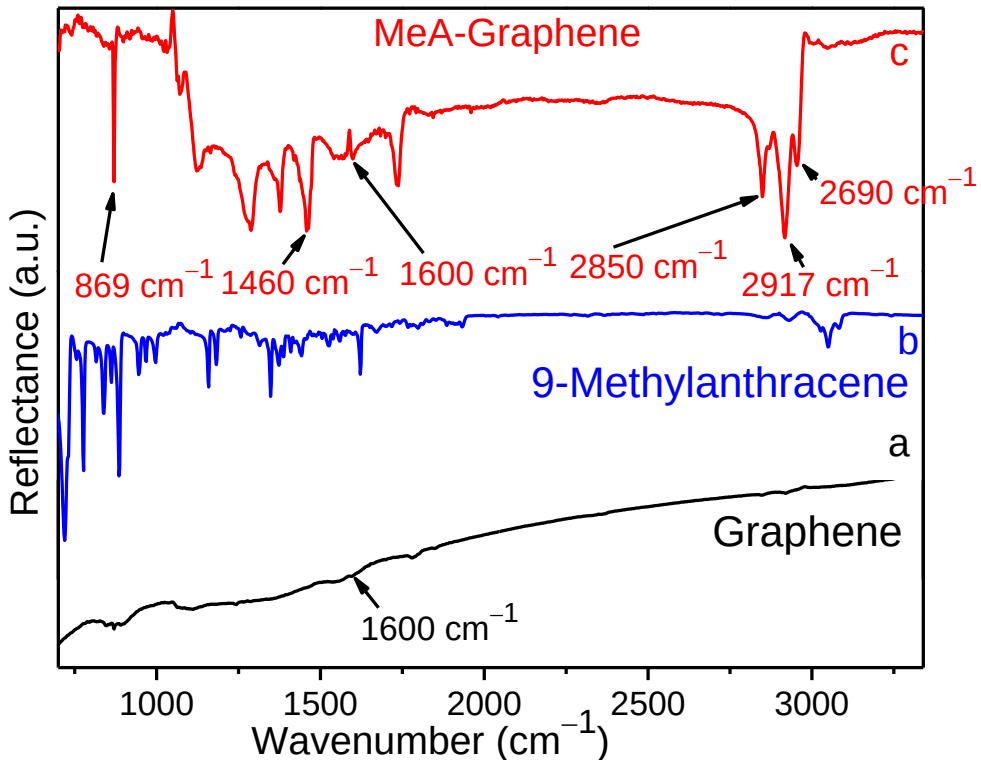

Figure 3.11. The FTIR reflectance spectra (ATR, Ge) of (a) exfoliated graphene, (b) 9-methylanthracene (MeA), and (c) MeA-Graphene, the Diels–Alder adduct of the 9-methylanthracene (MeA) and exfoliated graphene (XG).[18] Reprinted with permission from ref.[18] (Sarkar, S. et al. *J. Am. Chem. Soc.* **2011**, 133, 3324-3327; Copyright © 2011 American Chemical Society).

3.6.2. Reactions with 2,3-Dimethoxy-1,3-Butadiene (DMBD)

The use of graphite and graphene as a dienophile in the Diels-Alder reaction was also investigated by another electron-rich diene, 2,3-dimethoxy-1,3-butadiene (DMBD). The optimum temperature for the Diels–Alder reactions with DMBD was found to depend on the nature of the graphitic material as follows: HOPG (130 ^{o}C), μG (120 ^{o}C; **Figure 3.13-b**), XG_{flake} and XG_{sol} (130 ^{o}C; **Figure 3.12-a**), and EG (50 ^{o}C; **Figure 3.13-c**).[18] The reaction can be reversed in all cases at about 170 ^{o}C, switching the functionalized graphene back to the pristine material.

(A) Diels-Alder Chemistry of Scotch Tape Exfoliated SLG and BLG

Application of the Diels-Alder (DA) chemistry of graphene (SLG, BLG; dienophile) with a diene (2,3-dimethoxy-1,3-butadiene; DMBD), which leads to creation of 1,2-sp^3 centers on graphene lattice (**Figure 3.12-a**). As discussed in earlier chapters and in the reports on the Raman spectroscopy of graphene[211] that the creation of sp^3 centers on graphene lattice is accompanied by appearance of a new peak (called as D-peak, which is due to intervalley scattering) at ~1345 cm^{-1} in the Raman spectrum of graphene, which is otherwise absent in defect-free pristine SLG.[15] The pristine SLG is often distinct from graphene layers by the fact that it possesses a sharp single 2D peak (at ~2690 cm^{-1}) with a G peak (at ~1580 cm^{-1}) with the intensity of 2D greater than

the G peak (here I_{2D}/I_G = 3.11). Thus the ratio of D to G peaks (I_D/I_G) can quantify the relative content of the sp^3 carbon centers, and provides a useful index of the degree of chemical functionalization.[15] The DA chemistry of pristine SLG with DMBD leads to a graphene derivative (DA-SLG) leads to an increase of I_D/I_G ratio to 0.35 as compared to 0.01 in pristine SLG (**Figure 3.12-b**). Thermal retro-DA of the graphene adducts leads to clean regeneration of graphene at its nearly pristine state making reversible switching of the graphene devices feasible [**Figure 3.12-b-(iii)**].

Two dimensional Raman maps of the ratio of integrated area of D-band (centered at ~1355 cm^{-1}) to the integrated area of G-peak (centered at ~1581 cm^{-1}) with 3671 spectra each, at points spaced 1 μm apart, are collected in the selected ~80 μm $\times$ 50 μm sample areas of the graphene flakes on an oxidized silicon wafer (**Figure 3.12-c**) for comparison and to obtain statistical information of functionalization homogenity. The graphene flake studied here has both the single-layer (SLG, area 1, 3) and bilayer graphene (area 2) on oxidized silicon wafer, as was thoroughly confirmed by optical microscopy (**Figure 3.12-c**), Raman spectroscopy (**Figure 3.12-b**) and Raman band mapping experiments.

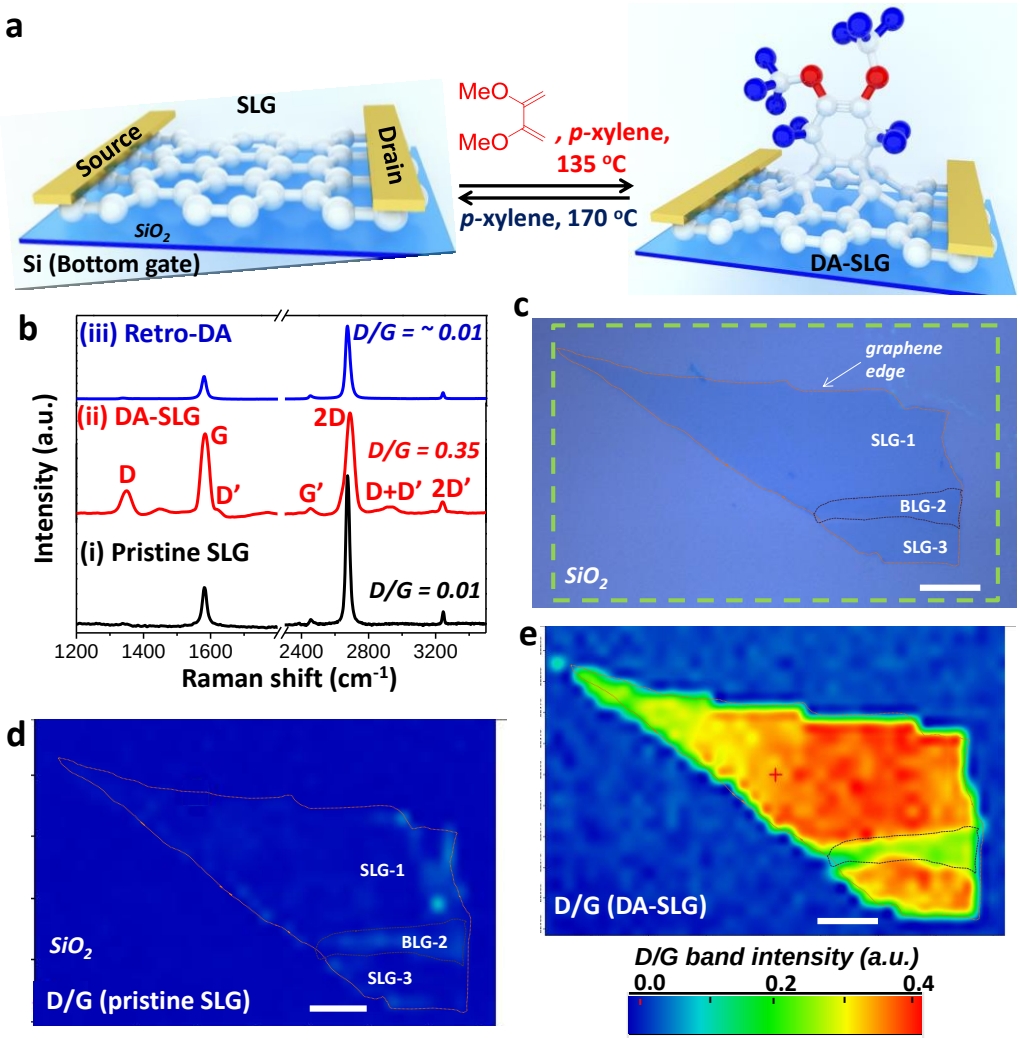

Figure 3.12. Diels-Alder chemistry of graphene (dienophile). a, Schematics of the Diels-Alder (DA) chemistry of single layer graphene, SLG (dienophile) device with 2,3-dimethoxy-1,3-butadiene (DMBD, a diene). The retro-Diels-Alder chemistry, which happens at 170 ^{o}C leads to graphene devices at its nearly pristine state. **b**, Evolution of Raman spectra (λ_{ex} = 532 nm, spot size = 0.7 μm) of SLG (i) before (pristine), (ii) after DA chemistry with DMBD (DA-SLG), and (iii) after retro-DA reaction. **c**, Optical image of a graphene flake showing both SLG and bilayer graphene (BLG). Raman mapping of the

selected area (shown by rectangular box) of the graphene flake in **figure c** for: **d**, the ratio of integrated area of D peak to G peak (A_D/A_G) for the pristine SLG and BLG flake (before reaction), confirming the presence of defect free graphene (negligible D peak). **e**, Raman imaging of the DA modified flake (DA-SLG) for the A_D/A_G shows that the SLG show pronounced increase in D to G band intensity than the BLG after the DA chemistry. Scale bar = 10 μm.

The pristine graphene used for this study was defect free over the whole regions (**Figure 3.12-d**). As can be seen in **Figure 3.12-e** that DA-SLG adduct has moderate degree of sp^3-centers over most of the SLG region (regions 1 and 3, as compared to pristine SLG), while the DA modified bilayer graphene (DA-BLG, region 2) shows low D/G ratio. Note that the relative ratios of intensities of Raman 2D to G band varies with different number of graphene layers: I_{2D}/I_G (= 3.11 for SLG in **Figure 3.12-b**) > I_{2D}/I_G (= 0.73 for BLG, not shown here).[22]

(B) Diels-Alder Chemistry of Microcrystalline Graphite (μG)

The reaction of microcrystalline graphite (μG) with the electron-rich diene, 2,3-dimethoxy-1,3-butadiene (DMBD) was found to be a particularly effective route for producing stable, colloidal dispersions of single–layer functionalized graphene flakes from graphite, as evidenced by the sharp 2D peak (located at ~ 2684 cm^{-1}, with I_{2D}/I_G = 0.73) in the Raman spectra of the resulting DMBD–μG materials (**Figure 3.13-b**).[18] There is considerable interest in using such

functionalization schemes to produce bulk quantities of solution re-dispersible graphene materials which do not readily aggregate in solution;[19,117,151] and the covalent Diels–Alder functionalization approach is a viable option in this regard, particularly because of the clean reversibility of the reaction.

(C) Diels-Alder Chemistry of Epitaxial Graphene (EG)

The electronic structure of the graphene surface after DA chemistry is of great interest from the standpoint of the application of organic chemical process lithography to the band gap engineering of graphene devices.[30] The transport properties of DMBD-EG (**Figure 3.13-d**) shows that the room temperature resistance of the functionalized sample is increased by 60% and the temperature dependence is activated (semiconducting). The temperature dependence of resistance, shown in Figure **3.13-d**, shows a change in the transport mechanism: EG exhibits a slight decrease of resistance with temperature with a cross-over to metallic behavior below 110K, whereas DMBD-EG shows non-metallic behavior over the whole temperature range, characteristic of weak localization.[212,213] This indicates that the Diels-Alder chemistry on the top layer of epitaxial graphene (EG) is quite efficient in modifying the electronic structure of the graphene sheet.

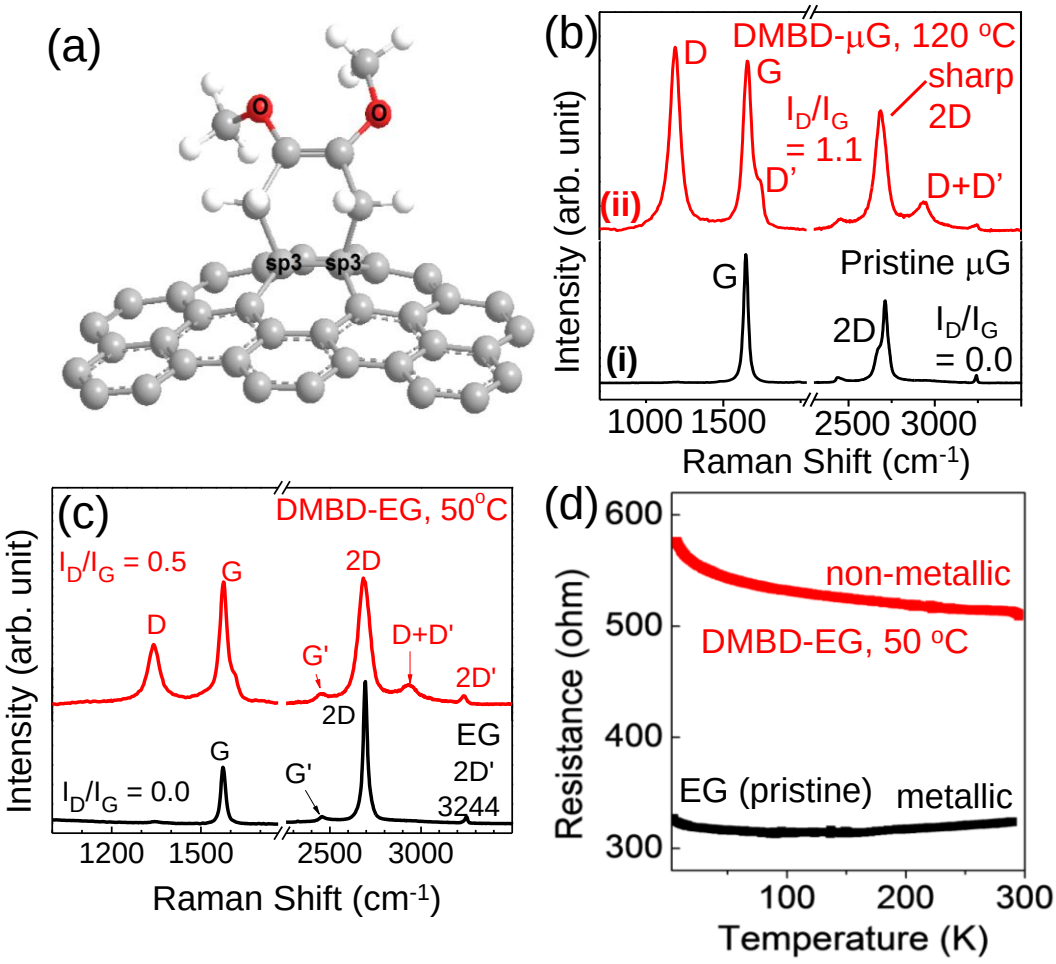

Figure 3.13. (a) Three-dimensional structure of the Diels-Alder adduct of graphene and 2,3-dimethoxy-1,3-butadiene (DMBD), showing the creation of a pair of sp^3 carbon centers in the graphene lattice and the generation of a slightly non-planar structure.[21] (b) Raman spectra (λ_{ex} = 532 nm) of pristine microcrystalline graphite (μG) and its Diels-Alder adduct, DMBD-μG obtained at 120 °C.[21] (c) Raman spectra (λ_{ex} = 532 nm) of pristine epitaxial graphene (EG) and its Diels-Alder adduct, DMBD-EG obtained at 50 °C.[18] (d) Temperature dependent resistance of EG wafer (before reaction) and DMBD-EG (after reaction); functionalization of EG with DMBD leads to a 60% increase in room

temperature resistance, and the DMBD-EG shows non-metallic behavior over the full temperature range.[18]

(D) Scanning Tunneling Microscopy (STM) of Pristine and the Diels-Alder Functionalized Epitaxial Graphene

A particularly direct probe of the electronic structure of the functionalized graphene surface is afforded by scanning tunneling microscopy (STM), which can also give the surface coverage of the functional groups and their periodicities over the whole graphene wafer; however, this technique typically requires ultra-high vacuum and cryogenic temperatures.[30,155,214]

Both theoretical calculations and experimental data have shown that the single atom sp^3 functionalization sites that result from a radical addition process, in both graphite and graphene, generate threefold symmetric patterns in the local density of states (LDOS) as a result of presence of the unpaired spin which is localized in the vicinity of the point of addition.[30,161,165,215,216] These patterns can be enhanced by two-dimensional fast Fourier transform (2D-FFT) filtering of STM images acquired under ambient conditions, and it has been shown that positive and negative spin densities become localized at the **A** and **B** sublattices, in a threefold symmetric super-lattice.[215] The Diels-Alder cycloaddition chemistry is expected to occur by the pairwise formation of 1,4-,

or 1,2-sp^3 carbon centers in the regular honeycomb lattice of sp^2 carbon atoms, and thus antiferromagnetic (diamagnetic) products are expected,[29] because this pattern of chemistry guarantees the balanced functionalization of the **A** and **B** graphene sublattices. Hence the electronic structure of the Diels-Alder functionalized graphene lattice will be completely different from that formed in the atom-by-atom reactions of graphene with nitrophenyl radicals or hydrogen atoms.[30,161,165,214-216]

The STM images of defect-free, pristine 1-3 layer EG and DMBD-EG are compared in **Figure 3.14**; the STM images are collected using a Digital Instruments Nanoscope IIIa multimode scanning probe microscope (Pt/Ir tips) under ambient conditions. The 2D FFT spectrum of the STM image of EG consists of six outer bright spots from the graphene super-lattice and six spots corresponding to the graphene lattice in the center, which appear as the large bright spot at the center in the insets of **Figure 3.14-a** and **3.14-d**. The higher order spots are filtered in the FFT spectrum (**Figure 3.14-b** and **3.14-e**), which improves the image by removing the noise, whereas in **Figure 3.14-c** and **3.14-f** the graphene lattice is also filtered by removing everything inside the largest circle circumscribed by the hexagon of the superlattice points, yielding an image which reflects the modified LDOS.[30] The 2D-FFT filtered LDOS given in **Figure 3.14-f** shows scattering and interference patterns over the entire image and it is

clear from **Figures 3.14-c** and **3.14-f** that the DA reaction with DMBD leads to a striking reconstruction of the epitaxial graphene electronic structure.

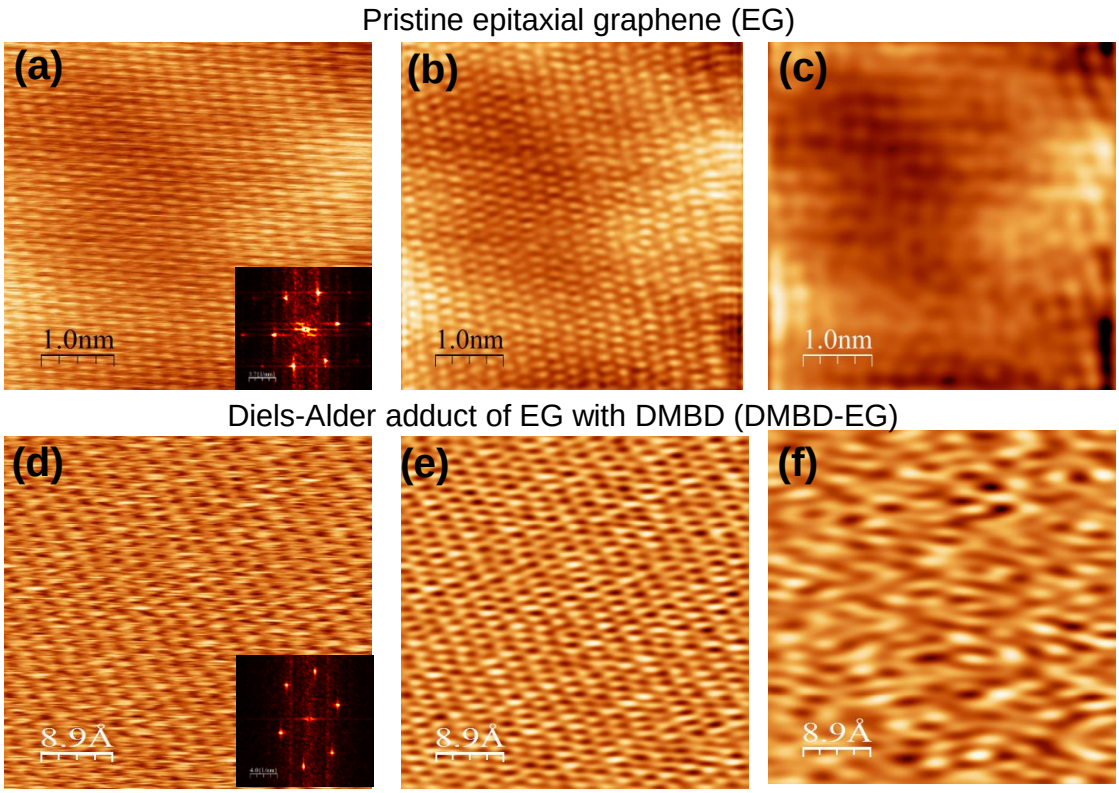

Figure 3.14. STM current images of pristine EG (a,b,c) and 2,3-dimethoxy-1,3-butadiene functionalized epitaxial graphene, DMBD-EG (d,e,f) under ambient conditions. (a) Pristine EG, V_{bias} = + 5.1 mV, I_t = 4.3 nA; 2D-FFT spectrum of the STM image is shown in the inset. (b) STM image of EG after subtracting noise. (c) 2D-FFT filtered STM image of EG. (d) DMBD-EG, V_{bias} = + 5 mV, I_t = 3 nA; 2D-FFT spectrum of the STM image is shown in the inset. (e) STM image of DMBD-EG after subtracting noise. (f) 2D-FFT filtered STM image of DMBD-EG.[21] Reprinted with permission from ref.[21] (Sarkar, S. et al. *Acc. Chem. Res.* **2012**, 45, 673-682; Copyright © 2012 American Chemical Society).

(E) Solution Spectroscopic Estimation of Surface Coverage of Functional Groups on Graphene

A prime question in chemical modification of graphene is to what extent the graphene surface is functionalized (surface coverage) and how the functional groups (new sp^3 centers) are distributed on graphene lattice. Accurate estimation of the density of functional groups over graphene still remains a major challenge.

To date the methods, such as correlating with the Raman I_D/I_G ratio,[91,93] electrochemical charge of the oxidation or reduction of the attached electro-active species,[15] TGA, XPS, STM etc., employed to do so are limited to the merits and drawbacks of the technique.[217] In search of a comprehensive technique to accurate estimate the graphene coverage, we have developed solution mid-IR and Raman spectroscopic approach for calculation of the coverage of the graphene surface with the DMBD group. Diels-Alder chemistry of DMBD with graphene converts the terminal olefinic $=C_{sp2}H_2$ groups to aliphatic secondary (2^o) $>C_{sp3}H_2$ (methylene) groups; such a conversion of C_{sp2}–H to C_{sp3}–H is accompanied by a large shift of mid-IR frequencies to lower wavenumber. We employ solution mid-IR spectroscopy of DMBD adduct of solvent exfoliated graphene (DMBD-XG_{sol}), and we monitor the changes in C–H stretches in solution mid-IR spectroscopy. Solid-state devices are difficult to

study; we, therefore, employed liquid-phase exfoliated graphene (XG_{sol})[149,218] for our solution studies.

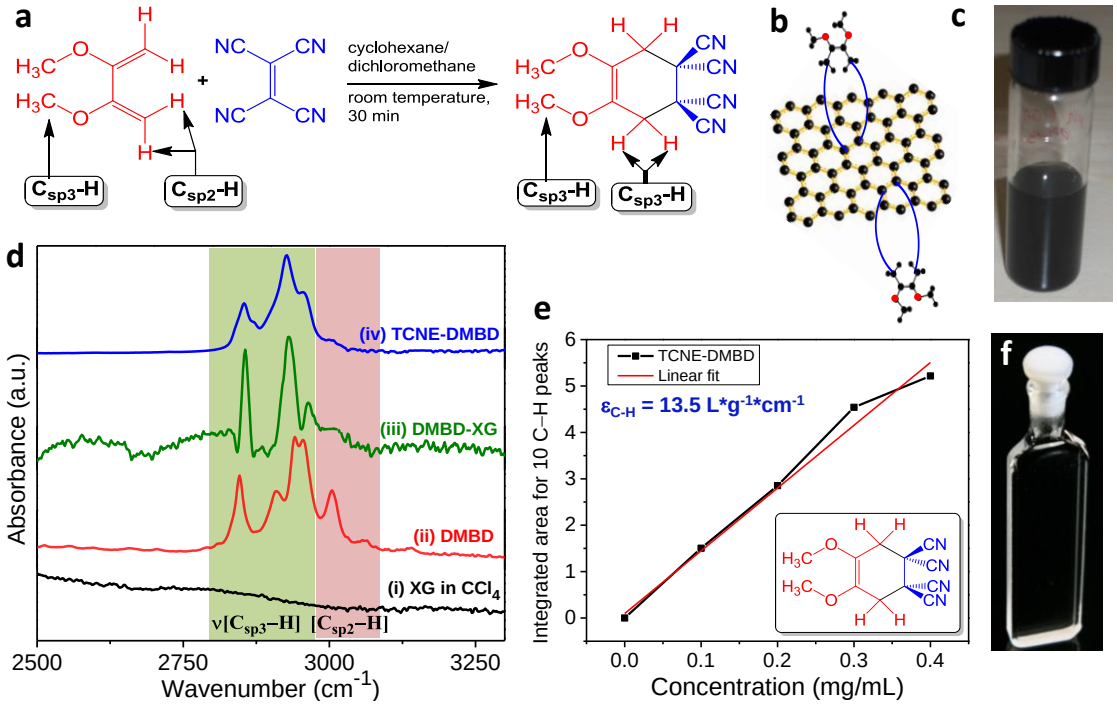

Figure 3.15. Solution spectroscopic estimation of Diels-Alder modified graphene dispersions. (a) Schematics of the room-temperature Diels-Alder reaction between 2,3-dimethoxy-1,3-butadiene (DMBD, a diene) and tetracyanoethylene (TCNE, a dienophile). (b) 3D structure of the adduct of DMBD and liquid-phase exfoliated graphene (XG_{sol}). (c) Picture of the solution of DMBD-XG. (d**)** Solution mid-IR spectroscopy (in CCl_4, 1 mm quartz cell) of (i) XG, (ii) DMBD, (iii) DMBD-XG and (iv) the DMBD-TCNE adduct. (e) Plot of integrated absorbance of 10 C-H peaks of TCNE-DMBD against concentration of the TCNE-DMBD solution. (f) Picture of the cell (1 m m) used for solution-IR spectroscopy.

In order to compare the C–H stretches of the DA adduct of exfoliated graphene (DMBD-XG_{sol}), a model DA adduct of small organic diene and dienophiles with similar C–H chemical environments was synthesized by a controlled reaction between DMBD and tetracyanoethylene (**Figure 3.15-5a**) and probed by solution mid-IR spectroscopy in carbon tetrachloride in quartz cell. As expected, the mid-IR C–H stretches of (DMBD-XG_{sol}, **Figure 3.15-b,c**) in Figure **3.15-d(iii)** is similar to that of TCNE-DMBD adduct (**Figure 3.15-d-iv**). From the plot of C–H absorbance (integrated area between 2700-3000 cm^{-1} as in **Figure 3.15-d**) against concentration of TCNE-DMBD yields the extinction coefficient per unit C–H peak as 13.52 $Lg^{-1}cm^{-1}$ (**Figure 3.15-e**). Solution Raman spectroscopy has revealed that the DMBD-XG_{sol} in solution stays as nearly monolayer of graphene, presumably due to the ability of the Diels-Alder chemistry to make solution re-dispersable graphene.[21] Taking account of all the solution spectroscopic studies we conclude that there is 1 functional group in about 1000 carbon atoms in the graphene lattice, or in other words, in this sample 500 carbon atoms of graphene have one sp^3 center.

3.7. APPLICATIONS: BAND GAP ENGINEERING AND HIGH MOBILITY GRAPHENE DEVICES

Graphene lattice is a bipartite lattice with two sublattices A and B, which are chemically equivalent, but crystallographically inequivalent.[22] The Diels-

Alder chemistry of graphene leads to the formation of a pair of sp^3 centers (or divacancies) on graphene lattice (**Figure 3.16-a**), and therefore, can offer the potential for balanced functionalization of graphene A and B sublattices. If we consider a Hamiltonian containing only nearest-neighbor hopping (uncompensated lattice) each A atom is coupled with only B atoms and vice versa.[219,220] Consequently, at very low concentration of vacancies (isolated simple vacancies, e.g. one produced by the chemisorption by single hydrogen atom or by single addition of aryl radicals),[112] the distribution of vacancies is locally uneven between the two sublattices and zero energy states necessarily appear.[220,221]

Theoretical studies on the quantum diffusion of electrons in graphene with local defects (e.g. chemically induced vacancies) have revealed that if vacancies are arranged by pair of nearest neighbor vacancies (divacancies, e.g. one produced by the present Diels-Alder method), the electronic structure at low defect concentration (low functional group coverage) is completely different.[222] Indeed in that case, the distribution of vacancies is locally even between the two sublattices, and zero energy state does not occur.

Earlier reports of calculation on the effect of such vacancies on electronic transport properties suggest the following. (1) For low coverage, around Dirac point, a single vacancy can cause more scattering, which will significantly

reduce the mean free path and, in turn, reduce the device mobility. (2) For high coverage (heavily functionalized samples), both the two conditions behaves similarly with highly resistive samples, and a transport gap should be observed. In our present case we believe that the mean free path should be main factor which will affect mobility. Based on this, the uneven distribution of defects should indeed affect transport properties of electrons.

Around the Dirac Point, at same coverage rate, even though the DOS of single vacancy and divacancy systems are in the same order; the mean free path (l_{mean}) of charge carriers in divacancy system is about one order larger than that of single vacancy system (for coverage <10%) and in case of graphene:[154,223]

$$\mu = \frac{el_{mean}}{m^* v_F} \qquad \text{.....(3.2)}$$

where μ is mobility of the sample; m^* is the effective mass of charge carriers, v_F is the Fermi velocity and e is elementary charge. This means that the mobility is proportional to mean free path. So for these lightly functionalized samples, around the Dirac Point the mobility of Diels-Alder modified (divacany) graphene system can be much higher than that of single vacancy systems.[20,222] This is indeed what we observe in our present application of Diels-Alder chemistry on single-layer graphene devices in which device mobility if not significantly reduced and preserved to a great extent.

After functionalization with the Diels-Alder method, we observed significant changes on transport properties: the conductance and mobility decreased by a factor of ~3 and *I(V)* curves became non-linear especially at low temperature (**Figure 3-16-b,c**). Typically, our devices can reach an acceptable on/off ratio ~10, which is comparable to previous organometallic hexahapto (η^6-) functionalization method.[224] Since the mobility of our devices only dropped by a factor of 2-3 after chemical treatment, which is much better than the previous reported results;[20,123,225] this enabled us to harvest even higher mobility from functionalized devices. At low temperature (~4.5 K), the mobility of functionalized devices is in the range of 1,000~6,000 $cm^2V^{-1}s^{-1}$. Even at room temperature, it still can reach 3,400 cm^2/Vs. This result impressively surpassed all the previously reported values in functionalized graphene-based device's field-effect mobility (~1-200 $cm^2V^{-1}s^{-1}$ in nitrophenyl functionalized SLG,[20] 10 $cm^2V^{-1}s^{-1}$ in graphane,[119] ~0.01-12 $cm^2V^{-1}s^{-1}$ in reduced single-layer graphene oxide,[225-227] 5 $cm^2V^{-1}s^{-1}$ in fluorographene[123]) and far exceeds the mobility of Si (~280 $cm^2V^{-1}s^{-1}$ in doped Si).[30]

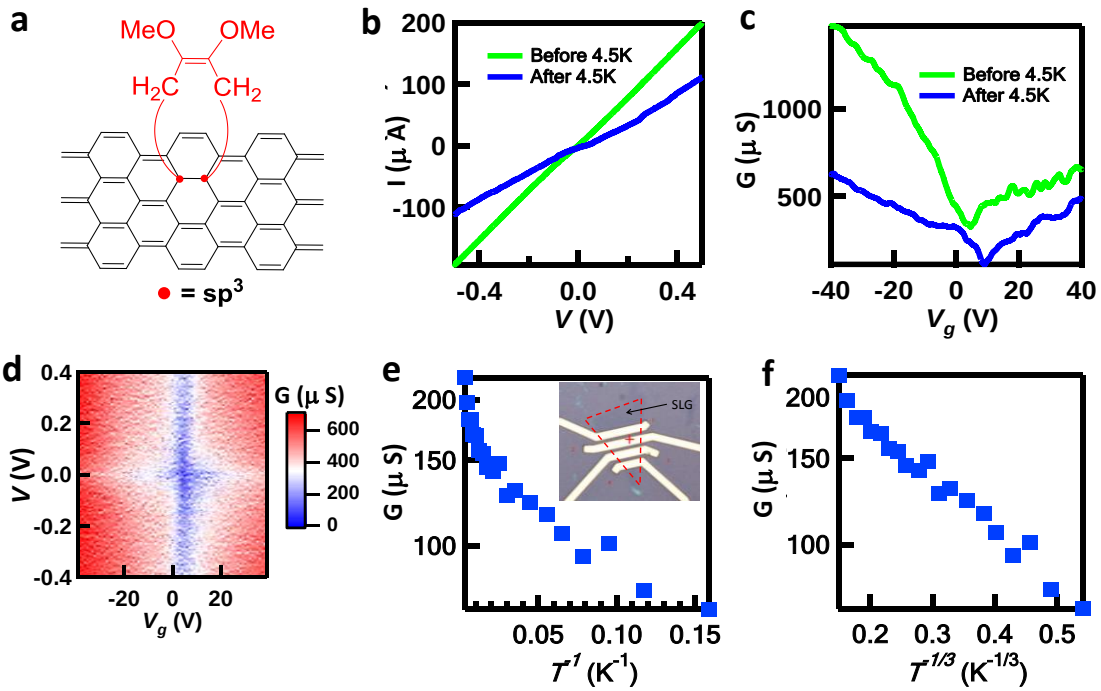

Figure 3.16. Low temperature electrical transport and investigation into the transport mechanism of Diels-Alder modified SLG FET device. (a) Chemical structure of a Diels-Alder functionalized graphene, with the location of sp^3 centers at A and B graphene sublattices are denoted by red circles. (b) *I(V)* curves at Dirac Point at 4.5 K of the device before and after DA functionalization. (c) *G* (V_g) characteristic of another device at 4.5 K before and after functionalization. (d) Conductance *G* as a function of bias *V* and gate V_g at 4.5 K of the same device. (e,f) Zero bias conductance, *G* at the Dirac point vs T^{-1} and $T^{-1/3}$ from the same functionalized graphene device. Optical image of a graphene devices is shown in the inset of Figure 3.16-e.

In order to reveal the mechanism of transport properties, we did temperature dependent measurement on functionalized devices. Based on our

previous results,[20] the two most common transport mechanisms in functionalized devices are: **a)** thermal activation, in which conductance decreases exponentially with the ratio between the activation barrier Δ and thermal energy k_BT, $G \propto e^{-\Delta/2k_BT}$ (k_B is Boltzmann constant); and **b.** variable range hopping (VRH), which displays a stretched exponential dependence $G \propto e^{-(T_0/T)^{\alpha}}$, where T_0 is a characteristic temperature and α ~ 1/(1+dimensional number) is the exponent. For a two dimensional system, α=1/3. To analyze the data, we plot zero-bias conductance *G* on a logarithmic scale as a function of T^{-1} or $T^{-1/3}$ (see **Figures 3.16-e** and **3.16-f**) In *G* v.s.T^{-1} plot, the data points do not fall on a straight line, suggesting that thermal activation is not the underlying transport mechanism in the functionalized devices. The data points in *G* v.s.$T^{-1/3}$ plot show a nice linearity, which strongly suggests transport behaviors are dominated by variable range hopping (VRH) mechanism. This is similar as lightly functionalized devices with aryl groups (radicals) method,[20] except we maintained the advantage of high mobility from the DA modified graphene (DA-SLG) samples.

3.8. CONCLUSION

In summary, we have shown the versatility of graphene as a Diels-Alder substrate and its ability to function as diene or dienophile (**Scheme 3.2**). As a result of the scope of Diels-Alder chemistry and the dual nature of the reactivity

of graphene, dienophiles and dienes with a wide range of modifiable chemical functionality can be employed, which provides a platform for post-grafting modification of graphene. The covalent functionalization of graphene via Diels-Alder reactions is a simple and efficient approach to reversibly engineer the band structure and conductivity of graphene for electronic and optical applications.

It should be mentioned that covalent modification of graphene to engineer a band gap in graphene has led to drastic reduction of device mobility and has, therefore, called for well-ordered structural patterning of graphene by chemistry. Construction of such “structured graphene” architectures is extremely challenging due to the multidimensional variables that influence the chemistry of graphene. Here we show that the application of the Diels-Alder (DA) chemistry to graphene, which is capable of simultaneous formation of a pair of sp^3-carbon centers (balanced divacancies) in graphene, can selectively produce DA-modified graphene devices with mobility between 1,000-6,000 $cm^2V^{-1}s^{-1}$ (with a variable range hopping transport mechanism), which far exceeds the mobility of doped silicon and other chemically-modified graphene devices reported so far. Additionally, current graphene literature also lacks of viable techniques for accurate estimation of surface density of functional groups on graphene. The present work also report on developing the solution Raman and infrared

spectroscopy approach for estimation of surface coverage or defect density on graphene, presenting a significant progress in this field.

CHAPTER 4. Organometallic Chemistry of Graphene and Carbon Nanotubes

4.1. INTRODUCTION

Organometallic complexes of carbon materials are potential candidates as reusable solid catalysts for organic synthetic applications,[228] in organometallic catalysis as electronically conjugated catalyst supports,[14] molecular wires,[229] in atomtronics and spintronics,[28] and they constitute ideal candidates for the realization of new electronic materials.[26,224] While conventional addition chemistry, in which the sp^2 conjugated carbon atoms are rehybridized to sp^3, has been widely explored in the new carbon allotropes (discussed in **Chapter 2-3**),[15] the participation of graphene and carbon nanotubes in organometallic chemical reactions has received limited attention.[28]

Fullerenes[230-233] and carbon nanotubes[234] are curved carbon materials with demonstrated ability to serve as primary ligands, while graphene represents a new class of extended periodic, planar two dimensional π-ligand, which has been recently reported to have a rich organometallic chemistry,[14,28,224] in analogy with the coordination chemistry of polyaromatic

hydrocarbons (PAHs).[235] The flat two-dimensional extended periodic π-surface of graphene exhibits a unique chemical reactivity as a result of the electronic structure at the Dirac point and this provides the opportunity to perform a wide range of chemical reactions.[14,21,26,27,30]

The strong interest in graphene has generated widespread interest in the chemistry of this material and its potential applications.[22] However it is clear that the future applications of graphene in carbon-based electronics require: (1) high quality electrical contacts to graphene, (2) introduction of a band gap (semiconducting behavior) in the zero-band-gap semi-metallic graphene, and (3) the production of high quality large-area graphene wafers, which will allow standard wafer-scale lithographic patterning and etching for scalable device fabrication.[10] While the 2D nature of graphene is compatible with standard organic chemistry processing and lithographic patterning of graphene wafers, defining high quality metal contacts to graphene calls for an in-depth understanding of the conditions necessary for the growth of uniform metal films (by e-beam evaporation or sputtering deposition) and the nature of metal–graphene interfaces at a fundamental level.[142] Additionally, the fundamental understanding of the interaction between mobile metal atoms or metal nano-clusters and graphitic surfaces is crucial from the standpoint of CVD growth of graphitic materials on metal surfaces (surface catalysis),[79] spintronics (spin filters),[143] electronic devices (ultrafast graphene transistors, memory

devices),[143] atomic interconnects,[144-147] and superconducting phenomena.

The main focus of this chapter is to discuss the chemical synthesis, nature of bonding, and applications of the organometallic complexes of single-walled carbon nanotubes (SWNTs)[14,144-146] and graphene.[14,28,224] while a brief mention of fullerene chemistry provides a well understood point of comparison.[230-233]

4.2. NATURE OF INTERACTIONS BETWEEN METALS AND GRAPHITIC SURFACES

There are two limiting cases for the interaction of a metal with a graphene surface – that which involves a **single metal atom** and that which involves the **bulk metal**.[27,28] In the former case the metal atoms are added individually to the graphene surface by either physical or chemical means. In the latter case, where a bulk metal is involved, the graphene is often transferred to the metallic surface, grown directly,[79] or the metal evaporated on the graphene sheet to serve as a contact. The great importance of the interaction of bulk metals and graphene surfaces is particularly related to the CVD growth of graphene and in defining bulk metal contacts (as in FET devices) to graphitic surfaces. We will distinguish between four limiting cases for the interaction of metal atoms with graphene surfaces:

(a) **Weak physisorption** of metal atoms generally occurs when the metal atom

has its d-orbitals filled (in the case of transition metals such as gold) or possesses an s,p-like metallic structure with free-electron-like parabolic band structure (such as Pb), together with a high work function.[143]

(b) **Ionic chemisorption** is characteristic of the interaction of metals of low ionization energy such as alkali metals (Li, Na, K) and alkaline earth metals (Ca, Sr, Ba). Metals with low work function lead to the injection of electrons into the conduction band of graphitic materials (n-type doping). Such a charge transfer interaction with the graphitic structure largely preserves the conjugation and band structure of the graphitic system.[236]

(c) **Covalent chemisorption** of metals to graphitic systems leads **to strong (destructive) rehybridization** of the graphitic band structure. One such example is the formation of metal carbides by the strong interaction between graphitic surface and metals leading to metal–carbon bond formation.

(d) **Covalent chemisorption** of metals to graphitic systems, which is accompanied by the formation of an **organometallic hexahapto(η^6)-metal bond**, preserves the graphitic band structure (constructive rehybridization), and this provides a distinct type of interaction between metals and graphitic surfaces.[14,144] We have recently discovered that the constructive rehybridization that accompanies the formation of bis-hexahapto-metal bonds, such as those in

(η^6-SWNT)Cr(η^6-SWNT), interconnects adjacent graphitic surfaces and significantly reduces the internanotube electrical junction resistance in single-walled carbon nanotube (SWNT) networks.[144-146]

In the traditional covalent chemistry of graphene, the sp^2 hybridized carbon atoms at the sites of covalent attachment of functional groups are converted into sp^3 centers, which can introduce a band gap into graphene, influence the electronic scattering, and create dielectric regions in a graphene wafer with drastically reduced device mobility (**Figure 4.1(a)**).[15,21,22] We refer to this phenomena as **destructive hybridization**. However, the organometallic hexahapto (η^6) functionalization of the two-dimensional (2D) graphene π-surface with transition metals does not bring about significant structural rehybridization of the graphitic surface, and provides a new way to modify graphitic structures that does not saturate the functionalized carbon atoms and by preserving their structural integrity, maintains the delocalization in these extended periodic π-electron systems (**Figure 4.1(b)**) and can also offer the possibility of three-dimensional (3D) interconnections between adjacent graphene sheets.[27] We refer this to as **constructive hybridization**.

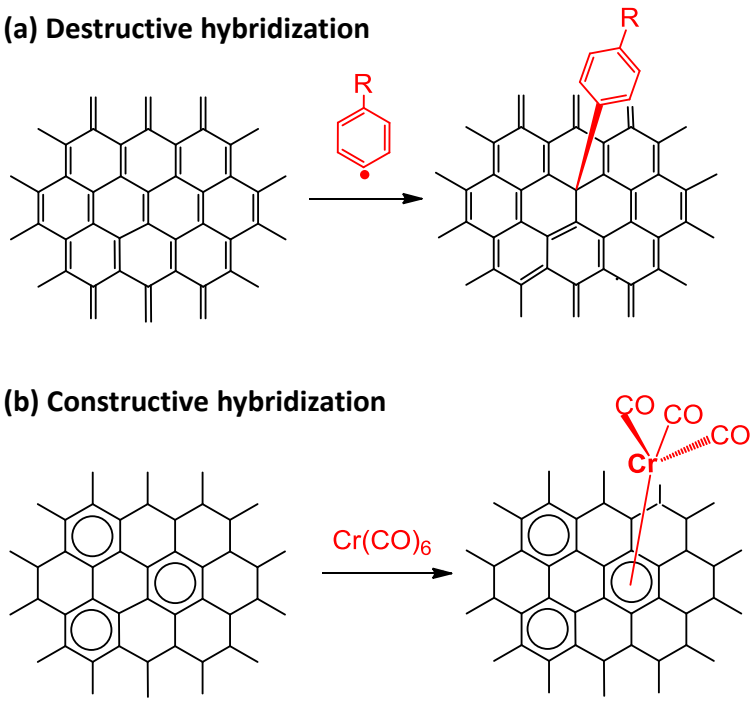

Figure 4.1. Schematics illustrating: (a) destructive hybridization: addition of nitrophenyl radicals to graphene, leading to creation of new sp^3 centers at the time of attachment, and (b) constructive hybridization: organometallic hexahapto complexation reactions of graphene.

From the standpoint of organometallic chemistry, if a chromium (Cr) atom is bonded in hexahapto (η^6) fashion to one of the graphene benzenoid rings, the complex is six electrons short of the stable 18-electron electron configuration.[14] Chromium atoms are mobile on graphitic surfaces,[14,237] and we found that Cr atoms on SWNTs promptly move to a carbon nanotube (CNT) junction to coordinate to the benzenoid rings of another SWNT so as to obtain the stable

18-electron configuration of (η^6-arene)$_2$Cr (where arene = SWNT).[144-146] A number of other transition metals such as Ti interact strongly with the graphene surface and this results in decreased mobility.[238,239] In contrast to these transition metals which strongly interact with the graphene surface, gold interacts weakly and the strength of the Au-Au interaction leads to ready cluster formation.[237,240]

4.3. BONDING IN THE ORGANOMETALLIC COMPLEXES OF THE EXTENDED PERIODIC π-ELECTRON SYSTEMS

Organometallic hexahapto (η^6-) complexation of graphene and carbon nanotubes, a new mode of covalent chemisorption on graphitic surfaces, makes use of the hexahapto-metal bond to electronically conjugate adjacent carbon surfaces, which contain the benzenoid ring system.[14,26,144-147] Electronic coupling of graphitic surfaces, comprised of polycyclic benzenoid ring systems,[241] is best exemplified by the well-known molecular complex, bis(benzene)chromium, [(η^6-C_6H_6)$_2$Cr] which is the quintessential case of a bis-hexahapto-metal bonded system.[242] Based on the gas phase structure of this compound,[243] the pyramidalization angle (**Figure 4.2**)[244] is calculated to be θ_P = 1.7^o, in the sense that the hydrogen atoms tilt toward the metal atom, compared to the normal tetrahedral angle of θ_P = 19.5^o for sp^3 hybridized carbon. In the highly condensed ring system of graphene, with a rigid network of benzene rings, the degree of pyramidalization given above represents an upper bound

and thus there will be very little geometric distortion on metal complexation of the graphitic benzenoid ring systems. Nevertheless these bonds are strong,[245] allow the metal d-orbitals to couple to the π-systems while preserving the band structure, and are capable of electrically interconnecting graphitic surfaces.[14,144-147] In addition to chromium, there are many metals with the ability to form such bonds and are therefore candidates for this type of chemistry.[242]

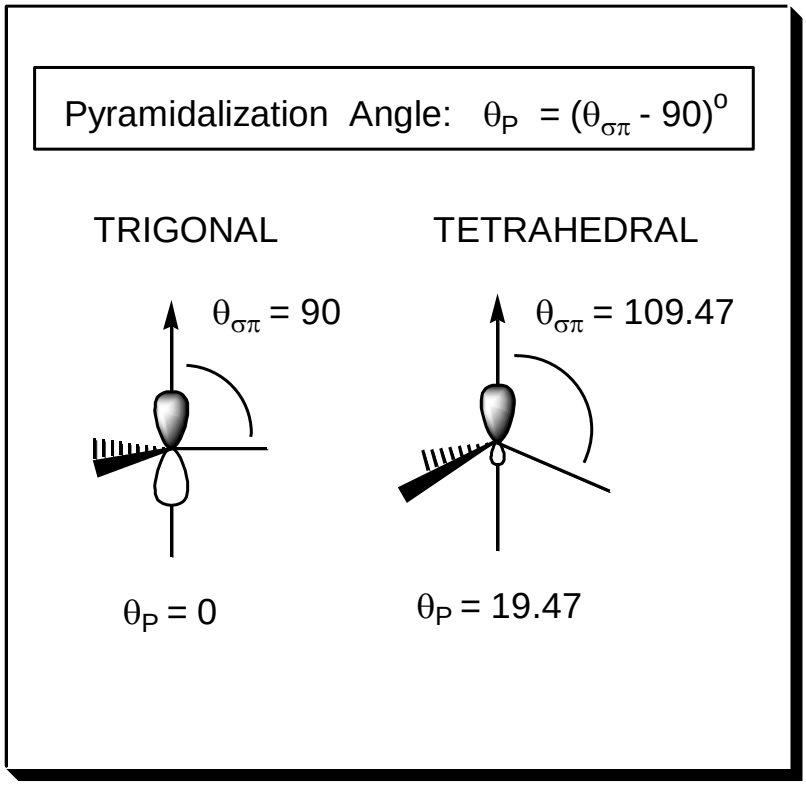

Figure 4.2. The pyramidalization angle (θ_P) for normal sp^2 (trigonal) and sp^3 (tetrahedral) hybridized carbon atoms, respectively.Adapted with permission from ref. [244] (Copyright © 2001 American Chemical Society).

The bis-hexahapto mode of bonding in carbon nanotubes and graphene can be understood within the conventional orbital interaction diagram for bis(benzene)chromium, [(η^6-C_6H_6)$_2$Cr] (**Figure 4.3**). All of the extended periodic π-electron graphitic structures are narrow or zero band gap materials and thus the electron-donor and electron-acceptor interactions between the HOMOs and LUMOs of the graphitic π-systems, and the d-orbitals of the transition metals will be enhanced by the high lying HOMO and low lying LUMO of the graphitic surfaces.[21,26]

The e_{1g} and e_{2u} benzene π-orbitals (**Figure 4.3**), which hybridize with the metal d-orbitals, are strongly involved in the construction of the hexahapto-metal-bonds in (η^6-C_6H_6)$_2$Cr, and are available at the Dirac point in graphene.[21,26] Thus the electronic structure of the graphitic π-electron systems is ideally suited for the realization of organometallic chemistry.[14,26,224]

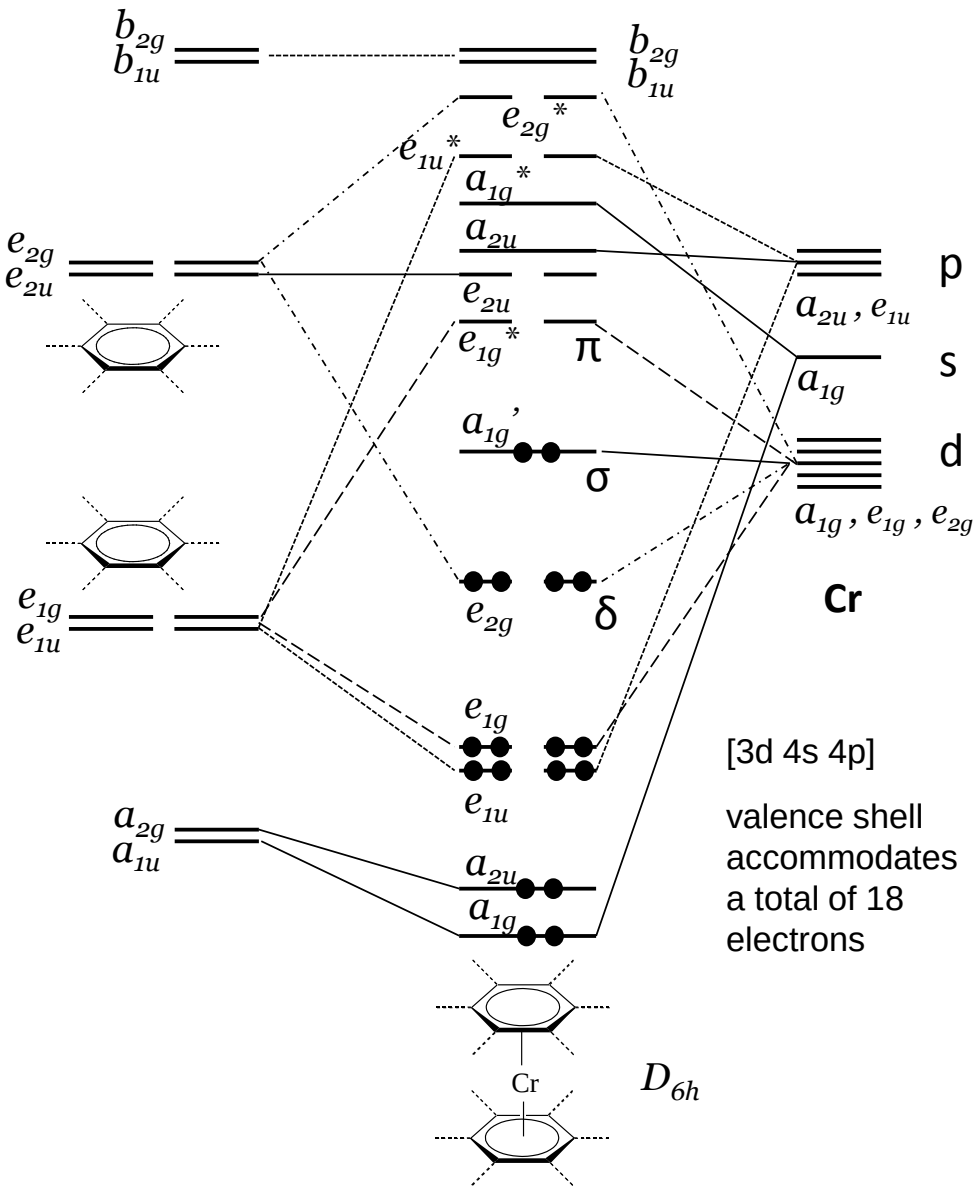

Figure 4.3. Orbital interaction diagram for bis(benzene)chromium, [(η^6-$C_6H_6)_2$Cr]. Adapted with permission from ref.[242] (Copyright © 2006 WILEY-VCH Verlag GmbH & Co. KGaA, Weinheim).

4.4. COMPARISON OF THE HEXAHAPTO COMPLEXATION ABILITY OF FULLERENE AND GRAPHENE

Compared to the fullerene molecules, which are curved in two dimensions, graphene has a flat surface and this makes it a suitable ligand for hexahapto (η^6)-complexation reactions.[146] The coordination chemistry of the fullerenes is dominated by mono (η^1)- and bihapto (η^2)- complexation.[230] It has been shown that the curvature in C_{60} significantly inhibits the potential of the molecule to function as a ligand in pentahapto (η^5)-, and hexahapto (η^6)-complexation reactions because the fullerene π-orbitals are directed away from the metal as a result of the rehybridization of the ring carbon atoms (**Figure 4.4**).[246,247] Nevertheless, the curvature can be ameliorated by functionalization,[247-249] and this has allowed the preparation of organometallic fullerene derivatives.[248,250] In C_{60} the π-orbital axis vectors are directed away from the center of the respective rings and make angles of 16.3^o (POAV2) to a normal to the plane of the five-membered rings and 25.8^o (POAV2) to a normal to the plane of the six-membered rings; hence, hexahapto (η^6)- coordination is even more strongly disfavored than pentahapto (η^5)-complexation.[247]

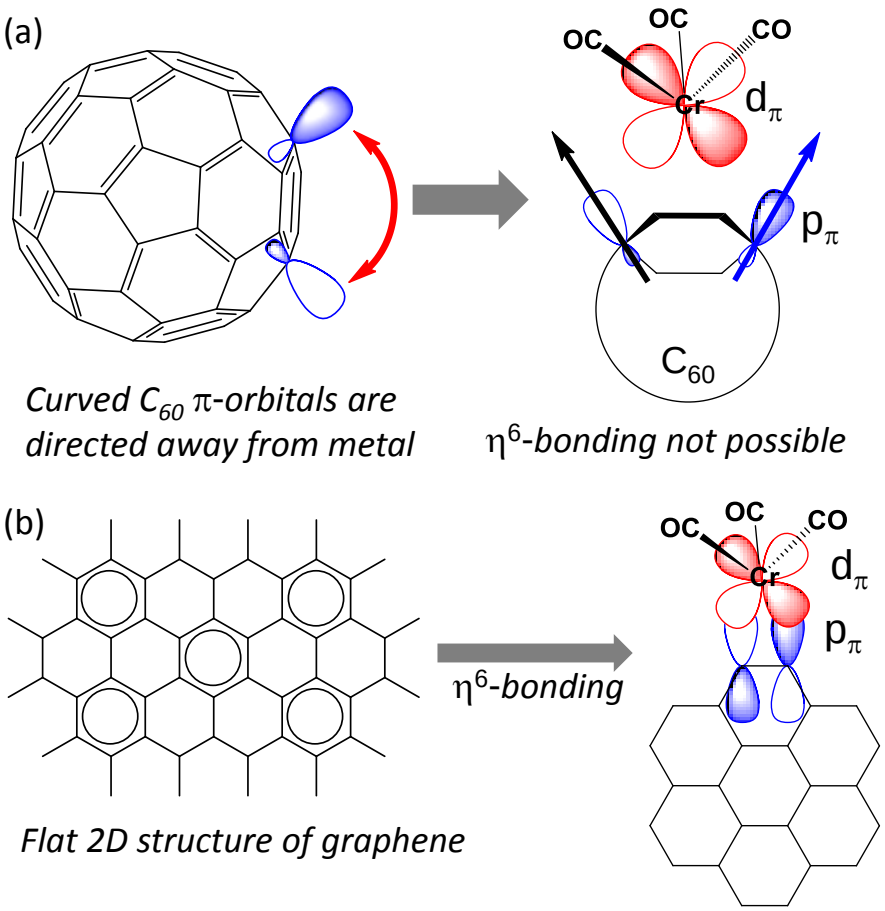

Figure 4.4. Comparison of the orientation of (a) fullerene π-orbitals and (b) graphene π-orbitals. The π-orbital axis vectors are shown in the case of C_{60}, and it is apparent that the curvature and rehybrization present in the fullerene structure severely inhibits its ability to function as a hexahapto ligand,[247] while the flat two-dimensional structure of graphene makes it an ideal hexahapto ligand.[26]

4.5. GENERAL APPROACH TO SYNTHESIS OF THE ORGANOMETALLIC COMPLEXES OF GRAPHENE AND CARBON NANOTUBES

Organometallic chemistry of carbon materials has received theoretical attention,[251-256] but the synthetic difficulties associated with finding suitable

reaction conditions for the formation of metal complexes together with the characterization of the products have been the main impediments to progress in the field.[253,257] The organometallic complexes of carbon nanotubes and graphene can be prepared by employing techniques used for the synthesis of small molecule arene-metal complexes, which have been reviewed in detail by Kundig.[258] Below we discuss the synthesis of (arene)metal carbonyls and bis(arene)metal complexes, where chromium metal is taken as the central metal atom and the arene = benzene, higher polycyclic aromatics, carbon nanotubes, or graphene.

4.5.1. Method A: (Arene)$Cr(CO)_3$ complexes are synthesized by thermolysis of $Cr(CO)_6$ under an inert atmosphere in the presence of an excess of the arene.[14,258] The reaction requires refluxing the mixture in a high-boiling-point solvent.[258] The solvent can be dibutylether/THF, 1,2-dimethoxyethane (DME), diglyme/THF, heptane/diglyme, α-picoline, decalin, decalin/ethyl formate or decalin/butyl acetate. The polar ether or ester additives (or solvents) promote carbonyl dissociation, stabilize intermediates, and the vigorous reflux of lower boiling additives (such as THF) washes the sublimed $Cr(CO)_6$ from the reflux condenser back into the reaction mixture. Prior to heating and mixing, solvents are usually degassed by several freeze/pump/thaw cycles or by bubbling inert gas through the solvent. A wide range of complexes of small aromatic molecules with useful functionalities have been prepared by a

combination of dibutyl ether/THF (9:1) in good yield with reaction times typically 1-4 days. Higher temperature shortens the reaction time, but increases the risk of decomposition of the products.[258]

4.5.2. Method B: This complexation method involves a procedure similar to *Method A*, but naphthalene (~0.25 equivalents) is added as an additional ligand in the reaction mixture (consisting of an arene, chromium hexacarbonyl in Bu_2O/THF),[259] which allows the reaction to occur at lower temperature. This is due to the in-situ formation of (naphthalene)$Cr(CO)_3$ complex, which is labile as a results of haptotropic slippage of the naphthalene ligand (change of hapticity from η^6- to η^4- or η^2-coordination), thus facilitating its dissociation and coordination of the new arene (facile arene exchange reaction).[224,260,261] The reactivity of naphthalene in promoting facile arene exchange has been widely explored for synthesis of (η^6-arene)Cr(η^6-naphthalene), (μ,η^6,η^6-naphthalene)-bis(η^6-benzene)dichromium as well as poly[(μ-η^6,η^6-naphthalene)chromium] compounds[262] under very mild reaction conditions, in which the ligand exchange reaction of (η^6-naphthalene)$_2$Cr[260] with fluorobenzene, benzene, toluene, mesitylene, and hexamethylbenzene in THF have been employed.[263]

4.5.3. Method C: Complexes of condensed aromatics are reported to be unstable towards polar solvents (THF, DMSO, acetone) and their synthesis

requires special attention,[258] or use of more labile $Cr(CO)_3L_3$ (L= CH_3CN, NH_3, pyridine) precursors, which allow the formation of (arene)$Cr(CO)_3$ complexes at much lower temperature.[224,258] The complexation reaction of graphene and $Cr(CO)_3(CH_3CN)_3$ has afforded (η^6-graphene)$Cr(CO)_3$ complexes at temperature as low as 50 ^oC.[224] Room temperature complexation of arene is accomplished by the reaction of $Cr(CO)_3(NH_3)_3$ with $BF_3.OEt_2$ in the presence of an arene.[264,265]

4.5.4. Method D: Timms first demonstrated the synthesis of organometallic complexes of transition metals using metal vapor synthesis (MVS) in 1969,[266,267] and the process has been used to synthesize a variety of compounds which incorporate metal-ligand bonds.[263] The electron beam evaporation technique was used as a source of metal vapors in 1973,[268] and the technique was shown to yield bis(arene)molybdenum complexes by condensation of molybdenum vapor with benzene, toluene, or mesitylene at 77K,[268] whereas the reaction of titanium vapour with benzene afforded extremely air-sensitive $(C_6H_6)_2Ti$.[269] The MVS technique is generally employed for the synthesis of bis(arene)-metal or related (arene)-metal-(arene) oligomeric complexes, and this method allowed the synthesis of a novel triple-decker sandwich complex: (η^6-mesitylene)$_2$(μ-η^6:η^6-mesitylene)Cr_2.[270]
We have employed a derivative of this method in which bis-hexahapto-metal complexes of carbon materials are synthesized by the controlled e-beam

evaporation of metal atoms onto thin films of carbon materials at room temperature with in situ measurement of properties such as the conductivity in a cryogenically pumped high vacuum chamber.[144-146]

4.6. GENERAL APPROACH TO THE DECOMPLEXATION OF THE METAL–GRAPHENE COMPLEXES

The ease of metal removal in the graphitic organometallic complexes is similar to that observed previously in small molecule chemistry. The (η^6-arene)metal$(CO)_3$ complexes are known to undergo loss of metal in high yields at the end of a synthetic sequence.[258,271] While the arene–metal bond can survive in a number of reaction environments, the (η^6-arene)$Cr(CO)_3$ complexes can be readily cleaved upon oxidation of the metal (with Ce(IV), Fe(III), I_2, hv/O_2).[258] The mildest procedure is the exposure of a solution of the complex in diethylether or acetonitrile to sunlight and air for few hours.[14] In small molecule chemistry, this method generally allows the isolation of the arene in yields that are >80%.[258]

In addition, the metal complexation chemistry can also be reversed by exchange with a competitive ligand (mesitylene or anisole).[14,224,258]

4.7. EXPERIMENTS

4.7.1. Preparation of the Chromium–SWNT Complex, (η^6–SWNT)Cr(η^6–benzene)

In a typical reaction, (η^6–benzene)$Cr(CO)_3$ (17 mg, 0.08 mmol, FW = 214.4) was added to a suspension of purified SWNTs (18 mg, 1.5 mmol of carbon atoms; purified SWNTs – P2-SWNT) in dry distilled THF (6 mL). The reaction mixture was sonicated for 2 min using an ultrasonic probe (Cole-Parmer, 50% amplitude) and then degassed with argon for 15 min in absence of light. The reaction mixture was heated at 72 °C for 72 h in the dark under a positive pressure of argon, after which it was cooled to room temperature. The suspension was filtered through a 0.2 μm PTFE membrane and the solid was washed with anhydrous ether. The resulting chromium-SWNTs complex (~21 mg, isolated yield) was dried overnight under vacuum in the dark.

4.7.2. Exfoliation of Microcrystalline Graphite

Microcrystalline graphite (1-2 μm, 500 mg, synthetic, Sigma-Aldrich) was sonicated in o-dichlorobenzene (~200 mL ODCB) for 1 h using a probe ultrasonic processor (Cole-Parmer) at 40% amplitude. The dispersion was centrifuged at 14000g for 30 min. The resulting supernatant (which yielded dispersions of graphene in *o*-dichlorobenzene)[202] was collected and concentrated under vacuum. The powdered exfoliated graphene was dried in

high vacuum overnight and used for subsequent reactions after re-dispersion in dry, distilled THF.

4.7.3. Reaction of Exfoliated graphene and (η^6–benzene)$Cr(CO)_3$

In a typical reaction, (η^6–benzene)$Cr(CO)_3$ (36 mg, 0.17 mmol, FW = 214.4) was added to a suspension of exfoliated graphene (20 mg, 1.67 mmol of carbon) in THF (4 mL). The reaction mixture was stirred vigorously and refluxed at 72^{o}C under argon, in the absence of light for 48 h. The resulting mixture was filtered using 0.2 µm PTFE filter paper and the solid was washed with fresh THF and ether (to remove excess chromium reagent). The resulting solid was dried under vacuum overnight in dark to obtain a silver-colored solid (~27 mg of solid was isolated).

4.7.4. Reaction of Exfoliated Graphene and $Cr(CO)_6$

$Cr(CO)_6$ [8.2 (47.8) mg, 0.04 (0.22) mmol, FW = 220.06] was added to a suspension of exfoliated graphene (20 mg) in THF [4 (10) mL] and dibutyl ether [2 (5) mL]. The black suspension was stirred vigorously and refluxed at 72 ^{o}C in the absence of light under an atmosphere of argon for 48 h. The reaction mixture was filtered using 0.2 µm PTFE filter paper and the solid was washed with fresh THF and ether. The resulting solid [~19 mg] was dried under vacuum overnight in the dark.

4.7.5. Reaction of HOPG and EG with $Cr(CO)_6$

HOPG (~0.28 cm^2) or EG on 4H-SiC (3.5 mm x 4.5 mm), was heated in a solution of $Cr(CO)_6$ (30 mg, 0.14 mmol) in THF (3 mL) and dibutyl ether (1 mL) under a positive pressure of argon at 72°C for 48 h without stirring, then washed with anhydrous ether and dried under a gentle flow of argon.

4.7.6. Reaction of HOPG and EG with (η^6–benzene)$Cr(CO)_3$

A piece of HOPG (~0.32 cm^2) or EG on 4H-SiC (3.5mm x 4.5mm) was heated in a solution of (η^6–benzene)$Cr(CO)_3$ (33 mg, 0.16 mmol) in THF (3 mL) under a positive pressure of argon at 72°C for 72 h without stirring, after which the sample was washed with THF and anhydrous ether and dried under a gentle flow of argon.

4.7.7. De-complexation of Graphene–Cr Complexes by Ambient Oxidation

To collect the Raman spectra of the graphene–Cr complexes, a dispersion of the sample was allowed to dry on a SiO_2 substrate; the color contrast with the substrate allowed identification of graphene samples of various thickness. After recording the Raman spectra of the products, the decomplexation reaction was carried out by adding a few drops of acetonitrile to the substrates and exposing them to sunlight, under a glass petridish; Raman

spectroscopy was used to follow the progress of the de-complexation reaction.

4.7.8. De-complexation of the Organometallic Complexes with Electron Rich Arenes

The Cr complexes of XG and HOPG were either refluxed or warmed (oil bath temperature of 100 °C for benzene, 150 °C for *p*-xylene and 150 °C for mesitylene) with the arene (~5 mL) under argon overnight. The resulting reaction mixture was filtered through a 0.2 μm PTFE membrane and the solid was washed with a copious amount of anhydrous diethylether. The resulting solid was dried for 1 h under vacuum and characterized by Raman spectroscopy.

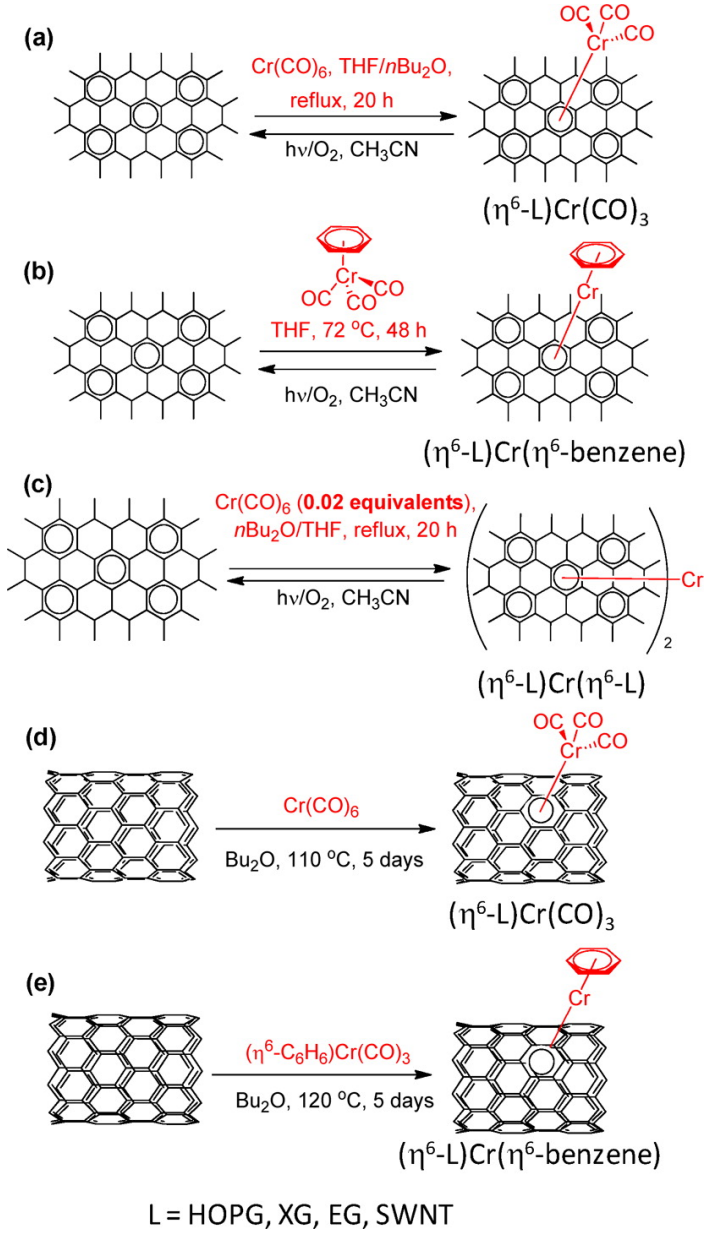

Figure 4.5. Organometallic reactions of graphene and SWNTs: Reactions of graphene with (a) chromium hexacarbonyl, (b) (η^6-benzene)$Cr(CO)_3$, and (c) with chromium hexacarbonyl, $Cr(CO)_6$ in the presence of excess exfoliated graphene (XG) to give the fully graphene-coordinated material, (η^6-XG)Cr(η^6-XG), in which two graphene sheets are interconnected by zero-valent chromium metal. Reactions of SWNTs with (d) chromium hexacarbonyl, $Cr(CO)_6$ and (e) (η^6-benzene)$Cr(CO)_3$. Adapted with permission from ref.[14] (Sarkar, S. et al.

Chem. Sci. **2011**, 2, 1326-1333; Copyright © 2011 The Royal Society of Chemistry).

4.8. RESULTS AND DISCUSSIONS

4.8.1. Synthesis and Charcaterization of the Reaction Product of EA-SWNTs and (η^6–benzene)$Cr(CO)_3$

The reaction of EA-SWNTs (average diameter D_{av} = 1.55 ±0.1 nm),[272,273] with (η^6– benzene)$Cr(CO)_3$ in tetrahydrofuran (THF), which is illustrated in **Figure 4.5-e**, gave rise to a black powder that was isolated by filtration. The changes in the Raman spectrum of SWNTs due to reaction is shown in **Figure 4.6-A**; the intensity of D-band increases relative to the G-band as previously observed for a sidewall functionalization process;[274] (I_D/I_G ~0.04 as compared to I_D/I_G ~ 0.01 in the pristine SWNTs). The SWNT radial breathing mode (RBM) is resonantly enhanced by interband electronic transitions and the frequency is inversely proportional to the diameter. Thus, when the SWNTs are chemically functionalized the band transition energies are modified and this may affect the resonance conditions in the Raman experiment and in cases where the chemical reaction is dependent on nanotube diameter and chirality the RBM band profile takes on a different shape due to changes in the resonance conditions of the various SWNT populations.[275] The inset in **Figure 4.6-A** shows such a change in the RBM profile; although nanotube chiralities cannot be assigned from a single excitation Raman spectrum, the loss of intensity at

the lower frequency of the RBM band indicates that the larger diameter SWNTs are preferentially removed from resonance by the chemical reaction.

The UV-vis-NIR absorption spectrum of the reaction product (**Figure 4.6-B**) shows a decrease in the intensities of all interband transitions; this is most clearly seen for the second semiconducting interband transition (S_{22}). It is apparent that the intensities of the larger diameter SWNTs are preferentially weakened in the product in accord with the previous discussion, which suggests that lower curvature structures will be the most reactive. The change of the SWNT spectra on reaction with benzene chromium tricarbonyl is qualitatively similar to that observed on side-wall functionalization with dichlorocarbene,[274] although the reaction does not proceed to the same degree, perhaps due to the incomplete dispersal of the current sample. The ATR-IR spectrum of the product does not show the C–O vibrations, but it will be of some interest to determine the mode of complexation as it is possible that chromium could bind to the interior wall of the carbon nanotubes.[247]

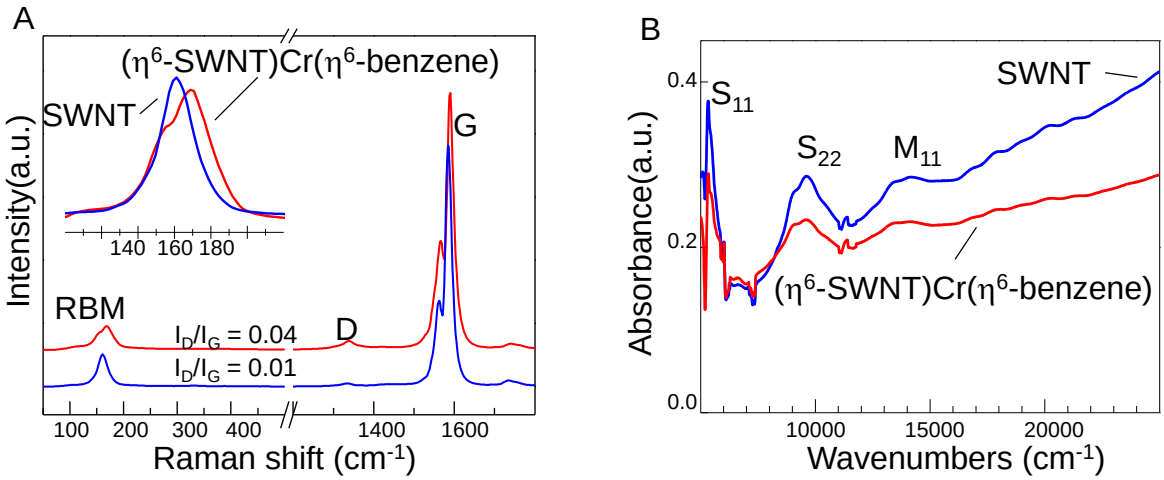

Figure 4.6. Characteristics of the (η^6–SWNT)Cr(η^6–benzene) complex of single–walled carbon nanotubes. A) Raman spectra of the starting SWNTs and the products, collected with λ_{ex} = 532 nm on solid samples. The inset shows the RBM region of the spectra; B) Absorbance spectra of the starting SWNTs and the products, collected on dispersions in dimethylformamide; the dispersions were prepared at approximately similar optical densities and the spectra are not normalized. The features on the lower energy side of the S_{11} band and on both sides of the S_{22} bands are due to water in the solvent. Reprinted with permission from ref.[14] (Sarkar, S. et al. *Chem. Sci.* **2011**, 2, 1326-1333; Copyright © 2011 The Royal Society of Chemistry).

In order to examine the effect of the complexation of SWNTs with Cr on the electronic structure of the material, films of pristine SWNTs and the (η^6–SWNT)Cr(η^6– benzene) product were prepared and transferred to a glass substrate with pre-deposited gold contacts.[276] The SWNT film thickness was estimated from the near-IR spectra of the films (absorbance at 550 nm)[277-279]

The conductivity of the functionalized SWNTs (σ_{RT} ~ 100 S cm^{-1}) decreased by a factor of 3 from the pristine value of σ_{RT} ~ 300 S cm^{-1}.[279]

4.8.2. Synthesis and Assignment of Product Structure of the Organometallic Complexes of Graphene

Graphene–metal complexes have been synthesized by **methods A**, **B**, and **C** as described in **Section 4.5**.[14] A typical sample of solvent exfoliated graphene (XG) consists of a mixture of multilayer-graphene flakes (micrometer dimensions), together with single layer graphene.

After reaction of XG with 0.13 equivalents of $Cr(CO)_6$ (**Figure 4.5-a**), the IR spectrum showed C–O stretching vibrations at 1939 cm^{-1} (**Figure 4.7-c**), and the product was assigned as (η^6-graphene)$Cr(CO)_3$. After the reaction of XG with 0.02 equivalents of $Cr(CO)_6$ (**Figure 4.5-c**), the C–O vibrations was not observed in the product, but the Cr_{2p} XPS spectrum shows the presence of Cr(0) and we assign the structure of the product as (η^6-graphene)$_2$Cr.[14] The observation of varying product structures as a function of the reagent stoichiometry is consistent with results reported for molecular chromium complexes.[270,280] Such (η^6-graphene)$_2$Cr complexes offer the possibility of three-dimensional interconnection between adjacent graphene sheets, providing the opportunity to extend the electronic structure of the two-

dimensional graphene sheets into three dimensions without creating pyramidalized sp^3 carbon center.[26,147]

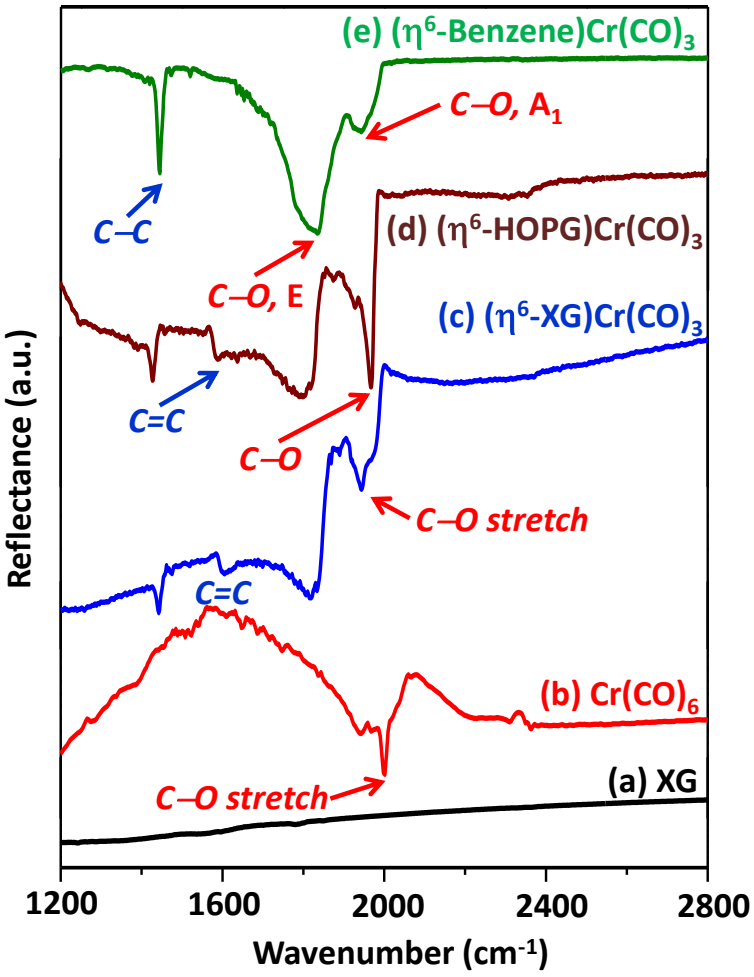

Figure 4.7. ATR-IR characterization of (a) exfoliated graphene (XG) and the organometallic complexes: (b) chromium hexacarbonyl, $Cr(CO)_6$, (c) (η^6-XG)$Cr(CO)_3$, (d) (η^6-HOPG)$Cr(CO)_3$, and (e) (η^6-benzene)$Cr(CO)_3$. Adapted with permission from ref.[14] (Sarkar, S. et al. *Chem. Sci.* **2011**, 2, 1326-1333; Copyright © 2011 The Royal Society of Chemistry).

The ATR-IR spectra of the reaction product of XG (or HOPG) and (η^6-benzene)$Cr(CO)_3$ showed the aromatic C–H vibration of benzene at lower frequency compared to that in the starting material[281] and do not show the C–O vibrations, indicating the formation of the (η^6-graphene)Cr(η^6-benzene) product (**Fig. 4.5-b**).We have also compared the organometallic complexation reactivity of graphene as a function of the number of layers (n), and observed that single layer graphene (n = 1) is more reactive than few-layer graphene (n ≥ 2) and HOPG (n = ∞).[224]

4.8.3. Characterization of the Organometallic Complexes of Graphene

Characterization data on the nature of the products from metal complexation reactions with the graphene surface can be obtained from infrared (ATR-IR), Raman, and UV-vis-NIR spectroscopy, while quantitative analytical information about the amount of chromium present in these complexes can be obtained using thermogravimetric analysis (TGA) and X-ray photoelectron spectroscopy (XPS). Solution UV-vis spectroscopy and the electrochemistry of well-dispersed organometallic complexes of carbon materials can be useful for identifying the nature of the metal-ligand bonding.[14,282]

ATR-IR spectroscopy, which relies on the C–O (or C–H) stretching frequencies of the residual ligands, is an extremely useful technique for the

characterization of organometallic complexes. Coordination of electron donating ligands such as benzene to $Cr(CO)_3$ leads to a decrease in the C–O stretching frequencies of the remaining CO ligands when compared to the $Cr(CO)_6$ starting material. For example, coordination of benzene to $–Cr(CO)_3$ moieties decreases the C–O stretching frequency from 2000 cm^{-1} [**Figure 4.7-b** in $Cr(CO)_6$][283] to 1854 and 1954 cm^{-1} (**Figure 4.7-e**). Coordination of HOPG to $–Cr(CO)_3$ moieties leads to a decrease of C–O stretching frequencies of the residual CO ligands to 1948 cm^{-1} (**Figure 4.7-d**),[14] while coordination of graphene (exfoliated graphene, XG) and SWNT-$CONH(CH_2)_{17}CH_3$ to $–Cr(CO)_3$ moieties leads to a decrease of the C–O stretching frequencies of the residual CO ligands to 1939 (**Figure 4.7-c**) and 1982 cm^{-1},[146] highlighting the trend in donating abilities of the ligands.

4.8.4. Decomplexation Reactions of Organometallic Complexes of Graphene

The ease of metal removal in the graphitic organometallic complexes is similar to that observed previously in small molecule chemistry and the (arene)metal$(CO)_3$ complexes undergo loss of metal selectively in high yields at the end of a synthetic sequence.[258,271,284] While the arene–metal bond can survive in a large number of reaction environments, the (arene)$Cr(CO)_3$ complexes can be readily cleaved upon oxidation of the metal (with Ce(IV),

Fe(III), I_2, hv/O_2). The mildest procedure is the exposure of a solution of the complex in diethylether or acetonitrile to sunlight and air for few hours.[14] In small molecule chemistry, this method generally allows the isolation of the arene in yields that are usually >80%.[258]

The process of decomplexation of graphene–metal bond can be followed by using Raman spectroscopy, in which the I_D/I_G ratio quantifies the relative extent of functionalization in any covalent chemistry of graphene.[14] Applying the same chemistry to the organometallic complexes of graphene, we find that the exposure of the (η^6-graphene)Cr(η^6-graphene) complex to light for 3 h in acetonitrile is sufficient to cleave the complex (I_D/I_G = 1.59 and 0.06 for the same sample before and after exposure to sunlight; **Figure 4.8-a**). The de-complexation of (η^6-graphene)Cr(η^6-benzene) requires longer exposure to sunlight; after exposure for 6 h the I_D/I_G ratio decreases from 1.40 to 0.18 (**Figure 4.8-b**), suggesting that the (η^6-graphene)Cr(η^6-graphene) complex is more reactive than (η^6-graphene)Cr(η^6-benzene).

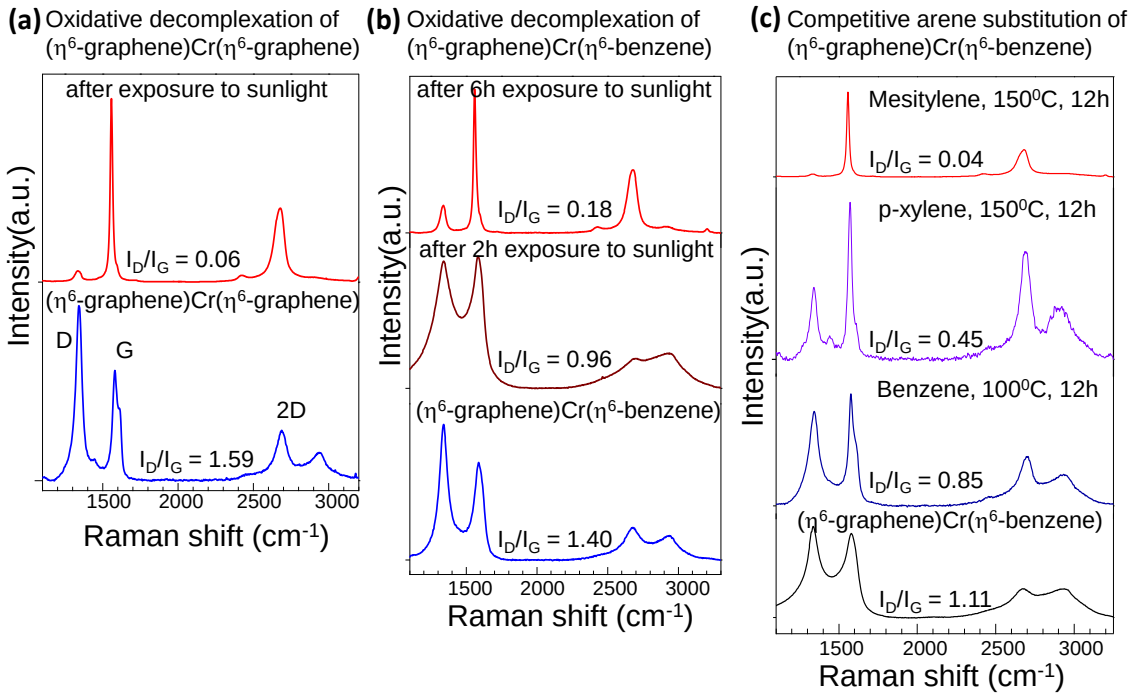

Figure 4.8. Monitoring of the decomplexation reactions with Raman spectroscopy: effect of sunlight on (a) (η^6-graphene)$_2$Cr and (b) (η^6-graphene)Cr(η^6-benzene) complexes. (c) Decomplexation of (η^6-graphene)Cr(η^6-benzene) with benzene, *p*-xylene and mesitylene via competitive arene exchange reactions. Reprinted with permission from ref.[14] (Sarkar, S. et al. *Chem. Sci.* **2011**, 2, 1326-1333; Copyright © 2011 The Royal Society of Chemistry).

Refluxing of an (arene)Cr(CO)$_3$ complex in pyridine is reported to cleave the arene–metal bond and allows recycling the Cr(0) complex in the form of Cr(CO)$_3$py$_3$,[258] while employing the same process to (η^6-graphene)Cr(CO)$_3$

complex leads to highly exfoliated graphene (very small flakes), which are well dispersed in pyridine.[14]

Another effective way to reverse the metal complexation involves refluxing the organometallic complexes with an electron-rich arene (such as mesitylene, anisole), which is able to replace the original ligand from the starting complex via arene exchange reaction.[14,224]

For example, decomplexation of (η^6-graphene)$Cr(CO)_3$ complexes with mesitylene or anisole led to the formation of (η^6-mesitylene)$Cr(CO)_3$ (**Figure 4.9-a**)[14] or (η^6-anisole)$Cr(CO)_3$[224] complexes (detected by ESI-mass spectrometry), with regeneration of pristine-like graphene (confirmed by Raman spectroscopy). Similarly, the decomplexation of the (η^6-graphene)Cr(η^6-benzene) sandwich complex with mesitylene led to graphene and a new complex, which was tentatively assigned as (η^6-mesitylene)Cr(η^6-benzene) (**Figure 4.9-b**).[14]

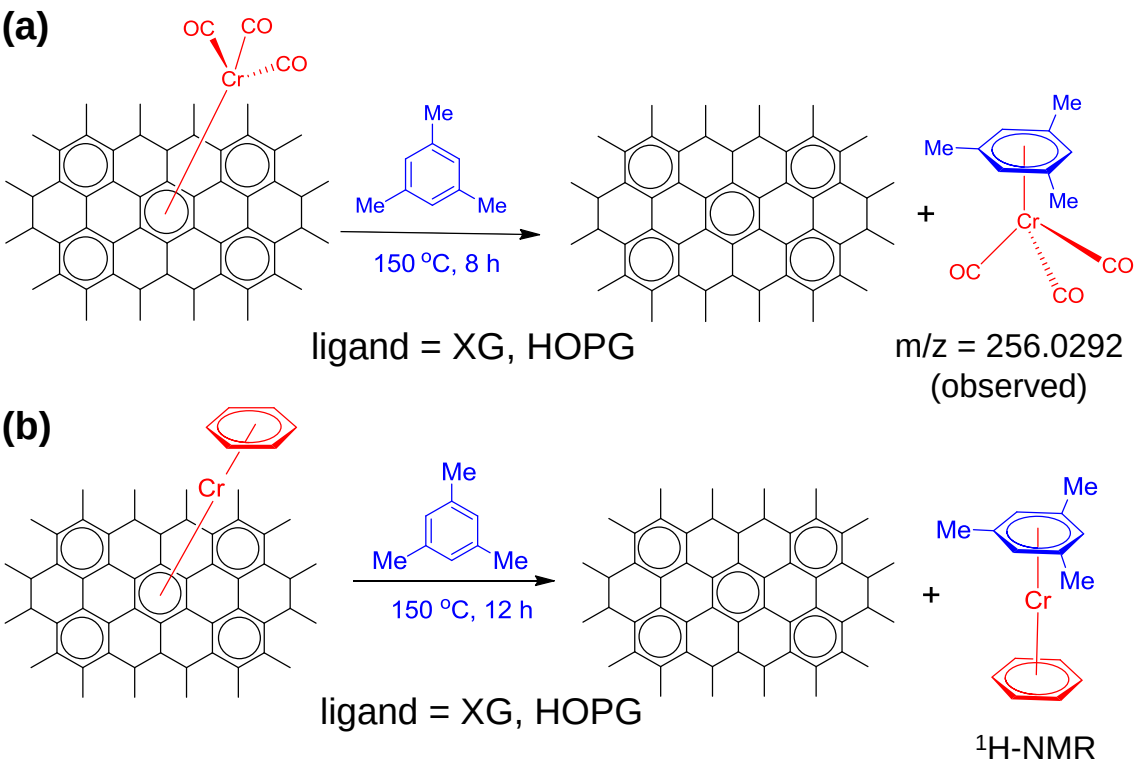

Figure 4.9. Decomplexation of the organometallic complexes of graphene by competitive arene exchange reactions with mesitylene. Reprinted with permission from ref.[14] (Sarkar, S. et al. *Chem. Sci.* **2011**, 2, 1326-1333; Copyright © 2011 The Royal Society of Chemistry).

The strength of the hexahapto graphene–Cr bond was investigated in a series of competition reactions with electron rich arenes.[14] Refluxing the (η^6-graphene)Cr(η^6-benzene) complex (I_D/I_G = 1.1, **Figure 4.8-c**) in benzene (oil bath temperature 100 °C; final I_D/I_G = 0.85) or *p*-xylene (oil bath temperature

150 ^{o}C; final I_D/I_G = 0.45) was insufficient to fully regenerate XG, whereas heating in mesitylene (oil bath temperature 150 ^{o}C) gave a final product with a Raman I_D/I_G = 0.04, indistinguishable from the starting graphene sample. Thus, it is apparent that the η^6 graphene–Cr bond is fairly robust; the (η^6-benzene)–Cr bond energy is reported to be 164 kJ mol^{-1} in (η^6-benzene)$_2$.[285]

4.9. APPLICATIONS: ATOMTRONICS USING ORGANOMETALLIC COMPLEXATION OF SWNTs and GRAPHENE

The electrical connection of graphitic surfaces to bulk metal wiring constitutes a major problem in most approaches to molecular electronics, individual carbon nanotube devices or graphene circuitry.[286-288] In an attempt to address this problem in materials with graphitic surfaces – carbon nanotubes, graphene and other forms of benzenoid-based carbon materials - we have used single atom bridges to develop a technology we term atomtronics.[28] The application of atomtronics to electrically connect graphene surfaces of SWNTs via bis-hexahapto-metal complexation reactions were first reported by our group.[144-146] Below we discuss the applications of the mono-hexahapto metal complexation chemistry (atomtronics approach) to single layer of graphene to produce high mobility graphene transistor (FET) devices.[14,224]

4.9.1. HIGH MOBILITY ORGANOMETALLIC GRAPHENE TRANSISTORS VIA MONO-HEXAHAPTO (η^6) – METAL COMPLEXATION REACTIONS

We have recently shown that the organometallic hexahapto (η^6)-chromium metal complexation of single-layer graphene (SLG), which involved constructive overlap between the graphene π-orbitals and the vacant metal d-orbital of the transition metal,[14] is effective in producing field effect transistor (FET) devices which retain a high carrier mobility and show an enhanced on-off ratio (**Figure 4.10**).[224] This η^6-mode of bonding is quite distinct from the modification in the electronic structure induced by conventional covalent σ-bonds, which result in the formation of sp^3 carbon centers in the graphene lattice with drastically reduced device mobility.[15,18,21,22,26] Thus the application of organometallic functionalization chemistry has enables the fabrication of FET devices, which retain high carrier mobility, presumably due to the fact that such organometallic hexahapto functionalization preserves the conjugation of these extended periodic π-electron systems and the functionalized carbon atoms remain a part of the electronic band structure. In other words, the degree of rehybridization at the site of complexation is insufficient to saturate the conjugated electronic structure, unlike those reactions that require destructive hybridization,[15] which when incorporated in electronic field effect devices show low conductivity and significantly reduced carrier mobility.[27]

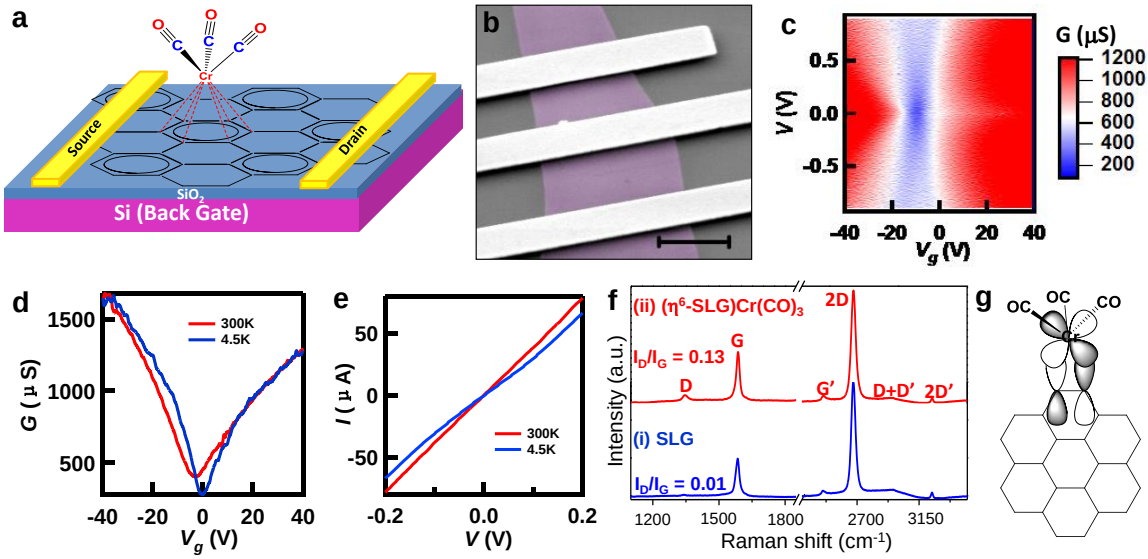

Figure 4.10. Fabrication of high mobility organometallic graphene transistor devices. (a) Schematics of a $(\eta^6\text{-SLG})Cr(CO)_3$ organometallic single-layer graphene (SLG) FET device on an oxidized silicon wafer with metal contacts (Au/Cr = 150 nm/10nm). (b) False-color scanning electron microscopic (SEM) of a typical graphene device (scale bar 2 μm), with color of graphene (SLG) matching to that seen in optical microscope. (c) Conductance *G* as a function of bias *V* and gate V_g at 4.5 K of a $(\eta^6\text{-SLG})Cr(CO)_3$ organometallic device. (d,e) *G(V)* characteristics and *I(V)* curves of a weakly functionalized device at 300 K and 4.5 K. The functionalized graphene device has mobility of ~2,000 $cm^2V^{-1}s^{-1}$ at room temperature and ~3,500 $cm^2V^{-1}s^{-1}$ at 4.5 K. (f) Comparison of Raman spectra (λ_{ex} = 0.7 μm) of a (i) pristine SLG and (ii) metal functionalized devices,

which shows a small increase in I_D/I_G (from 0.01 to 0.13). (g) Schematic illustration of our analysis of the flat two-dimensional structure of graphene as an ideal hexahapto ligand. Reprinted with permission from ref.[224] (Sarkar, S. et al. *Adv. Mater.* **2013**, 25, 1131-1136; Copyright © 2013 WILEY-VCH Verlag GmbH & Co. KGaA, Weinheim).

4.9.2. CORRELATION BETWEEN SURFACE COVERAGE AND BAND GAP IN THE ORGANOMETALLIC COMPLEXES OF GRAPHENE

To understand the transport mechanism of the functionalized graphene FET devices, the temperature dependence of conductance at the Dirac point and in the highly-doped regimes, were recorded in the range of 4 K to 300 K. The two most common transport mechanisms in functionalized devices are: (1) thermal activation over an energy gap ($2E_A$),[20] in which conductance decreases exponentially with the ratio between the activation energy E_A and thermal energy k_BT, $G(T) = G_0 + A\exp(-E_A / k_BT)$ (equation 4.1), where G_0 = the constant background conductance, which is ascribed to the noise floor of the measurement setup, k_B = Boltzmann constant, and (or) (2) variable range hopping (VRH), which displays a stretched exponential dependence $G(T) = A\exp\left[-(T_0/T)^{\alpha}\right]$ (equation 4.2), where T_0 is a characteristic temperature and α~ ½ to ¼ is the exponent.[20] To analyze the data, we plot G on a logarithmic scale as a function of T^{-1} and $T^{-1/3}$.[224] Both plots exhibit some scatter

but the thermally activated regression analysis (equation 4.1) gives values for the energy gap of $2E_A$ = 3 meV (Dirac point), $2E_A$ = 1 meV [highly doped regime (gate voltage of -42V)]; the largest energy gap that we observed in this study was for a device with a gap of $2E_A$ = 14 meV. Thus the data are consistent with the formation of a band gap of $2E_A \approx 10$ meV.[20] A possible complication in analyzing the transport data is the mobility (dynamic nature) of the chromium atoms [–$Cr(CO)_3$ moieties] on the graphene surface which may be evident in the data at high temperatures; such fluxional behavior has been observed in previous studies of polyaromatic hydrocarbon ligands,[235,289] and this may be operative on the two-dimensional surface of the organometallic (η^6-SLG)$Cr(CO)_3$ complexes.[14]

We performed X-ray photoelectron spectroscopy (XPS) to estimate the coverage of the -$Cr(CO)_3$ units on the graphene surface. Because of the very small dimensions of the micromechanically exfoliated single-layer graphene (SLG) flakes and the fact that the presence of additional graphitic flakes on the silicon substrates is unavoidable, CVD-grown SLG (4 mm $\times$ 4 mm, on Cu-substrate) was prepared for the XPS experiments. The SLG samples were functionalized with chromium hexacarbonyl following the procedure described in Method ***C*** as in the ***Section 4.5***. The survey spectrum of the functionalized samples in **Figure 4.11** illustrates the doublet peak corresponding to Cr2p orbitals. The elemental composition was estimated from the areas of the peaks

after Shirley background correction and the corresponding sensitivity factors. The analysis gave a C:Cr ratio of about 18 :1, which in the ideal case gives a structure such as that illustrated in the inset of **Figure 4.11**.

Recent theoretical studies on our experimentally realized organometallic complexes of graphene, such as (η^6-SLG)$Cr(CO)_3$ have indicated a computed band gap of 1.08 V for the composition of C:Cr = 18:1 (as determined from our XPS studies)[224] using density functional theory (DFT) calculations.[290] Our experimentally observed band gap of ~10 meV in the chromium complexes of SLG is explained by Dai and coworkers as originating from regions with low coverage, in view of the much smaller experimental band gap: (η^6-SLG)$Cr(CO)_3$ with C:Cr = 32:1 (54 meV) and C:Cr = 50:1 (20 meV).[290]

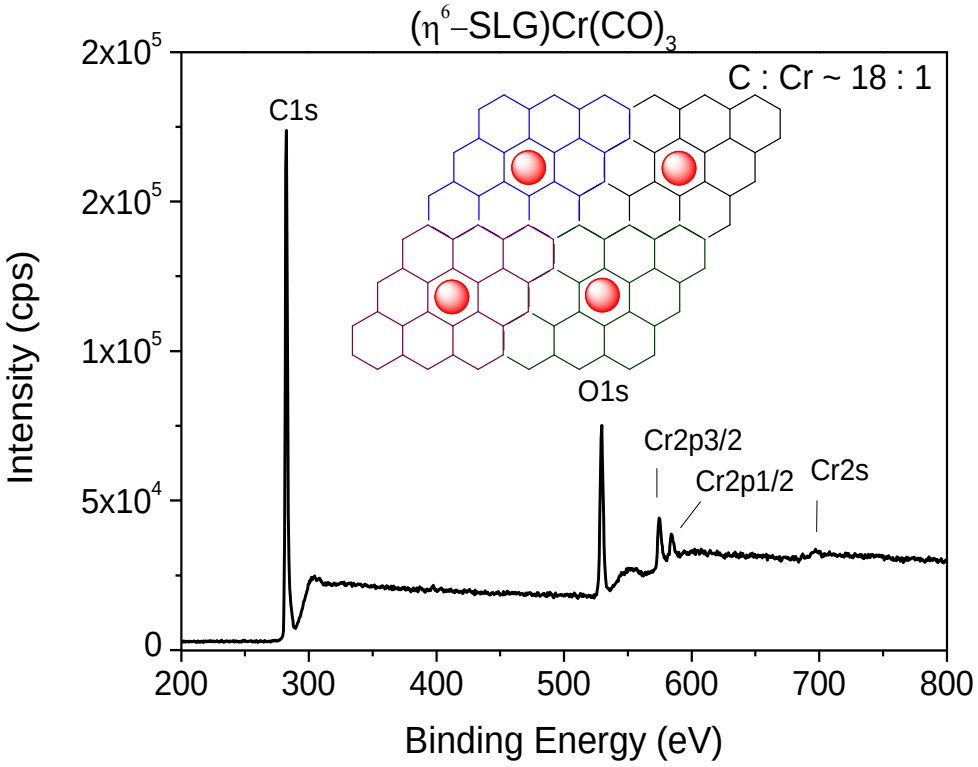

Figure 4.11. Survey spectrum of CVD-grown single-layer graphene (SLG) functionalized with chromium(0)tricarbonyl moieties. The inset shows the structure corresponding to the C:Cr ratio of 18:1 estimated from the C1s and Cr2p peaks, taking into account the sensitivity factors for carbon and chromium. Reprinted with permission from ref.[224] (Sarkar, S. et al. *Adv. Mater.* **2013**, 25, 1131-1136; Copyright © 2013 WILEY-VCH Verlag GmbH & Co. KGaA, Weinheim).

4.10. CONCLUSION

The mobile nature of metal atoms on π-conjugated graphitic surfaces can

lead to several interesting physicochemical phenomena including self-assembled metal nanoclusters with unique morphology, atomic interconnects for 3D electronics based on 1D SWNTs or 2D graphene structures (atomtronics), novel catalyst architectures, and organometallic transistor devices. This is a fertile area for new science and technology and we can expect even more interesting results in the next few years.[28]

This hexahapto (η^6-) bonding mode, unlike previous methodologies,[15,22] leads to an enhancement in the conductivity by increasing the dimensionality of the electronic structure.[144] Such atomic, chemically formed interconnects are entirely distinct from those that depend on the physical adsorption of bulk metals, which have been labeled as a “performance killer” in the formation of metal/graphene contacts.[287]

The organometallic approach discussed in this chapter may lead to new material phenomena in a number of fields, such as organometallic catalysis (for example, in fuel cells, hydrogenation and water splitting reactions),[14] memory devices,[143] high mobility organometallic transistor devices,[224] advanced energy devices, and new electronic materials of enhanced dimensionality including atomic spintronics,[255] and superconductivity.

REFERENCES

(1) Castro Neto, A. H. The Carbon New Age. *Mater. Today* **2010**, *13*, 12-17.

(2) Berger, C.; Song, Z.; Li, T.; Li, X.; Ogbazghi, A. Y.; Feng, R.; Dai, Z.; Marchenkov, A. N.; Conrad, E. H.; First, P. N.; de Heer, W. A. Ultrathin Epitaxial Graphite: 2D Electron Gas Properties and a Route Toward Graphene-Based Nanoelectronics. *J. Phys. Chem. B* **2004**, *108*, 19912-19916.

(3) Novoselov, K. S.; Geim, A. K.; Morozov, S. V.; Jiang, D.; Zhang, Y.; Dubonos, S. V.; Grigorieva, I. V.; Firsov, A. A. Electric Field Effect in Atomically Thin Carbon Films. *Science* **2004**, *306*, 666-669.

(4) de Heer, W. A.; Berger, C.; Wu, X. S.; First, P. N.; Conrad, E. H.; Li, X. B.; Li, T. B.; Sprinkle, M.; Hass, J.; Sadowski, M. L.; Potemski, M.; Martinez, G. Epitaxial Graphene. *Solid State Commun.* **2007**, *143*, 92-100.

(5) Boehm, H. P. Graphene-How a Laboratory Curiosity Suddenly Became Extremely Interesting. *Angew. Chem. Int. Ed.* **2010**, *49*, 9332-9335.

(6) First, P. N.; de Heer, W. A.; Seyller, T.; Berger, C.; Stroscio, J. A.; Moon, J. S. Epitaxial Graphenes on Silicon Carbide. *MRS Bulletin* **2010**, *35*, 296-305.

(7) Geim, A. K.; Novoselov, K. S. The Rise of Graphene. *Nat. Mater.* **2007**, *6*, 183-191.

(8) Novoselov, K. S.; Falko, V. I.; Colombo, L.; Gellert, P. R.; Schwab, M. G.; Kim, K. A Roadmap for Graphene. *Nature* **2012**, *490*, 192-200.

(9) Zhang, Y.; Tan, Y. W.; Stormer, H. L.; Kim, P. Experimental Observation of the Quantum Hall effect and Berry's Phase in Graphene. *Nature* **2005**, *438*, 201-204.

(10) de Heer, W. A.; Berger, C.; Wu, X.; Sprinkle, M.; Hu, Y.; Ruan, M.; Stroscio, J.; First, P. N.; Haddon, R. C.; Piot, B.; Faugeras, C.; Potemski, M.; Moon, J.-S. Epitaxial Graphene Electronic Structure and Transport. *J. Phys. D: Appl. Phys.* **2010**, *43*, 374007.

(11) Wu, J. S.; Pisula, W.; Mullen, K. Graphenes as Potential Material for Electronics. *Chem. Rev.* **2007**, *107*, 718-747.

(12) Bekyarova, E.; Itkis, M. E.; Ramesh, P.; Haddon, R. C. Chemical Approach to the Realization of Electronic Devices in Epitaxial Graphene. *Phys. Stat. Sol. RRL* **2009**, *3*, 184-186.

(13) Loh, K. P.; Bao, Q. L.; Ang, P. K.; Yang, J. X. The Chemistry of Graphene. *J. Mater. Chem.* **2010**, *20*, 2277-2289.

(14) Sarkar, S.; Niyogi, S.; Bekyarova, E.; Haddon, R. C. Organometallic Chemistry of Extended Periodic π-Electron Systems: Hexahapto-Chromium Complexes of Graphene and Single-Walled Carbon Nanotubes. *Chem. Sci.* **2011**, *2*, 1326-1333.

(15) Sarkar, S.; Bekyarova, E.; Haddon, R. C. Reversible Grafting of α-Naphthylmethyl Radicals to Epitaxial Graphene. *Angew. Chem. Int. Ed.* **2012**, *51*, 4901-4904.

(16) Novoselov, K. S.; Geim, A. K.; Morozov, S. V.; Jiang, D.; Katsnelson, M. I.; Grigorieva, I. V.; Dubonos, S. V.; Firsov, A. A. Two-dimensional Gas of Massless Dirac Fermions in Graphene. *Nature* **2005**, *438*, 197-200.

(17) Castro Neto, A. H.; Guinea, F.; Peres, N. M. R.; Novoselov, K. S.; Geim, A. K. The Electronic Properties of Graphene. *Rev. Mod. Phys.* **2009**, *81*, 109-162.

(18) Sarkar, S.; Bekyarova, E.; Niyogi, S.; Haddon, R. C. Diels-Alder Chemistry of Graphite and Graphene: Graphene as Diene and Dienophile. *J. Am. Chem. Soc.* **2011**, *133*, 3324-3327.

(19) Swager, T. M. Functional Graphene: Top-Down Chemistry of the p-Surface. *ACS Macro Lett.* **2012**, *1*, 3-5.

(20) Zhang, H.; Bekyarova, E.; Huang, J.-W.; Zhao, Z.; Bao, W.; Wang, F.; Haddon, R. C.; Lau, C. N. Aryl Functionalization as a Route to Band Gap Engineering in Single Layer Graphene Devices. *Nano Lett.* **2011**, *11*, 4047-4051.

(21) Sarkar, S.; Bekyarova, E.; Haddon, R. C. Chemistry at the Dirac Point: Diels-Alder Reactivity of Graphene. *Acc. Chem. Res.* **2012**, *45*, 673-682.

(22) Sarkar, S.; Bekyarova, E.; Haddon, R. C. Covalent Chemistry in Graphene Electronics. *Mater. Today* **2012**, *15*, 276-285.

(23) Woodward, R. B.; Hoffmann, R. *The Conservation of Orbital Symmetry*; VCH: Weinheim, Chapter 3, 1970.

(24) Fukui, K. Theory of Orientation and Stereoselection. *Top. Curr. Chem.* **1970**, *15*, 1-85.

(25) Houk, K. N. The Frontier Molecular Orbital Theory of Cycloaddition Reactions. *Acc. Chem. Res.* **1975**, *8*, 361-369.

(26) Bekyarova, E.; Sarkar, S.; Niyogi, S.; Itkis, M. E.; Haddon, R. C. Advances in the Chemical Modification of Epitaxial Graphene. *J. Phys. D: Appl. Phys.* **2012**, *45*, 154009.

(27) Bekyarova, E.; Sarkar, S.; Wang, F.; Itkis, M. E.; Kalinina, I.; Tian, X.; Haddon, R. C. Effect of Covalent Chemistry on the Electronic Structure and Properties of Carbon Nanotubes and Graphene. *Acc. Chem. Res.* **2013**, *46*, 65-76.

(28) Sarkar, S.; Moser, M. L.; Tian, X.; Haddon, R. C. Metals on Graphene and Carbon Nanotube Surfaces: From Mobile Atoms to Atomtronics to Bulk Metals to Clusters and Catalysts. *Chem. Mater.* **2014**, *26*, DOI: 10.1021/cm4025809.

(29) Hong, J.; Niyogi, S.; Bekyarova, E.; Itkis, M. E.; Palanisamy, R.; Amos, N.; Litvinov, D.; Berger, C.; de Heer, W. A.; Khizroev, S.; Haddon, R. C. Effect of Nitrophenyl Functionalization on the Magnetic Properties of Epitaxial Graphene. *Small* **2011**, *7*, 1175-1180.

(30) Niyogi, S.; Bekyarova, E.; Hong, J.; Khizroev, S.; Berger, C.; de Heer, W. A.; Haddon, R. C. Covalent Chemistry for Graphene Electronics. *J. Phys. Chem. Lett.* **2011**, *2*, 2487-2498.

(31) Hong, J.; Bekyarova, E.; Liang, P.; de Heer, W. A.; Haddon, R. C.; Khizroev, S. Room-Temperature Magnetic Ordering in Functionalized Graphene. *Sci. Rep.* **2012**, *2*, 624.

(32) Hong, J.; Bekyarova, E.; de Heer, W. A.; Haddon, R. C.; Khizroev, S. Chemically Engineered Graphene-Based 2D Organic Molecular Magnet. *ACS Nano* **2013**, 7, 10011-10022.

(33) Mohanty, N.; Berry, V. Graphene-Based Single-Bacterium Resolution Biodevice and DNA Transistor: Interfacing Graphene Derivatives with Nanoscale and Microscale Biocomponents. *Nano Lett.* **2008**, *8*, 4469-4476.

(34) Collins, W. R.; Lewandowski, W.; Schmois, E.; Walish, J.; Swager, T. M. Claisen Rearrangement of Graphite Oxide: A Route to Covalently Functionalized Graphenes. *Angew. Chem. Int. Ed.* **2011**, *50*, 8848-8852, *Angew. Chem.* **2011**, 123, 9010-9014.

(35) Haddon, R. C. Chemistry of the Fullerenes: The Manifestation of Strain in a Class of Continuous Aromatic Molecules. *Science* **1993**, *261*, 1545-1550.

(36) Niyogi, S.; Hamon, M. A.; Hu, H.; Zhao, B.; Bhowmik, P.; Sen, R.; Itkis, M. E.; Haddon, R. C. Chemistry of Single-Walled Carbon Nanotubes. *Acc. Chem. Res.* **2002**, *35*, 1105-1113.

(37) Haddon, R. C.; Lamola, A. A. The Molecular Electronic Device and the Biochip Computer: Present Status. *Proc. Nat. Acad. Sci. USA* **1985**, *82*, 1874.

(38) Boehm, H. P.; Stumpp, E. Citation Errors Concerning the First Report on Exfoliated Graphite. *Carbon* **2007**, *45*, 1381-1383.

(39) Schafhaeutl, C. Ueber die Verbindungen des Kohlenstoffes mit Silicium, Eisen und anderen Metallen, welche die verschiedenen Gallungen von Roheisen, Stahl und Schmiedeeisen bilden. *J. Prakt. Chem.* **1840**, *21*, 129-157.

(40) Schafhaeutl, C. *Phil. Mag.* **1840**, *16*, 570.

(41) Dreyer, D. R.; Park, S.; Bielawski, C. W.; Ruoff, R. S. The Chemistry of Graphene Oxide. *Chem. Soc. Rev.* **2010**, *39*, 228-240.

(42) Dresselhaus, M. S.; Dresselhaus, G. Intercalation compounds of graphite. *Advances in Physics* **2002**, *51*, 1-186.

(43) Novoselov, K. S.; Jiang, D.; Schedin, F.; Booth, T. J.; Khotkevich, V. V.; Morozov, S. V.; Geim, A. K. Two-Dimensional Atomic Crystals. *Proc. Nat. Acad. Sci. USA* **2005**, *102*, 10451-10453.

(44) Dreyer, D. R.; Ruoff, R. S.; Bielawski, C. W. From Conception to Realization: An Historial Account of Graphene and Some Perspectives for Its Future. *Angew. Chem. Int. Ed.* **2010**, *49*, 9336-9344.

(45) Jang, B.; Zhamu, A. Processing of nanographene platelets (NGPs) and NGP nanocomposites: a review. *Journal of Materials Science* **2008**, *43*, 5092-5101.

(46) Geim, A. K. Graphene: Status and Prospects. *Science* **2009**, *324*, 1530-1534.

(47) Allen, M. J.; Tung, V. C.; Kaner, R. B. Honeycomb Carbon: A Review of Graphene. *Chem. Rev.* **2010**, *110*, 132-145.

(48) Workshop, S. s. Electro-Plating on Non-Metallic Substances. *Vol. II: Dyeing to Japanning. Spon* **1921**, 132.

(49) Belash, I. T.; Zharikov, O. V.; Palnichenko, A. V. Superconductivity of GiC with Li, Na and K. *Synth. Met.* **1990**, 455-460.

(50) Brodie, B. C. On The Atomic Weight of Graphite. *Philosophical Transactions of the Royal Society of London* **1859**, *149*, 249-259.

(51) Staudenmaier, L. Verfahren zur Darstellung der Graphitsäure. *Ber. Dtsch. Chem. Ges.* **1898**, *31*, 1481-1487.

(52) Marcano, D. C.; Kosynkin, D. V.; Berlin, J. M.; Sinitskii, A.; Sun, Z. Z.; Slesarev, A.; Alemany, L. B.; Lu, W.; Tour, J. M. Improved Synthesis of Graphene Oxide. *ACS Nano* **2010**, *4*, 4806-4814.

(53) Zhu, Y.; James, D. K.; Tour, J. M. New Routes to Graphene, Graphene Oxide and Their Related Applications. *Adv. Mater.* **2012**, *24*, 4924-4955.

(54) Wallace, P. R. The Band Theory of Graphite. *Phys. Rev.* **1947**, *71*, 622-634.

(55) Boehm, H. P.; Clauss, A.; Fischer, G. O.; Hofmann, U. *Z. Naturf.* **1962**, *17*, 150.

(56) Boehm, H. P.; Clauss, A.; Hofmann, U.; Fischer, G. O. *Proceedings of the Fifth Conference on Carbon*: Pergamon Press, Heidelberg, Germany, 1962.

(57) Morgan, A. E.; Somorjai, G. A. Low Energy Electron Diffraction Studies of Gas Adsorption on the Platinum(100) Single Crystal Surface. *Surf. Sci.* **1968**, *12*, 405-425.

(58) May, J. W. Platinum Surface LEED Rings. *Surf. Sci.* **1969**, *17*, 267-270.

(59) Blakely, J. M.; S., K. J.; Potter, H. C. Segregation of Carbon to the (100) Surface of Nickel. *J. Appl. Phys.* **1970**, *41*, 2693-2697.

(60) Patil, H. R.; Blakely, J. M. Electron Energy Losses in Thin Graphite Layers on the (111) Face of Nickel. *J. Appl. Phys.* **1974**, *45*, 3806-3808.

(61) Hamilton, J. C.; Blakely, J. M. Carbon Layer Formation on the Pt (111) Surface as a Function of Temperature. *J. Vac. Sci. Technol. B* **1978**, *15*, 559-562.

(62) Eizenberg, M.; Blakely, J. M. Carbon Monolayer Phase Condensation on Ni(111). *Surf. Sci.* **1979**, *82*, 228-236.

(63) Eizenberg, M.; Blakely, J. M. Carbon Interaction with Nickel Surfaces - Monolayer Formation and Structural Stability. *J. Chem. Phys.* **1979**, *71*, 3467-3477.

(64) Hamilton, J. C.; Blakely, J. M. Carbon Segregation to Single-Crystal Surfaces of Pt,Pd and Co. *Surf. Sci.* **1980**, *91*, 199-217.

(65) Shelton, J. C.; Patil, H. R.; Blakely, J. M. Equilibrium Segregation of Carbon to a Nickel(111) Surface. Surface Phase Transition. *Surf. Sci.* **1974**, *43*, 493-520.

(66) Land, T. A.; Michely, T.; Behm, R. J.; Hemminger, J. C.; Comsa, G. STM Investigation of Single Layer Graphite Structures Produced on Platinum(111) by Hydrocarbon Decomposition. *Surf. Sci.* **1992**, *264*, 261-270.

(67) van Bommel, A. J.; Crombeen, J. E.; van Tooren, A. LEED and Auger Electron Observations of the SiC(0001) Surface. *Surf. Sci.* **1975**, *48*, 463-472.

(68) Badami, B. V. X-Ray Studies of Graphite Formed by Decomposing Silicon Carbide. *Carbon* **1965**, *3*, 53-54.

(69) Boehm, H. P.; Setton, R.; Stumpp, E. Nomenclature and Terminology of Graphite-Intercalation Compounds. *Carbon* **1986**, *24*, 241-245.

(70) Boehm, H. P.; Setton, R.; Stumpp, E. Nomenclature and Terminology of Graphite-Intercalation Compounds (IUPAC Recommendations 1994). *Pure and Applied Chemistry* **1994**, *66*, 1893-1901.

(71) Boehm, H. P. Some Aspects of the Surface Chemistry of Carbon Blacks and Other Carbons. *Carbon* **1994**, *32*, 759-769.

(72) Boehm, H. P. Surface Oxides on Carbon and their Analysis: A Critical Assessment. *Carbon* **2002**, *40*, 145-149.

(73) IUPAC *in Compendium of Chemical Terminology*; 2nd ed. ed.: Blackwell Scientific, Oxford, 1997.

(74) Bolotin, K. I.; Sikes, K. J.; Jiang, Z.; Klima, M.; Fudenberg, G.; Hone, J.; Kim, P.; Stormer, H. L. Ultrahigh Electron Mobility in Suspended Graphene. *Solid State Commun.* **2008**, *146*, 351-355.

(75) Morozov, S. V.; Novoselov, K. S.; Katsnelson, M. I.; Schedin, F.; Elias, D. C.; Jaszczak, J. A.; Geim, A. K. Giant Intrinsic Carrier Mobilities in Graphene and its Bilayer. *Phys. Rev. Lett.* **2008**, *1*, 016602-4.

(76) Frank, I. W.; Tanenbaum, D. M.; van der Zande, A. M.; McEuen, P. L. Mechanical Properties of Suspended Graphene Sheets. *J. Vac. Sci. Tech. B* **2007**, *25*, 2558.

(77) Berger, C.; Song, Z. M.; Li, X. B.; Wu, X. S.; Brown, N.; Naud, C.; Mayou, D.; Li, T. B.; Hass, J.; Marchenkov, A. N.; Conrad, E. H.; First, P. N.; de Heer,

W. A. Electronic Confinement and Coherence in Patterned Epitaxial Graphene. *Science* **2006**, *312*, 1191-1196.

(78) Novoselov, K. S.; McCann, E.; Morozov, S. V.; Fal'ko, V. I.; Katsnelson, M. I.; Zeitler, U.; Jiang, D.; Schedin, F.; Geim, A. K. Unconventional Quantum Hall Effect and Berry's Phase of 2p in Bilayer Graphene. *Nature Phys.* **2006**, *2*, 177-180.

(79) Li, X. S.; Cai, W. W.; An, J. H.; Kim, S.; Nah, J.; Yang, D. X.; Piner, R.; Velamakanni, A.; Jung, I.; Tutuc, E.; Banerjee, S. K.; Colombo, L.; Ruoff, R. S. Large-Area Synthesis of High-Quality and Uniform Graphene Films on Copper Foils. *Science* **2009**, *324*, 1312-1314.

(80) Xiong, W.; Zhou, Y. S.; Jiang, L. J.; Sarkar, A.; Mahjouri-Samani, M.; Xie, Z. Q.; Gao, Y.; Ianno, N. J.; Jiang, L.; Lu, Y. F. Single-Step Formation of Graphene on Dielectric Surfaces. *Adv. Mater.* **2013**, *25*, 630-634.

(81) Kosynkin, D. V.; Higginbotham, A. L.; Sinitskii, A.; Lomeda, J. R.; DImiev, A.; Price, B. K.; Tour, J. M. Longitudinal Unzipping of Carbon Nanotubes to Form Graphene Nanoribbons. *Nature* **2009**, *458*, 872-876.

(82) Sprinkle, M.; Ruan, M.; Hu, Y.; Hankinson, J.; Rubio-Roy, M.; Zhang, B.; Wu, X.; Berger, C.; de Heer, W. A. Scalable Templated Growth of Graphene Nanoribbons on SiC. *Nat. Nanotechnol.* **2010**, *5*, 727-731.

(83) Fujita, M.; Wakabayashi, K.; Nakada, K.; Kusakabe, K. Peculiar Localized State at Zigzag Graphite Edge. *J. Phys. Soc. Jpn* **1996**, *65*, 1920-1923.

(84) Nakada, K.; Fujita, M.; Dresselhaus, G.; Dresselhaus, M. S. Edge State in Graphene Ribbons: Nanometer Size Effect and Edge State Dependence. *Phys Rev. B* **1996**, *54*, 17954-17961.

(85) Wakabayashi, K.; Fujita, M.; Ajiki, H.; Sigrist, M. Electronic and Magnetic Properties of Nanographite Ribbons. *Phys Rev. B* **1999**, *59*, 8271-8282.

(86) Hass, J.; de Heer, W. A.; Conrad, E. H. The Growth and Morphology of Epitaxial Multilayer Graphene. *J. Phys.: Condens. Matter* **2008**, *20*, 323202 1-27.

(87) Zhou, S. Y.; Gweon, G. H.; Fedorov, A. V.; First, P. N.; De Heer, W. A.; Lee, D. H.; Guinea, F.; Neto, A. H. C.; Lanzara, A. Substrate-Induced Bandgap Opening in Epitaxial Graphene. *Nat. Mater.* **2007**, *6*, 770-775.

(88) Ferrari, A. C.; Meyer, J. C.; Scardaci, V.; Casiraghi, C.; Lazzeri, M.; Mauri, F.; Piscanec, S.; Jiang, D.; Novoselov, K. S.; Roth, S.; Geim, A. K. Raman Spectrum of Graphene and Graphene Layers. *Phys. Rev. Lett.* **2006**, *97*, 187401-1-187401-4.

(89) Ferrari, A. C. Raman Spectroscopy of Graphene and Graphite: Disorder, Electron-Phonon Coupling, Doping and Nonadiabatic Effects. *Solid State Commun.* **2007**, *143*, 47-57.

(90) Malard, L. M.; Pimenta, M. A.; Dresselhaus, G.; Dresselhaus, M. S. Raman Spectroscopy in Graphene. *Phys. Report* **2009**, *473*, 51-87.

(91) Niyogi, S.; Bekyarova, E.; Itkis, M. E.; Zhang, H.; Shepperd, K.; Hick, J.; Sprinkle, M.; Berger, C.; Lau, C. N.; de Heer, W. A.; Conrad, E. H.; Haddon, R. C. Spectroscopy of Covalently Functionalized Graphene. *Nano. Lett.* **2010**, *10*, 4061–4066.

(92) Ramesh, P.; Itkis, M. E.; Bekyarova, E.; Wang, F.; Niyogi, S.; Chi, X.; Berger, C.; de Heer, W. A.; Haddon, R. C. Electro-Oxidized Epitaxial Graphene Channel Field-Effect Transistors with Single-Walled Carbon Nanotube Thin Film Gate Electrode. *J. Am. Chem. Soc.* **2010**, *132*, 14429–14436.

(93) Lucchese, M. M.; Stavale, F.; Ferreira, E. H. M.; Vilani, C.; Moutinho, M. V. O.; Capaz, R. B.; Achete, C. A.; Jorio, A. Quantifying Ion-Induced Defects and Raman Relaxation Length in Graphene. *Carbon* **2010**, *48*, 1592-1597.

(94) Dong, X. C.; Fu, D. L.; Fang, W. J.; Shi, Y. M.; Chen, P.; Li, L. J. Doping Single-Layer Graphene with Aromatic Molecules. *Small* **2009**, *5*, 1422-1426.

(95) Robinson, J. A.; Wetherington, M.; Tedesco, J. L.; Campbell, P. M.; Weng, X.; Stitt, J.; Fanton, M. A.; Frantz, E.; Snyder, D.; VanMil, B. L.; Jernigan, G. G.; Myers-Ward, R. L.; Eddy Jr., C. R.; Gaskill, D. K. Correlating Raman Spectral Signatures with Carrier Mobility in Epitaxial Graphene: A Guide to Achieving High Mobility on the Wafer Scale. *Nano Lett.* **2009**, *9*, 2873-2876.

(96) Wang, Q. H.; Jin, Z.; Kim, K. K.; Hilmer, A. J.; Paulus, G. L. C.; Shih, C. J.; Ham, M. H.; Sanchez-Yamagishi, J. D.; Watanabe, K.; Taniguchi, T.; Kong, J.; Jarillo-Herrero, P.; Strano, M. S. Understanding and Controlling the Substrate Effect on Graphene Electron-Transfer Chemistry via Reactivity Imprint Lithography. *Nat. Chem.* **2012**, *4*, 724-732.

(97) Yan, L.; Zheng, Y. B.; Zhao, F.; Li, S. J.; Gao, X. F.; Xu, B. Q.; Weiss, P. S.; Zhao, Y. L. Chemistry and Physics of a Single Atomic Layer: Strategies and Challenges for Functionalization of Graphene and Graphene-Based Materials. *Chem. Soc. Rev.* **2012**, *41*, 97-114.

(98) Sharma, R.; Baik, J. H.; Perera, C. J.; Strano, M. S. Anomalously Large Reactivity of Single Graphene Layers and Edges toward Electron Transfer Chemistries. *Nano Lett.* **2010**, *10*, 398-405.

(99) Boukhvalov, D. W.; Katsnelson, M. I. Chemical Functionalization of Graphene. *J. Phys: Condens. Matter* **2009**, *21*, 344205(12pp).

(100) Boukhvalov, D. W. Modeling of Epitaxial Graphene Functionalization. *Nanotech.* **2011**, *22*, 055708 (5pp).

(101) Boukhvalov, D. W.; Katsnelson, M. I. Enhancement of Chemical Activity in Corrugated Graphene. *J. Phys. Chem. C* **2009**, *113*, 14176-14178.

(102) Deng, S. L.; Zhang, Y.; Brozena, A. H.; Mayes, M. L.; Banerjee, P.; Chiou, W. A.; Rubloff, G. W.; Schatz, G. C.; Wang, Y. H. Confined Propagation of Covalent Chemical Reactions on Single-Walled Carbon Nanotubes. *Nat. Commun.* **2011**, *2*, 382.

(103) Yang, Z. Q.; Sun, Y. Q.; Alemany, L. B.; Narayanan, T. N.; Billups, W. E. Birch Reduction of Graphite. Edge and Interior Functionalization by Hydrogen. *J. Am. Chem. Soc* **2012**, *134*, 18689-18694.

(104) Liu, H.; Ryu, S.; Chen, Z.; Steigerwald, M. L.; Nuckolls, C.; Brus, L. E. Photochemical Reactivity of Graphene. *J. Am. Chem. Soc.* **2009**, *131*, 17099-17101.

(105) Kudin, K. N.; Ozbas, B.; Schniepp, H. C.; Prud'homme, R. K.; Aksay, I. A.; Car, R. Raman Spectra of Graphite Oxide and Functionalized Graphene Sheets. *Nano Lett* **2008**, *8*, 36-41.

(106) Ryu, S.; Han, M. Y.; Maultzsch, J.; Heinz, T. F.; Kim, P.; Steigerwald, M.; Brus, L. E. Reversible Basal Plane Hydrogenation of Graphene. *Nano Lett.* **2008**, *8*, 4597-4602.

(107) Jiang, D. E.; Sumpter, B. G.; Dai, S. Unique Chemical Reactivity of a Graphene Nanoribbon's Zigzag Edge. *J. Chem. Phys.* **2007**, *126*, 134701.

(108) Wassmann, T.; Seitsonen, A. P.; Saitta, A. M.; Lazzeri, M.; Mauri, F. Clar's Theory, p-Electron Distribution, and Geometry of Graphene Nanoribbons *J. Am. Chem. Soc.* **2010**, *132*, 3440-3451.

(109) Strom, T. A.; Dillon, E. P.; Hamilton, C. E.; Barron, A. R. Nitrene Addition to Exfoliated Graphene: A One-step Route to Highly Functionalized Graphene. *Chem. Commun.* **2010**, *46*, 4097-4099.

(110) Economopoulos, S. P.; Rotas, G.; Miyata, Y.; Shinohara, H.; Tagmatarchis, N. Exfoliation and Chemical Modification Using Microwave Irradiation Affording Highly Functionalized Graphene. *ACS Nano* **2010**, *4*, 7499-7507.

(111) Quintana, M.; Spyrou, K.; Grzelczak, M.; Browne, W. R.; Rudolf, P.; Prato, M. Functionalization of Graphene via 1,3-Dipolar Cycloaddition. *ACS Nano* **2010**, *4*, 3527-3533.

(112) Bekyarova, E.; Itkis, M. E.; Ramesh, P.; Berger, C.; Sprinkle, M.; de Heer, W. A.; Haddon, R. C. Chemical Modification of Epitaxial Graphene:

Spontaneous Grafting of Aryl Groups. *J. Am. Chem. Soc.* **2009**, *131*, 1336-1337.

(113) Liu, L. H.; Lerner, M. M.; Yan, M. D. Derivitization of Pristine Graphene with Well-Defined Chemical Functionalities. *Nano Lett.* **2010**, *10*, 3754-3756.

(114) Yuan, J.; Chen, G.; Weng, W.; Xu, Y. One-Step Functionalization of Graphene with Cyclopentadienyl-Capped Macromolecules via Diels–Alder "Click" Chemistry. *J. Mater. Chem.* **2012**, *22*, 7929-7936.

(115) Bian, S.; Scott, A. M.; Cao, Y.; Liang, Y.; Osuna, S.; Houk, K. N.; Braunschweig, A. B. Covalently Patterned Graphene Surfaces by a Force-Accelerated Diels–Alder Reaction. *J. Am. Chem. Soc* **2013**, *135*, 9240–9243.

(116) Seo, J.-M.; Jeon, I.-Y.; Baek, J.-B. Mechanochemically Driven Solid-State Diels-Alder Reaction of Graphite into Graphene Nanoplatelets. *Chem. Sci.* **2013**, *4*, 4273-4277.

(117) Zhong, X.; Jin, J.; Li, S.; Niu, Z.; Hu, W.; Li, R.; Ma, J. Aryne Cycloaddition: Highly Efficient Chemical Modification of Graphene. *Chem. Commun.* **2010**, *46*, 7340-7342.

(118) Stankovich, S.; Dikin, D. A.; Piner, R. D.; Kohlhaas, K. A.; Kleinhammes, A.; Jia, Y.; Wu, Y.; Nguyen, S. T.; Ruoff, R. S. Synthesis of Graphene-Based Nanosheets via Chemical Reduction of Exfoliated Graphite Oxide. *Carbon* **2007**, *45*, 1558-1565.

(119) Elias, D. C.; Nair, R. R.; Mohiuddin, T. M. G.; Morozov, S. V. B., P.; Halsall, M. P.; Ferrari, A. C.; Boukhvalov, D. W.; Katsnelson, M. I.; Geim, A. K.; Novoselov, K. S. Control of Graphene's Properties by Reversible Hydrogenation: Evidence for Graphane. *Science* **2009**, *323*, 610-613.

(120) Worsley, K. A.; Ramesh, P.; Mandal, S. K.; Niyogi, S.; Itkis, M. E.; Haddon, R. C. Soluble Graphene Derived from Graphite Fluoride. *Chem. Phys. Lett.* **2007**, *445*, 51 - 56.

(121) Bon, S. B.; Valentini, L.; Verdejo, R.; Fierro, J. L. G.; Peponi, L.; Lopez-Manchado, M. A.; Kenny, J. M. Plasma Fluorination of Chemically Derived

Graphene Sheets and Subsequent Modification With Butylamine. *Chem. Mater.* **2009**, *21*, 3433-3438.

(122) Withers, F.; Dubois, M.; Savchenko, A. K. Electron Properties of Fluorinated Single-layer Graphene Transistors. *Phys. Rev. B* **2010**, *82*, 073403-4.

(123) Robinson, J. T.; Burgess, J. S.; Junkermeier, C. E.; Badescu, S. C.; Reinecke, T. L.; Perkins, F. K.; Zalalutdniov, M. K.; Baldwin, J. W.; Culbertson, J. C.; Sheehan, P. E.; Snow, E. S. Properties of Fluorinated Graphene Films. *Nano Lett.* **2010**, *10*, 3001-3005.

(124) Zhou, J.; Liang, Q. F.; Dong, J. M. Enhanced Spin-orbit Coupling in Hydrogenated and Fluorinated Graphene. *Carbon* **2010**, *48*, 1405-1409.

(125) Haddon, R. C. Graphene: Noble No More. *Acc. Chem. Res.* **2013**, *46*, 1-3.

(126) Sun, Z. Z.; Kohama, S.; Zhang, Z. X.; Lomeda, J. R.; Tour, J. M. Soluble Graphene Through Edge-selective Functionalization. *Nano Res.* **2010**, *3*, 117-125.

(127) Gizzatov, A.; Dimiev, A.; Mackeyev, Y.; Tour, J. M.; Wilson, L. J. Highly Water Soluble Multi-layer Graphene Nanoribbons and Related Honey-comb Carbon Nanostructures. *Chem. Commun.* **2012**, *48*, 5602-5604.

(128) Jha, N.; Ramesh, P.; Bekyarova, E.; Itkis, M. E.; Haddon, R. C. High Energy Density Supercapacitor Based on a Hybrid Carbon Nanotube–Reduced Graphite Oxide Architecture. *Adv. Energy Mater.* **2012**, *2*, 438-444.

(129) Schedin, F.; Geim, A. K.; Morozov, S. V.; Hill, E. W.; Blake, P.; Katsnelson, M. I.; Novoselov, K. S. Detection of Individual Gas Molecules Adsorbed on Graphene. *Nat. Mater.* **2007**, *6*, 652-655.

(130) Li, X. S.; Zhu, Y. W.; Cai, W. W.; Borysiak, M.; Han, B. Y.; Chen, D.; Piner, R. D.; Colombo, L.; Ruoff, R. S. Transfer of Large-Area Graphene Films for High-Performance Transparent Conductive Electrodes. *Nano Letters* **2009**, *9*, 4359-4363.

(131) Nair, R. R.; Blake, P.; Grigorenko, A. N.; Novoselov, K. S.; Booth, T. J.; Stauber, T.; Peres, N. M. R.; Geim, A. K. Fine Structure Constant Defines Visual Transparency of Graphene. *Science* **2008**, *320*, 1308.

(132) Stankovich, S.; Dikin, D. A.; Dommett, G. H. B.; Kohlhaas, K. M.; Zimney, E. J.; Stach, E. A.; Piner, R. D.; Nguyen, S. T.; Ruoff, R. S. Graphene-Based Composite Materials. *Nature* **2006**, *442*, 282-286.

(133) Tian, X.; Itkis, M. E.; Bekyarova, E.; Haddon, R. C. Anisotropic Thermal and Electrical Properties of Thin Thermal Interface Layers of Graphite Nanoplatelet-Based Composites *Sci. Rep.* **2013**, *3*, 1710.

(134) Yu, A.; Ramesh, P.; Sun, X.; Bekyarova, E.; Itkis, M. E.; Haddon, R. C. Enhanced Thermal Conductivity in a Hybrid Graphite Nanoplatelet - Carbon Nanotube Filler for Epoxy Composites. *Adv. Mater.* **2008**, *20*, 4740-4744.

(135) Seol, J. H.; Jo, I.; Moore, A. L.; Lindsay, L.; Aitken, Z. H.; Pettes, M. T.; Li, X.; Yao, Z.; Huang, R.; Broido, D.; Mingo, N.; Ruoff, R. S.; Shi, L. Two-Dimensional Phonon Transport in Supported Graphene. *Science* **2010**, *328*, 213.

(136) Stoller, M. D.; Park, S. J.; Zhu, Y. W.; An, J. H.; Ruoff, R. S. Graphene-Based Ultracapacitors. *Nano Lett.* **2008**, *8*, 3498-3502.

(137) Banerjee, S.; Sardar, M.; Gayathri, N.; Tyagi, A. K.; Raj, B. Enhanced Conductivity in Graphene Layers and at Their Edges. *Appl. Phys. Lett.* **2006**, *88*, 062111.

(138) Kobayashi, Y.; Fukui, K.; Enoki, T.; Kusakabe, K.; Kaburagi, Y. Observation of Zigzag and Armchair Edges of Graphite Using Scanning Tunneling Microscopy and Spectroscopy. *Phys. Rev. B* **2005**, *71*, 193406.

(139) Radovic, L. R.; Bockrath, B. On the Chemical Nature of Graphene Edges: Origin of Stability and Potential for Magnetism in Carbon Materials. *J. Am. Chem. Soc.* **2005**, *127*, 5917-5927.

(140) Malig, J.; Englert, J. M.; Hirschi, A.; Guldi, D. M. Wet Chemistry of Graphene. *Interface* **2011**, *20*, 53-56.

(141) Han, M. Y.; Ozyilmaz, B.; Zhang, Y. B.; Kim, P. Energy Band-Gap Engineering of Graphene Nanoribbons. *Phys. Rev. Lett.* **2007**, *98*, 206805-4.

(142) Schultz, B. J.; Jaye, C.; Lysaght, P. S.; Fischer, D. A.; Prendergast, D.; Banerjee, S. On Chemical Bonding and Electronic Structure of Graphene-Metal Contacts. *Chem. Sci.* **2013**, *4*, 494-502.

(143) Liu, X.; Wang, C.-Z.; Hupalo, M.; Lin, H.-Q.; Ho, K.-M.; Tringides, M. C. Metals on Graphene: Interactions, Growth Morphology, and Thermal Stability. *Crystals* **2013**, *3*, 79-111.

(144) Wang, F.; Itkis, M. E.; Bekyarova, E.; Tian, X.; Sarkar, S.; Pekker, A.; Kalinina, I.; Moser, M.; Haddon, R. C. Effect of First Row Transition Metals on the Conductivity of Semiconducting Single-Walled Carbon Nanotube Networks. *Appl. Phys. Lett.* **2012**, *100*, 223111.

(145) Wang, F.; Itkis, M. E.; Bekyarova, E.; Sarkar, S.; Tian, X.; Haddon, R. C. Solid-State Bis-Hexahapto-Metal Complexation of Single-Walled Carbon Nanotubes. *J. Phys. Org. Chem.* **2012**, *25*, 607-610.

(146) Kalinina, I.; Bekyarova, E.; Sarkar, S.; Wang, F.; Itkis, M. E.; Tian, X.; Niyogi, S.; Jha, N.; Haddon, R. C. Hexahapto-Metal Complexes of Single-Walled Carbon Nanotubes. *Macromol. Chem. Phys.* **2012**, *213*, 1001-1019.

(147) Tian, X.; Sarkar, S.; Moser, M. L.; Wang, F.; Pekker, A.; Bekyarova, E.; Itkis, M. E.; Haddon, R. C. Effect of Group 6 Transition Metal Coordination on the Conductivity of Graphite Nanoplatelets. *Mater. Lett.* **2012**, *80*, 171-174.

(148) Rao, C. N. R.; Sood, A. K.; Subrahmanyam, K. S.; Govindaraj, A. Graphene: The New Two-Dimensional Nanomaterial. *Angew. Chem. Int. Ed.* **2009**, *48*, 7752-7777; *Angew. Chem.* **2009**, 121, 7890–7916.

(149) Coleman, J. N. Liquid-Phase Exfoliation of Nanotubes and Graphene. *Adv. Funct. Mater.* **2009**, *19*, 3680-3695.

(150) Koehler, F. M.; Jacobsen, A.; Ensslin, K.; Stampfer, C.; Stark, W. J. Selective Chemical Modification of Graphene Surfaces: Distinction Between Single- and Bilayer Graphene. *Small* **2010**, *6*, 1125-1130.

(151) Englert, J. E., J. M.; Dotzer, C.; Yang, G. A.; Schmid, M.; Papp, C.; Gottfried, J. M.; Steinruck, H. P.; Spiecker, E.; Hauke, F.; Hirsch, A. Covalent Bulk Functionalization of Graphene. *Nat. Chem.* **2011**, *3*, 279-286.

(152) Koehler, F. M.; Luechinger, N. A.; Ziegler, D.; Athanassiou, E. K.; Grass, R. N.; Rossi, A.; Hierold, C.; Stemmer, A.; Stark, W. J. Permanent Pattern-Resolved Adjustment of the Surface Potential of Graphene-Like Carbon through Chemical Functionalization. *Angew. Chem. Int. Ed.* **2009**, *48*, 224-227.

(153) Sinitskii, A.; Dimiev, A.; Corley, D. A.; Fursina, A. A.; Kosynkin, D. V.; Tour, J. M. Kinetics of Diazonium Functionalization of Chemically Converted Graphene Nanoribbons. *ACS Nano* **2010**, *4*, 1949-1954.

(154) Shih, C. J.; Wang, Q. H.; Jin, Z.; Paulus, G. L. C.; Blankschtein, D.; Jarillo-Herrero, P.; Strano, M. S. Disorder Imposed Limits of Mono- and Bilayer Graphene Electronic Modification Using Covalent Chemistry. *Nano Lett.* **2013**, *13*, 809-817.

(155) Hossain, M. Z.; Walsh, M.; Hersam, M. C. Scanning Tunneling Microscopy, Spectroscopy, and Nanolithography of Epitaxial graphene Chemically Modified with Aryl Moieties. *J. Am. Chem. Soc.* **2010**, *132*, 15399-15403.

(156) Andrieux, C. P.; Gonzalez, F.; Saveant, J. M. Derivatization of Carbon Surfaces by Anodic Oxidation of Arylacetates. Electrochemical Manipulation of the Grafted Films. *J. Am. Chem. Soc.* **1997**, *119*, 4292-4300.

(157) Kolbe, H. Electrochemical Oxidation of Alkyl- or Aryl- Acetates. *Ann. Chem.* **1849**, *69*, 257.

(158) Wurtz, A. *Ann. Chim. Phys.* **1855**, *44*, 291.

(159) Schafer, H. J. Anodic and Cathodic C-C Bond Formation. *Angew. Chem. Int. Ed.* **1981**, *20*, 911-934.

(160) Whangbo, M.-H.; Hoffmann, R.; Woodward, R. B. Conjugated One and Two Dimensional Polymers. *Proc. Royal Soc. Lond. A* **1979**, *366*, 23-46.

(161) Ruffieux, P.; Groning, O.; Schwaller, P.; Schlapbach, L.; Groning, P. Hydrogen Atoms Cause Long-Range Electronic Effects on Graphite. *Phys. Rev. Lett.* **2000**, *84*, 4910-4913.

(162) Boukhvalov, D. W.; Katsnelson, M. I. Tuning the Gap in Bilayer Graphene using Chemical Functionalization: Density Functional Calculations. *Phys. Rev. B* **2008**, *78*, 085413.

(163) Borden, W. T.; Davidson, E. R. Theoretical Studies of Diradicals Containing Four pi Electrons. *Acc. Chem. Res.* **1981**, *14*, 69-76.

(164) Borden, W. T.; Iwamura, H.; Berson, J. A. Violations of Hund's Rule in Non-Kekule Hydrocarbons: Theoretical Prediction and Experimental Verification. *Acc. Chem. Res.* **1994**, *27*, 109-116.

(165) Yazyev, O. V. Emergence of Magnetism in Graphene Materials and Nanostructures. *Rep. Prog. Phys.* **2010**, *73*, 056501.

(166) Sofo, J. O.; Chaudhari, A. S.; Barber, G. D. Graphane: A Two-Dimensional Hydrocarbon. *Phys Rev. B* **2007**, *75*, 153401.

(167) Lebegue, S.; Klintenberg, M.; Eriksson, O.; Katsnelson, M. I. Accurate Eelectronic Band Gap of Pure and Functionalized Graphane from GW Calculations. *Physical Review B* **2009**, *79*, 245117(5).

(168) Nair, R. R.; Ren, W.; Jalil, R.; Riaz, I.; Kravets, V. G.; Britnell, L.; Blake, P.; Schedin, F.; Mayorov, A. S.; Yuan, S.; Katsnelson, M. I.; Cheng, H. M.; Strupinski, W.; Bulusheva, L. G.; Okotrub, A. V.; Grigorieva, I. V.; Grigorenko, A. N.; Novoselov, K. S.; Geim, A. K. Fluorographene: A Two-Dimensional Counterpart of Teflon. *Small* **2010**, *6*, 2877-2884.

(169) Jeon, K. J.; Lee, Z.; Pollak, E.; Moreschini, L.; Bostwick, A.; Park, C. M.; Mendelsberg, R.; Radmilovic, V.; Kostecki, R.; Richardson, T. J.; Rotenberg, E. Fluorographene: A Wide Bandgap Semiconductor with Ultraviolet Luminescence. *ACS Nano* **2011**, *5*, 1042-1046.

(170) Zhu, H.; Huang, P.; Jing, L.; Zuo, T.; Zhao, Y. L.; Gao, X. Microstructure Evolution of Diazonium Functionalized Graphene: A Potential Approach to Change Graphene Electronic Structure. *J. Mater. Chem* **2012**, *22*, 2063-2068.

(171) Barzola-Quiquia, J.; Yao, J. L.; Rodiger, P.; Schindler, K.; Esquinazi, P. Sample Size Effects on the Transport Characteristics of Mesoscopic Graphite Samples. *Phys. Stat. Sol. (a)* **2008**, *205*, 2924-2933.

(172) Garcia, N.; Esquinazi, P.; Barzola-Quiquia, J.; Ming, B.; Spoddig, D. Transition from Ohmic to Ballistic Transport in Oriented Graphite: Measurements and Numerical Simulations. *Phys. Rev. B* **2008**, *78*, 035413.

(173) Arndt, A.; Spoddig, D.; Esquinazi, P.; Barzola-Quiquia, J.; Dusari, S.; Butz, T. Electric Carrier Concenrtation in Graphite: Dependence of Electrical Resistivity and Magnetoresistance on Defect Concentration. *Phys. Rev. B* **2009**, *80*, 195402.

(174) Ristein, J.; Stief, R. T.; Ley, L.; Beyer, W. A Comparative Analysis of a-C : H by Infrared Spectroscopy and Mass Selected Thermal Effusion. *J. App. Phys.* **1998**, *84*, 3836-3847.

(175) Lin-Vien, D.; Colthup, N. B.; Fateley, W. G.; Grasselli, J. G. The Handbook of Infrared and Raman Characteristic Frequencies of Organic Molecules **1991**, *1st edition, Academic Press*.

(176) Hass, J.; Varchon, F.; Millan-Otoya, J. E.; Sprinkle, M.; Sharma, N.; De Heer, W. A.; Berger, C.; First, P. N.; Magaud, L.; Conrad, E. H. Why Multilayer Graphene on 4H-SiC(000(1)over-bar) Behaves Like a Single Sheet of Graphene. *Phys. Rev. Lett.* **2008**, *100*, 125504-4-.

(177) Nicolaou, K. C.; Snyder, S. A.; Montagnon, T.; Vassilikogiannakis, G. The Diels-Alder Reaction in Total Synthesis. *Angew. Chem. Int. Ed.* **2002**, *41*, 1668-1698.

(178) Rotello, V. M.; Howard, J. B.; Yadav, T.; Conn, M. M.; Viani, E.; Giovane, L. M.; Lafleur, A. L. Isolation of Fullerene Products from Flames - Structure and Synthesis of the C60-Cyclopentadiene Adduct. *Tet. Lett.* **1993**, *34*, 1561-1562.

(179) Tsuda, M.; Ishida, T.; Nogami, T.; Kurono, S.; Ohashi, M. Isolation and Characterization of Diels-Alder Adducts of C-60 with Anthracene and Cyclopentadiene. *J. Chem. Soc. Chem. Commun.* **1993**, 1296-1298.

(180) Wilson, S. R.; Yurchenko, M. E.; Schuster, D. I.; Khong, A.; Saunders, M. Synthesis of Fluorous Fullerene Adducts: Reversible Solubilization of Fullerenes in Perfluorinated Solvents. *J. Org. Chem* **2000**, *65*, 2619-2623.

(181) Schlueter, J. A.; Seaman, J. M.; Taha, S.; Cohen, H.; Lykke, K. R.; Wang, H. H.; Williams, J. M. Synthesis, Purification, and Characterization of the 1/1 Addition Product of C_{60} and Anthracene. *J. Chem. Soc. Chem. Commun.* **1993**, 972-974.

(182) Lamparth, I.; Maichlemossmer, C.; Hirsch, A. Reversible Template-Directed Activation of Equatorial Double-Bonds of the Fullerene Framework - Regioselective Direct Synthesis, Crystal-Structure, and Aromatic Properties of T_h-$C_{66}(COOEt)_{12}$. *Angew. Chem. Int. Ed.* **1995**, *34*, 1607-1609.

(183) Diekers, M.; Hirsch, A.; Pyo, S.; Rivera, J.; Echegoyen, L. Synthesis and Electrochemical Properties of New C-60-Acceptor and -Donor Dyads. *Eur. J. Org. Chem.* **1998**, 1111-1121.

(184) Segura, J. L.; Martin, N. o-Quinodimethanes: Efficient Intermediates in Organic Synthesis. *Chem. Rev.* **1999**, *99*, 3199-3246.

(185) Langa, F.; DelaCruz, P.; DelaHoz, A.; DiazOrtiz, A.; DiezBarra, E. Microwave Irradiation: More Than Just a Method for Accelerating Reactions. *Contemp. Org. Synth.* **1997**, *4*, 373-386.

(186) Meidine, M. F.; Roers, R.; Langley, G. J.; Avent, A. G.; Darwish, A. D.; Firth, S.; Kroto, H. W.; Taylor, R.; Walton, D. R. M. Formation and Stabilization of the Hexa-Cyclopentadiene Adduct of C_{60}. *J. Chem. Soc. Chem. Commun.* **1993**, 1342-1344.

(187) Miller, G. P.; Tetreau, M. C. Facile, Completely Regioselective 1,4-Hydrogenations of C_{60}-Diaryltetrazine Monoadducts. *Org. Lett.* **2000**, *2*, 3091-3094.

(188) Lu, X.; Tian, F.; Wang, N. Q.; Zhang, Q. N. Organic Functionalization of the Sidewalls of Carbon Nanotubes by Diels-Alder reactions: A Theoretical Prediction. *Org. Lett.* **2002**, *4*, 4313-4315.

(189) Delgado, J. L.; de la Cruz, P.; Langa, F.; Urbina, A.; Casado, J.; Navarrete, J. T. L. Microwave Assisted Sidewall Functionalization of Single-wall Carbon Nanotubes by Diels-Alder Cycloaddition. *Chem. Commun.* **2004**, *15*, 1734-1735.

(190) Zhang, L.; Yang, J. Z.; Edwards, C. L.; Alemany, L. B.; Khabashesku, V. N.; Barron, A. R. Diels-Alder Addition to Fluorinated Single Walled Carbon Nanotubes. *Chem. Commun.* **2005**, 3265-3267.

(191) Menard-Moyon, C.; Dumas, F.; Doris, E.; Mioskowski, C. Functionalization of Single-Wall Carbon Nanotubes by Tandem High-pressure/$Cr(CO)_6$ Activation of Diels-Alder Cycloaddition. *J. Am. Chem. Soc.* **2006**, *128*, 14764-14765.

(192) Munirasu, S.; Albuerne, J.; Boschetti-de-Fierro, A.; Abetz, V. Functionalization of Carbon Materials Using the Diels-Alder Reaction. *Macromol. Rapid Commun.* **2010**, *31*, 574-579.

(193) Kanungo, M.; Lu, H.; Malliaras, G. G.; Blanchet, G. B. Suppression of Metallic Conductivity of Single-Walled Carbon Nanotubes by Cycloaddition Reactions. *Science* **2009**, *323*, 234-237.

(194) Chuang, S. C.; Sander, M.; Jarrosson, T.; James, S.; Rozumov, E.; Khan, S. I.; Rubin, Y. Approaches to Open Fullerenes: Synthesis and Kinetic Stability of Diels-Alder Adducts of Substituted Isobenzofurans and C_{60}. *J. Org. Chem* **2007**, *72*, 2716-2723.

(195) Hoke, S. H.; Molstad, J.; Dilettato, D.; Jay, M. J.; Carlson, D.; Kahr, B.; Cooks, R. G. Reaction of Fullerenes and Benzyne. *J. Org. Chem* **1992**, *57*, 5069-5071.

(196) Sun, J. T.; Zhao, L. Y.; Hong, C. Y.; Pan, C. Y. Selective Diels-Alder Cycloaddition on Semiconducting Single-Walled Carbon Nanotubes for Potential Separation Application. *Chem. Commun.* **2011**, *47*, 10704-10706.

(197) Criado, A.; Gomez-Escalonilla, M. J.; Fierro, J. L. G.; Urbina, A.; Pena, D.; Guitian, E.; Langa, F. Cycloaddition of Benzyne to SWNT: Towards CNT-Based Paddle Wheels. *Chem. Commun.* **2010**, *46*, 1272-1274.

(198) Fort, E. H.; Donovan, P. M.; Scott, L. T. Diels-Alder Reactivity of Polycyclic Aromatic Hydrocarbon Bay Regions: Implications for Metal-Free Growth of Single-Chirality Carbon Nanotubes. *J. Am. Chem. Soc.* **2009**, *131*, 16006-16007.

(199) Denis, P. A. Organic Chemistry of Graphene: The Diels-Alder Reaction. *Chem. Eur. J.* **2013**, 19, 15719-15725.

(200) Cao, Y.; Osuna, S.; Liang, Y.; Haddon, R. C.; Houk, K. N. Diels–Alder Reactions of Graphene: Computational Predictions of Products and Sites of Reaction. *J. Am. Chem. Soc* **2013**, 135, 17643-17649.

(201) Ferrari, A. C.; Robertson, J. Interpretation of Raman spectra of disordered and amorphous carbon. *Phys. Rev. B* **2000**, *61*, 14095-14107.

(202) Hamilton, C. E.; Lomeda, J. R.; Sun, Z. Z.; Tour, J. M.; Barron, A. R. High-Yield Organic Dispersions of Unfunctionalized Graphene. *Nano Lett.* **2009**, *9*, 3460-3462.

(203) Fukui, K. Recognition of Stereochemical Paths by Orbital Interaction. *Acc. Chem. Res.* **1971**, *4*, 57-64.

(204) Houk, K. N.; Li, Y.; Evanseck, J. D. Transition Structures of Hydrocarbon Pericylic Reactions. *Angew. Chem. Int. Ed.* **1992**, *31*, 682-708.

(205) Townshend, R. E.; Ramunni, G.; Segal, G.; Hehre, W. J.; Salem, L. Organic Transitions States. V. The Diels-Alder Reaction. *J. Am. Chem. Soc.* **1976**, *98*, 2190-2198.

(206) Houk, K. N.; Munchausen, L. L. Ionization Potentials, Electron Affinities, and Reactivities of Cyanoalkenes and Related Electron-Deficient Alkenes. A

Frontier Molecular Orbital Treatment of Cyanoalkene Reactivities in Cycloadditon, Electrophilic, Nucleophilic, and Radical Reactions. *J. Am. Chem. Soc.* **1976**, *98*, 937-946.

(207) Mathieu, C.; Barrett, N.; Rault, J.; Mi, Y. Y.; Zhang, B.; de Heer, W. A.; Berger, C.; Conrad, E. H.; Renault, O. Microscopic Correlation Between Chemical and Electronic States in Epitaxial Graphene on SiC(0001). *Phys. Rev. B* **2011**, *83*, 235436.

(208) Luo, Z.; Yu, T.; Kim, K.-j.; Ni, Z.; You, Y.; Lim, S.; Shen, Z.; Wang, S.; Lin, J. Thickness-Dependent Reversible Hydrogenation of Graphene Layers. *ACS Nano* **2009**, *3*, 1781-1788.

(209) Farmer, D. B.; Golizadeh-Mojarad, R.; Perebeinos, V.; Lin, Y.-M.; Tulevski, G. S.; Tsang, J. C.; Avouris, P. Chemical Doping and Electron-Hole Conduction Asymmetry in Graphene Devices. *Nano. Lett.* **2009**, *9*, 388-392.

(210) Ryan, M. E.; Hynes, A. M.; Badyal, J. P. S. Pulsed Plasma Polymerization of Maleic Anhydride. *Chem. Mater.* **1996**, *8*, 37-42.

(211) Ferrari, A. C.; Basko, D. M. Raman Spectroscopy as a Versatile Tool for Studying the Properties of Graphene. *Nature Nanotech.* **2013**, *8*, 235-246.

(212) Thouless, D. J. Maximum Metallic Resistance in Thin Wires. *Phys. Rev. Lett.* **1977**, *39*, 1167-1170.

(213) Abrahams, E.; Anderson, P. W.; Licciardello, D. C.; Ramakrishnan, T. V. Scaling Theory of Localization: Absence of Quantum Diffusion in Two Dimensions. *Phys. Rev. Lett.* **1979**, *42*, 673-676.

(214) Balog, R.; Jorgensen, B.; Wells, J.; Laegsgaard, E.; Hofmann, P.; Besenbacher, F.; Hornekaer, L. Atomic Hydrogen Adsorbate Structures on Graphene. *J. Am. Chem. Soc.* **2009**, *131*, 8744-8745.

(215) Kelly, K. F.; Halas, N. J. Determination of a and b Site Defects on Graphite Using C_{60}-Adsorbed STM Tips. *Surf. Sci.* **1998**, *416*, L1085-L1089.

(216) Ruffieux, P.; Melle-Franco, M.; Groning, O.; Bielmann, M.; Zerbetto, F.; Groning, P. Charge-Density Oscillation on Graphite Induced by the Interference of Electron Waves. *Phys. Rev. B* **2005**, *71*, 153403.

(217) Itkis, M. E.; Perea, D.; Jung, R.; Niyogi, S.; Haddon, R. C. Comparison of Analytical Techniques for Purity Evaluation of Single-Walled Carbon Nanotubes. *J. Am. Chem. Soc.* **2005**, *127*, 3439-3448.

(218) Hernandez, Y.; Nicolosi, V.; Lotya, M.; Blighe, F. M.; Sun, Z. Y.; De, S.; McGovern, I. T.; Holland, B.; Byrne, M.; Gun'ko, Y. K.; Boland, J. J.; Niraj, P.; Duesberg, G.; Krishnamurthy, S.; Goodhue, R.; Hutchison, J.; Scardaci, V.; Ferrari, A. C.; Coleman, J. N. High-Yield Production of Graphene by Liquid-Phase Exfoliation of Graphite. *Nature Nanotech.* **2008**, *3*, 563-568.

(219) Pereira, V. M.; Guinea, F.; dos Santos, J. M. B. L.; Peres, N. M. R.; Castro Neto, A. H. Disorder Induced Localized States in Graphene. *Phys. Rev. Lett.* **2006**, *96*, 036801.

(220) Pereira, V. M.; dos Santos, J. M. B. L.; Castro Neto, A. H. Modeling Disorder in Graphene. *Phys Rev. B.* **2008**, *77*, 1151109.

(221) Brouwer, P. W.; Racine, E.; Furusaki, A.; Hatsugai, Y.; Morita, Y.; Mudry, C. Zero Modes in the Random Hopping Model. *Phys. Rev. B* **2002**, *66*, 014204.

(222) De Laissardiere, G. T.; Mayou, D. Electronic Transport in Graphene: Quantum Effects and Role of Local Defects. *Mod. Phys. Lett. B* **2011**, *25*, 1019-1028.

(223) Zhang, Z. M. *Nano/Microscale Heat Transfer*; McGraw Hill, N.Y.: New York, 2007.

(224) Sarkar, S.; Zhang, H.; Huang, J.-W.; Wang, F.; Bekyarova, E.; Lau, C. N.; Haddon, R. C. Organometallic Hexahapto Functionalization of Single Layer Graphene as a Route to High Mobility Graphene Devices. *Adv. Mater.* **2013**, *25*, 1131-1136.

(225) Tung, V. C.; Allen, M. J.; Yang, Y.; Kaner, R. B. High-throughput Solution Processing of Large-Scale Graphene. *Nat. Nanotech.* **2009**, *4*, 25-29.

(226) Eda, G.; Fanchini, G.; Chhowalla, M. Large-Area Ultrathin Films of Reduced Graphene Oxide as a Transparent and Flexible Electronic Material. *Nat. Nanotech.* **2008**, *3*, 270-274.

(227) Gomez-Navarro, C.; Weitz, T. R.; Bittner, A. M.; Scolari, M.; Mews, A.; Kern, K. Electronic Transport Properties of Individual Chemically Reduced Graphene Oxide Sheets. *Nano Lett.* **2009**, *7*, 3499-3503.

(228) Banerjee, S.; Wong, S. S. Structural Characterization, Optical Properties, and Improved Solubility of Carbon Nanotubes Functionalized with Wilkinson's Catalyst. *J. Am. Chem. Soc.* **2002**, *124*, 8940-8948.

(229) Jiang, J.; Smith, J. R.; Luo, Y.; Grennberg, H.; Ottosson, H. Multidecker Bis(benzene)chromium: Opportunities for Design of Rigid and Highly Flexible Molecular Wires. *J. Phys. Chem. C* **2011**, *115*, 785-790.

(230) Balch, A. L.; Catalano, V. J.; Lee, J. W. Accumulating Evidence for the Selective Reactivity of the 6-6 Ring Fusion of C_{60}. Preparation and Structure of $(\eta^2\text{-}C_{60})Ir(CO)Cl(PPh_3)_2 \cdot 5C_6H_6$. *Inorg. Chem.* **1991**, *30*, 3980-3981.

(231) Balch, A. L.; Catalano, V. J.; Lee, J. W.; Olmstead, M. M.; Parkin, S. R. $(\eta^2\text{-}C70)Ir(CO)Cl(PPh_3)_2$). *J. Am. Chem. Soc.* **1991**, *113*, 8953-8955.

(232) Balch, A. L.; Lee, J. W.; Olmstead, M. M. Structure of a Product of Double Addition to C70: $[C_{70}\{Ir(CO)Cl(PPhMe_2)_2\}_2] \cdot 3C_6H_6$. *Angew. Chem. Int. Ed. Engl.,* **1991**, *31*, 1356-1358.

(233) Balch, A. L.; Olmstead, M. M. Reactions of Transition Metal Complexes with Fullerenes (C_{60}, C_{70}, etc.) and Related Materials. *Chem. Rev.* **1998**, *98*, 2123-2165.

(234) Banerjee, S.; Wong, S. S. Functionalization of Carbon Nanotubes with a Metal-Containing Molecular Complex. *Nano Lett.* **2002**, *2*, 49-53.

(235) Filatov, A. S.; Petrukhina, M. A. Probing the Binding Sites and Coordination Limits of Buckybowls in a Solvent-free Environment: Experimental and Theoretical Assessment. *Coord. Chem. Rev.* **2010**, *254*, 2234-2246.

(236) Lee, R. S.; Kim, H. J.; Fischer, J. E.; Thess, A.; Smalley, R. E. Conductivity Enhancement in Single-Walled Carbon Nanotube Bundles Doped with K and Br. *Nature* **1997**, *388*, 255-257.

(237) Zan, R.; Bangert, U.; Ramasse, Q.; Novoselov, K. S. Metal-Graphene Interaction Studied via Atomic Resolution Scanning Transmission Electron Microscopy. *Nano. Lett.* **2011**, *11*, 1087-1092.

(238) Chan, K. T.; Neaton, J. B.; Cohen, M. L. First-Principles Study of Adatom Adsorption on Graphene. *Phy. Rev. B* **2008**, *77*, 235430.

(239) Wang, W. H.; Han, W.; Pi, K.; McCreary, K. M.; Miao, F.; Bao, W.; Lau, C. N.; Kawakami, R. K. Growth of Atomically Smooth MgO Films on Graphene by Molecular Beam Epitaxy. *App. Phys. Lett.* **2008**, *93*, 183107.

(240) Gan, Y. J.; Sun, L. T.; Banhart, F. One- and Two-Dimensional Diffusion of Metal Atoms in Graphene. *Small* **2008**, *4*, 587-591.

(241) Elschenbroich, C.; Mockel, R.; Vasil'kov, A.; Metz, B.; Harms, K. Chromium Sandwich Complexes of Polycyclic Aromatic Hydrocarbons: Triphenylene and Fluoranthene as η^6 ligands. *European Journal of Inorganic Chemistry* **1998**, 1391-1401.

(242) Elschenbroich, C. *Organometallics*; Third ed.; Wiley-VCH: Weinheim, 2006.

(243) Haaland, A. The Molecular Structure of Gaseous Dibenzene Chromium, $(C_6H_6)_2Cr$. *Acta Chem. Scand.* **1965**, *19*, 4146.

(244) Haddon, R. C. Comment on the Relationship of the Pyramidalization Angle at a Conjugated Carbon Atom to the Sigma Bond Angles. *J. Phys. Chem. A* **2001**, *105*, 4164-4165.

(245) King, W. A.; Di Bella, S.; Lanza, G.; Khan, K.; Duncalf, D. J.; Cloke, F. G. N.; Fragala, I. L.; Marks, T. J. Metal-Ligand Bonding and Bonding Energetics in Zerovalent Lanthanide, Group 3, Group 4, and Group 6 Bis(arene) Sandwich Complexes. A Combined Solution Thermochemical and ab Initio Quantum Chemical Investigation. *J. Am. Chem. Soc.* **1996**, *118*, 627-635.

(246) Rogers, J. R.; Marynick, D. S. Theoretical Estimates of the Eta-6 Bonding Capability of Buckminsterfullerene in Transition-Metal Complexes. *Chem Phys Lett* **1993**, *205*, 197-199.

(247) Haddon, R. C. Organometallic Chemistry of the Fullerenes: η^2 and η^5-π Complexes. *J. Comp. Chem.* **1998**, *19*, 139-143.

(248) Sawamura, M.; Iikura, H.; Nakamura, E. First Pentahaptofullerene Metal Complexes. *J. Am. Chem. Soc.* **1996**, *118*, 12850-12851.

(249) Matsuo, Y.; Tahara, K.; Nakamura, E. Synthesis and Electrochemistry of Double-decker Buckyferrocenes. *J. Am. Chem. Soc.* **2006**, *128*, 7154-7155.

(250) Sawamura, M.; Kuninobu, Y.; Toganoh, M.; Matsuo, Y.; Yamanaka, M.; Nakamura, E. Hybrid of Ferrocene and Fullerene. *J. Am. Chem. Soc.* **2002**, *124*, 9354-9355.

(251) Nunzi, F.; Mercuri, F.; Sgamelotti, A. The Coordination Chemistry of Carbon Nanotubes: a Density Functional Study through a Cluster Model Approach. *J. Phys. Chem. B* **2002**, *106*, 10622-10633.

(252) Nunzi, F.; Mercuri, F.; Sgamelotti, A. The Interaction of $Cr(CO)_3$ on the (n,0) Nanotube Side-Walls: a Density Functional Study through a Cluster Model Approach. *Mol. Phys.* **2003**, *101*, 2047-2054.

(253) Nunzi, F.; Mercuri, F.; de Angelis, F.; Sgamelotti, A.; Re, N.; Giannozi, P. Coordination and Haptotropic Rearrangement of $Cr(CO)_3$ on (n, 0) Nanotube Sidewalls: A Dynamical Density Functional Study. *J. Phys. Chem. B* **2004**, *108*, 5243-5249.

(254) Nunzi, F.; Sgamellotti, A.; De Angelis, F. $Cr(CO)_3$-Activated Diels-Alder Reaction on Single-Wall Carbon Nanotubes: A DFT Investigation. *Chem. Eur. J.* **2009**, *15*, 4182-4189.

(255) Avdoshenko, S. M.; Ioffe, I. N.; Cuniberti, G.; Dunsch, L.; Popov, A. A. Organometallic Complexes of Graphene: Toward Atomic Spintronics Using a Graphene Web. *ACS Nano* **2011**, *5*, 9939-9949.

(256) Li, E. Y.; Marzari, N. Improving the Electrical Conductivity of Carbon Nanotube Networks: A First-Pronciples Study. *ACS Nano* **2011**, *5*, 9726-9736.

(257) Dagani, R. Putting the 'Nano' into Composites. *Chem. Eng. News* **1999**, *77*, 25.

(258) Kundig, E. P. Synthesis of Transition Metal η^6-Arene Complexes. *Topics Organomet. Chem.* **2004**, *7*, 3-20.

(259) Kondo, Y.; Green, J. R.; Ho, J. W. Tartrate-Derived Aryl Aldehyde Acetals in the Asymmetric Directed Metalation of Chromium Tricarbonyl Arene Complexes. *J. Org. Chem.* **1993**, *58*, 6182-6189.

(260) Kundig, E. P.; Timms, P. L. Metal Atom Preparation and Ligand Displacement Reactions of Bisnaphthalene Chromium and Related Compounds. *J. Chem. Soc. Chem. Commun.* **1977**, 912-913.

(261) Kundig, E. P.; Perret, C.; Spichiger, S.; Bernardinelli, G. Naphthalene Complexes .5. Arene Exchange-Reactions in Naphthalenechromium Complexes. *J. Organomet. Chem.* **1985**, *286*, 183-200.

(262) Bush, B. F.; Lagowski, J. J. Chemistry of Bis(η^6-naphhtalene)chromium Ligand Exchange Reactions: Synthesis and Characterization of Poly[(μ- η^6,η^6-naphthalene)chromium] *Organometallics* **1988**, *7*, 1945-1948.

(263) Bush, B. F.; Lynch, V. M.; Lagowski, J. J. Transition-Metal Organometallic Compounds. 8. Arene Exchange Reactions of Bis(naphthalene) chromium. *Organometallics* **1987**, *6*, 1267-1275.

(264) Vebrel, J.; Mercier, R.; Belleney, J. A Direct and Efficient Complexation of Some Indenes and Dihydronaphthalenes with $(NH_3)_3Cr(CO)_3$. *J. Orgmet. Chem.* **1982**, *235*, 197-200.

(265) Morley, J. A.; Woolsey, N. F. Metal Arene Complexes in Organic-Synthesis - Hydroxylation, Trimethylsilylation, and Carbethoxylation of Some Polycyclic Aromatic-Hydrocarbons Utilizing η^6-Arene Chromium Tricarbonyl Complexes. *J. Org. Chem.* **1992**, *57*, 6487-6495.

(266) Timms, P. L. The Formation of Complexes from Transition-metal Vapours. *Chem. Commun.* **1969**, 1033.

(267) Timms, P. L. Low Temperature Condensation of High Temperature Species as a Synthetic Method. *Adv. Inorg. Chem. Radiochem.* **1972**, *14*, 121-171.

(268) Green, M. L. H.; Silverthorn, W. E. *J. Chem. Soc., Dalton* **1973**, *301*.

(269) Benfield, F. W. S.; Green, M. L. H.; Ogden, J. S.; Young, D. Synthesis of Bis-p-Benzene-Titanium and -Molybdenum using Metal Vapours. *J. Chem. Soc., Chem. Commun.* **1973**, 866-867.

(270) Lamanna, W. M. Metal Vapor Synthesis of a Novel Triple-Decker Sandwich Complex: (η^6-Mesitylene)$_2$(μ-η^6:η^6-Mesitylene)Cr$_2$. *J. Am. Chem. Soc.* **1986**, *108*, 2096-2097.

(271) Pampaloni, G. Aromatic Hydrocarbons as Ligands. Recent Advances in the Synthesis, the Reactivity and the Applications of bis(η^6-arene) Complexes. *Coord. Chem. Rev.* **2010**, *254*, 402-419.

(272) Hamon, M. A.; Itkis, M. E.; Niyogi, S.; Alvaraez, T.; Kuper, C.; Menon, M.; Haddon, R. C. Effect of Rehybridization on the Electronic Structure of Single-Walled Carbon Nanotubes. *J. Am. Chem. Soc.* **2001**, *123*, 11292-11293.

(273) Wang, F.; Itkis, M. E.; Haddon, R. C. Enhanced Electromodulation of Infrared Transmittance in Semitransparent Films of Large Diameter Semiconducting Single-Walled Carbon Nanotubes. *Nano Lett.* **2010**, *10*, 937-942.

(274) Hu, H.; Zhao, B.; Hamon, M. A.; Kamaras, K.; Itkis, M. E.; Haddon, R. C. Sidewall Functionalization of Single-Walled Carbon Nanotubes by Addition of Dichlorocarbene. *J. Am. Chem. Soc.* **2003**, *125*, 14893-14900.

(275) Strano, M. S.; Huffman, C. B.; Moore, V. C.; O'Connell, M. J.; Haroz, E. H.; Hubbard, J.; Miller, M.; Rialon, K.; Kittrell, C.; Ramesh, S.; Hauge, R. H.; Smalley, R. E. Reversible, Band-Gap-Selective Protonation of Single-Walled Carbon Nanotubes in Solution. *J. Phys. Chem. B* **2003**, *107*, 6979-6985.

(276) Wu, Z.; Chen, Z.; Du, X.; Logan, J. M.; Sippel, J.; Nikolou, M.; Kamaras, K.; Reynolds, J. R.; Tanner, D. B.; Hebard, A. F.; Rinzler, A. G. Transparent, Conductive Carbon Nanotube Films. *Science* **2004**, *305*, 1273-1276.

(277) Zhao, B.; Itkis, M. E.; Niyogi, S.; Hu, H.; Perea, D.; Haddon, R. C. Extinction Coefficients and Purity of Single-Walled Carbon Nanotubes. *J. Nanosci. Nanotechnol.* **2004**, *4*, 995-1004.

(278) Zhao, B.; Itkis, M. E.; Niyogi, S.; Hu, H.; Zhang, J.; Haddon, R. C. Study of the Extinction Coefficients of Single-Walled Carbon Nanotubes and Related Carbon Materials. *J. Phys. Chem. B* **2004**, *108*, 8136-8141.

(279) Bekyarova, E.; Itkis, M. E.; Cabrera, N.; Zhao, B.; Yu, A.; Gao, J.; Haddon, R. C. Electronic Properties of Single-Walled Carbon Nanotube Networks. *J. Am. Chem. Soc.* **2005**, *127*, 5990-5995.

(280) Calhorda, M. J.; Frazao, C. F.; Simoes, J. A. M. Metal-Carbon Bond Strengths in $Cr(CO)_6$, $Cr(\eta^6\text{-}C_6H_6)_2$, and $Cr(CO)_3(\eta^6\text{-}C_6H_6)$. *J. Orgmet. Chem.* **1984**, *262*, 305-314.

(281) Stanghellini, P. L.; Diana, E.; Arrais, A.; Rossin, A.; Kettle, S. F. A. Benzene and Tropylium Metal Complexes. Intra- and Intermolecular Interaction Evidenced by Vibrational Analysis: The Blue-shift Hydrogen Bond. *Organometallics* **2006**, *25*, 5024-5030.

(282) Lundquist, R. T.; Cais, M. Ultraviolet Spectra of Organometallic Compounds. *J. Org. Chem.* **1962**, *27*, 1167-1172.

(283) Cotton, F. A.; Wilkinson, G.; Murillo, C. A.; Bochmann, M. *Adv. Inorg. Chem.*; Sixth Edition ed.; John Wiley & Sons: New York, 1999.

(284) Pape, A. R.; Kaliappan, K. P.; Kundig, E. P. Transition-Metal-Mediated Dearomatization Reactions. *Chem. Rev.* **2000**, *100*, 2917-2940.

(285) Skinner, H. A.; Connor, J. A. Metal-Ligand Bond-Energies in Organometallic Compounds. *Pure Appl. Chem.* **1985**, *57*, 79-88.

(286) Frank, S.; Poncharal, P.; Wang, Z. L.; de Heer, W. A. Carbon Nanotube Quantum Resistors. *Science* **1998**, *280*, 1744-1746.

(287) Nagashio, K.; Nishimura, T.; Kita, K.; Toriumi, A. Metal/Graphene Contact as a Performance Killer of Ultra-High Mobility Graphene - Analysis of Intrinsic Mobiity and Contact Resistance. *IEEE Int. Electron Dev. Meeting* **2009**, 23.2.1.

(288) Kim, B. K.; Jeon, E. K.; Kim, J. J.; Lee, J. O. Positioning of the Fermi Level in Graphene Devices with Asymmetric Metal Electrodes. *J. Nanomater.* **2010**, DOI:10.1155/2010/575472.

(289) Jimenez-Halla, J. O. C.; Robles, J.; Sola, M. Intramolecular Haptotropic Rearrangements of the Tricarbonylchromium Complex in Small Polycyclic Aromatic Hydrocarbons. *Organometallics* **2008**, *27*, 5230-5240.

(290) Dai, J.; Zhao, Y.; Wu, X.; Zeng, X. C.; Yang, J. Organometallic Hexahapto-Functionalized Graphene: Band Gap Engineering with Minute Distortion to the Planar Structure. *J. Phys. Chem. C* **2013**, *117*, 22156-22161.